

**COPY** 1  
2

# FLIGHT TESTS OF THE MICROWAVE LANDING SYSTEM MULTIMODE DIGITAL PROCESSOR

FEDERAL AVIATION ADMINISTRATION

FEB 12 1981

TECHNICAL CENTER LIBRARY  
ATLANTIC CITY, N.J. 08405

John Warren



**FINAL REPORT**

**JANUARY 1981**

Document is available to the U.S. public through  
the National Technical Information Service,  
Springfield, Virginia 22161.

Prepared for

**U. S. DEPARTMENT OF TRANSPORTATION  
FEDERAL AVIATION ADMINISTRATION  
TECHNICAL CENTER  
Atlantic City Airport, N.J. 08405**

#### NOTICE

This document is disseminated under the sponsorship of the Department of Transportation in the interest of information exchange. The United States Government assumes no liability for the contents or use thereof.

The United States Government does not endorse products or manufacturers. Trade or manufacturer's names appear herein solely because they are considered essential to the object of this report.

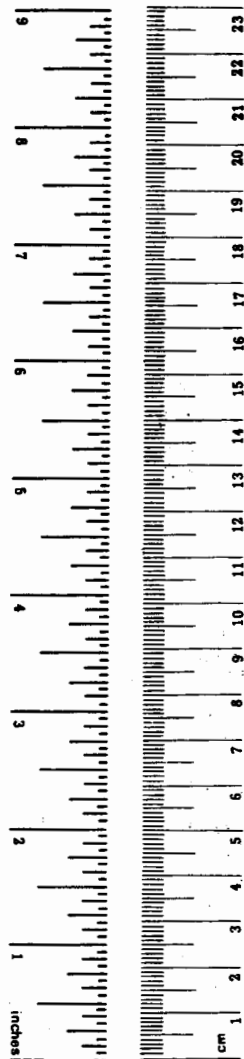
1. Report No. FAA-CT-80-19		2. Government Accession No.		3. Recipient's Catalog No.	
4. Title and Subtitle FLIGHT TESTS OF THE MICROWAVE LANDING SYSTEM MULTIMODE DIGITAL PROCESSOR				5. Report Date January 1981	
				6. Performing Organization Code	
7. Author(s) John Warren				8. Performing Organization Report No. FAA-CT-80-19	
9. Performing Organization Name and Address Federal Aviation Administration Technical Center Atlantic City Airport, New Jersey 08405				10. Work Unit No. (TRAIS)	
				11. Contract or Grant No. 075-725-420	
12. Sponsoring Agency Name and Address U.S. Department of Transportation Federal Aviation Administration Technical Center Atlantic City Airport, New Jersey 08405				13. Type of Report and Period Covered Final August 1980 - November 1980	
				14. Sponsoring Agency Code	
15. Supplementary Notes					
16. Abstract  Flight tests were performed in order to evaluate four digital airborne processing techniques. Four techniques used for processing Microwave Landing System (MLS) time reference scanning beam (TRSB) signals are: (1) dwell-gate processing (DGP), (2) single-edge processing (SEP), (3) dual-edge processing (DEP), and (4) split-gate processing (SPGT). These techniques were flight tested under standard partial orbits, glide slopes, and aircraft shadowing. Overall, the SPGT and DGP techniques resulted in about the same errors. The SEP data were noisier than the DGP but usually had about the same bias. The DEP technique was always inferior to the DGP. Aircraft shadowing errors were excessive for all techniques and should be avoided by operating procedures when an aircraft nears the touchdown region. It is recommended that the DEP algorithm be changed for improved noise performance and flight tests be performed using all four processing techniques in a specular multipath environment and under conditions using two azimuth antennas having different beam widths (these tests were not performed because of equipment nonavailability during flight testing).					
17. Key Words Microwave Landing System Time Reference Scanning Beam Multimode Digital Processor CALSPAN Processor			18. Distribution Statement Document is available to the U.S. public through the National Technical Information Service, Springfield, Virginia 22161		
19. Security Classif. (of this report) Unclassified		20. Security Classif. (of this page) Unclassified		21. No. of Pages 74	22. Price

## METRIC CONVERSION FACTORS

### Approximate Conversions to Metric Measures

Symbol	When You Know	Multiply by	To Find	Symbol
<b>LENGTH</b>				
in	inches	2.5	centimeters	cm
ft	feet	30	centimeters	cm
yd	yards	0.9	meters	m
mi	miles	1.6	kilometers	km
<b>AREA</b>				
in <sup>2</sup>	square inches	6.5	square centimeters	cm <sup>2</sup>
ft <sup>2</sup>	square feet	0.09	square meters	m <sup>2</sup>
yd <sup>2</sup>	square yards	0.8	square meters	m <sup>2</sup>
mi <sup>2</sup>	square miles	2.6	square kilometers	km <sup>2</sup>
	acres	0.4	hectares	ha
<b>MASS (weight)</b>				
oz	ounces	28	grams	g
lb	pounds	0.45	kilograms	kg
	short tons (2000 lb)	0.9	tonnes	t
<b>VOLUME</b>				
tsp	teaspoons	5	milliliters	ml
Tbsp	tablespoons	15	milliliters	ml
fl oz	fluid ounces	30	milliliters	ml
c	cups	0.24	liters	l
pt	pints	0.47	liters	l
qt	quarts	0.95	liters	l
gal	gallons	3.8	liters	l
ft <sup>3</sup>	cubic feet	0.03	cubic meters	m <sup>3</sup>
yd <sup>3</sup>	cubic yards	0.76	cubic meters	m <sup>3</sup>
<b>TEMPERATURE (exact)</b>				
°F	Fahrenheit temperature	5/9 (after subtracting 32)	Celsius temperature	°C

\* 1 in = 2.54 (exactly). For other exact conversions and more detailed tables, see NBS Misc. Publ. 286, Units of Weights and Measures, Price \$2.25, SD Catalog No. C13.10:286.



### Approximate Conversions from Metric Measures

Symbol	When You Know	Multiply by	To Find	Symbol
<b>LENGTH</b>				
mm	millimeters	0.04	inches	in
cm	centimeters	0.4	inches	in
m	meters	3.3	feet	ft
m	meters	1.1	yards	yd
km	kilometers	0.6	miles	mi
<b>AREA</b>				
cm <sup>2</sup>	square centimeters	0.16	square inches	in <sup>2</sup>
m <sup>2</sup>	square meters	1.2	square yards	yd <sup>2</sup>
km <sup>2</sup>	square kilometers	0.4	square miles	mi <sup>2</sup>
ha	hectares (10,000 m <sup>2</sup> )	2.5	acres	
<b>MASS (weight)</b>				
g	grams	0.035	ounces	oz
kg	kilograms	2.2	pounds	lb
t	tonnes (1000 kg)	1.1	short tons	
<b>VOLUME</b>				
ml	milliliters	0.03	fluid ounces	fl oz
l	liters	2.1	pints	pt
l	liters	1.06	quarts	qt
l	liters	0.26	gallons	gal
m <sup>3</sup>	cubic meters	35	cubic feet	ft <sup>3</sup>
m <sup>3</sup>	cubic meters	1.3	cubic yards	yd <sup>3</sup>
<b>TEMPERATURE (exact)</b>				
°C	Celsius temperature	9/5 (then add 32)	Fahrenheit temperature	°F

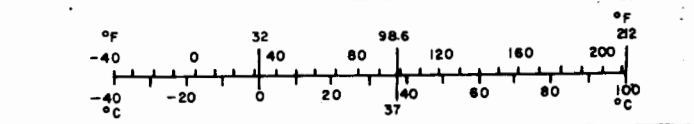


## TABLE OF CONTENTS

	Page
INTRODUCTION	1
Objective	1
Background	1
DISCUSSION	1
Equipment Description and Layout	1
Description of the Four Processing Techniques	2
Technical Approach	5
Flight Test Results	6
SUMMARY AND CONCLUSIONS	7
Single-Edge Processing	7
Split-Gate Processing	8
Dwell-Gate Processing	8
Dual-Edge Processing	8
Aircraft Shadowing	8
RECOMMENDATIONS	8
REFERENCES	9
APPENDIX	

## INTRODUCTION

### OBJECTIVE.

The objective was to perform flight tests which would be used to make a relative comparison of four time reference scanning beam (TRSB) digital processing techniques using the CALSPAN Corporation multimode processor. The four techniques for processing Microwave Landing System (MLS) TRSB signals are: (1) dwell-gate processing (DGP), (2) single-edge processing (SEP), (3) dual-edge processing (DEP), and (4) split-gate processing (SPGT).

### BACKGROUND.

The TRSB MLS developed by the Federal Aviation Administration (FAA) under a joint Department of Transportation, Department of Defense, and National Aeronautics and Space Administration program is designed to meet extended requirements in volumetric coverage, guidance accuracy, and integrity to satisfy the increasing needs of aviation. It is to be a common civil-military system and will provide operational capabilities and equipment suitability for all classes of users.

The key to the successful achievement of the MLS operational objectives is the availability of an economic airborne receiver signal processor design which can accurately estimate the aircraft's angular position in the presence of strong specular multipath and receiver noise. Specular multipath, as used in this report, refers to either vertical or lateral reflections which distort one edge of the scanning beam.

Early in the prototype hardware phase of the United States program for TRSB, the DGP, which operates on the received beam envelope, was selected because of its simplicity. This technique permitted significant reductions in the size, complexity, and production cost of the

avionics through the use of a readily available low-cost microprocessor such as the Intel 8080.

## DISCUSSION

### EQUIPMENT DESCRIPTION AND LAYOUT.

The Bendix test bed MLS was used as the TRSB signal source. The azimuth subsystem was located at the approach of runway 13 (FAA Technical Center) with Technical Center coordinates (right-handed rectangular cartesian coordinate system) of:

X: 111815.926  
Y: 115489.583  
Z: 10082.730

This subsystem uses 117 radiating elements and 117 phase shifters to produce the scanning action. It has a 1° beam which scans ±60° in azimuth and has elevation coverage from 1° to 20°.

The elevation unit was located about 429 feet from the centerline of runway 13/31 and 9,731 feet from the azimuth site at the Technical Center coordinates of:

X: 112244.954  
Y: 105758.803  
Z: 10068.059

It uses 81 radiating elements and 81 phase shifters for coverage in elevation from 1° to 20°. It has a 1° beam with azimuthal coverage of about ±55° (the signal is reduced in power beyond the ±40° limits).

The elevation unit has a monitor pole whose base is located at coordinates of:

X: 112262.31  
Y: 105660.454  
Z: 10058.817

The monitor antenna is about 12.5 feet from the base with a 2-foot (3/8 inch

diameter) lightning rod on top. It is located at an MLS azimuth angle of  $-10^\circ$  relative to the elevation unit. A negative MLS azimuth angle would place an aircraft on approach to the right of the runway.

Runway 13/31 is along the y-axis of the Technical Center coordinate system. The threshold of runway 31 is located at:

X: 111816.19  
Y: 104707.71  
Z: 10063.24

The tracking system used was the Technical Center theodolite system. The Technical Center coordinates of each of the three theodolites are:

<u>No.</u>	<u>X</u>	<u>Y</u>	<u>Z</u>
P8	115636.46	103214.78	10111.875
P29	109304.34	113190.56	10146.28
P36	115771.81	113297.69	10113.51

A general error analysis of the theodolite system is presented in reference 1.

The Bendix Small Community MLS receiver was used to receive the radiofrequency (RF) signals and to output video signals and DPSK (differential phase shift keying) decodes for function identification to the CALSPAN processor. The primary aircraft used for these tests was the Aerocommander (N50), with the MLS quarter wave stub antenna placed about 2 feet in back of the nose and about 1 foot above the centerline. The theodolites tracked the nose of the aircraft but the antenna position was corrected for in the tracking software.

#### DESCRIPTION OF THE FOUR PROCESSING TECHNIQUES.

The four processing techniques discussed are described in reference 2.

#### 1. Dwell-Gate Processor.

The DGP sets a threshold at 3 decibels (dB) below the peak value of the stored video signal as indicated in figure 1a. It then searches for an amplitude rise and fall through the threshold level that includes the peak. The rise and fall times must be separated by at least 20 microseconds ( $\mu s$ ) to be accepted. The times of occurrence of these passages are linearly interpolated to  $1/4 \mu s$  within an  $8 \mu s$  sampling interval. This process is carried out for both the TO and FRO scans. The raw angle is computed from the time difference.

The output angle is provided by a digital filter using the raw angle input. This filtered angle is also used to set the position of the tracking gates on the next scan. The raw dwell gate width, the time between the signal's rise and fall, is averaged by a low pass filter ( $\omega = 0.05$  radians/second). The average dwell gate width is used to set the tracking gate width.

A frame count is incremented whenever a successful angle computation is made and decremented otherwise. The DGP angle output is flagged at any time the frame count is below a threshold value.

Previous simulation tests and theory (reference 3) indicate DGP would be most useful with all azimuth signal levels and long-range elevation signal levels; i.e., low signal-to-noise ratios.

#### 2. Single-Edge Processor.

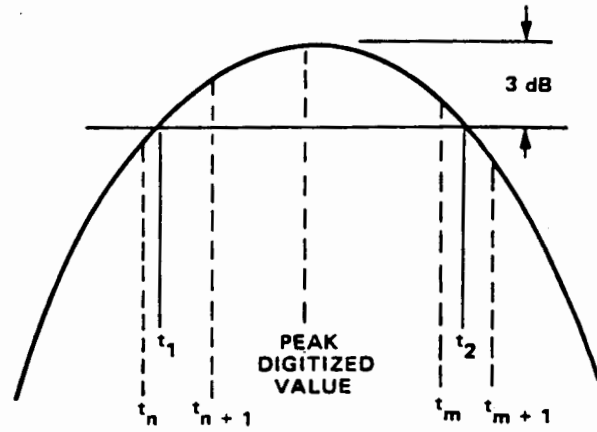
The SEP (figure 1b) looks for a change in slope on the one edge of the beam in order to avoid multipath perturbations of the beam peak and its other edge. Since multipath typically distorts the inside edges of the elevation beam, the SEP uses the leading beam edge on the TO scan and the trailing edge on the FRO scan.

1a Dwell Gate Processor

$t_1$  and  $t_2$  found by interpolation between sampling points (dashed lines)

$$\text{Dwell Gate Width} = t_2 - t_1$$

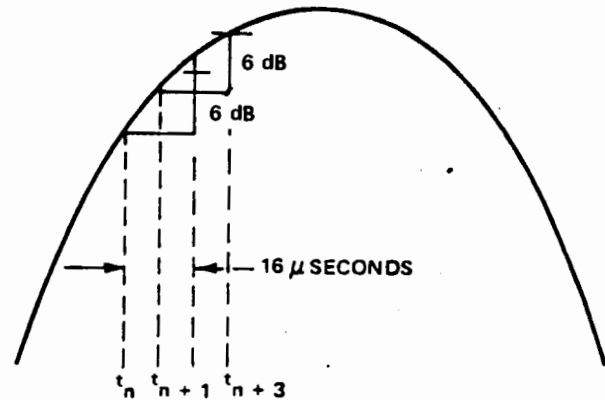
$$\text{Beam Center Time} = \frac{t_1 + t_2}{2}$$



1b Single Edge Processor

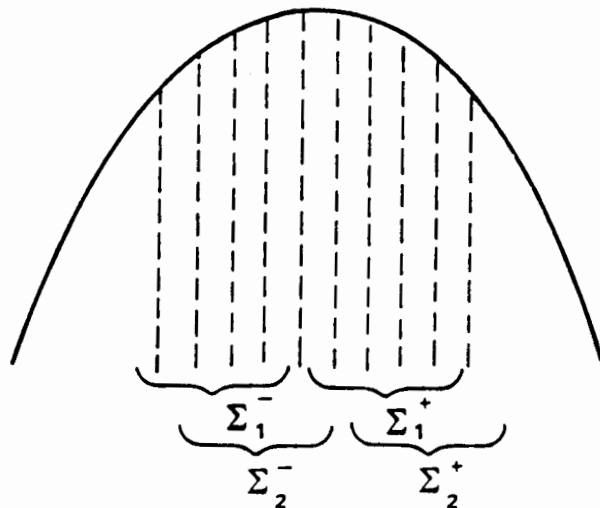
Time of 6 dB in 16 microseconds slope found by interpolation between times of greater and less slope

(Equivalent to analog delay and compare thresholding.)



1c Split Gate Processor

Difference of sums of four amplitudes on either side of peak ( $\Sigma_1^+ - \Sigma_1^-$ ) is interpolated with shifted difference ( $\Sigma_2^+ - \Sigma_2^-$ ) to determine beam centroid.



80-19-1

FIGURE 1. ILLUSTRATION OF PROCESSING PROCEDURES

Inside edge refers to the TO beam and FRO beam edges nearest each other as displayed on a voltage-time trace.

The stored beam shape is examined and the slope is compared to 6 dB in 16  $\mu$ s (two sampling intervals) as indicated in figure 1b. The slope first exceeds this value and then drops below it. A linear interpolation estimates the time to 1/4  $\mu$ s. The angle determined by the beam outside edge times is greater than that indicated by the beam centers, so a bias correction is necessary to produce the true angle. This correction is taken as the difference between the SEP and DGP angles averaged over about 20 seconds. Specifications for the CALSPAN software required a detection level of 9 dB instead of the 6 dB level, which was used erroneously. However, post-flight simulation tests of limited extent at CALSPAN indicate this difference is not significant.

A count is kept of the number of SEP corrections averaged. If multipath occurs, as indicated by a deviation of the raw SEP correction from the average correction ( $> 2 \mu$ s), the correction is not averaged and the count is decremented. Should the count fall to zero, approximately 30 seconds for a full count, the average correction is discarded and a new average correction started.

The SEP may fail if the beam amplitude falls too low or the beam is greatly distorted. A frame count is incremented on successful measurements and decremented on failures. The angle data is flagged if this count falls to zero.

Bench and simulation tests (reference 3) indicate this technique is an improvement over other processing techniques when the received signal exhibits specular multipath.

### 3. Dual-Edge Processor.

The dual-edge processor makes single-edge measurements on the inside and outside edges of the scanning beam using the same subroutines as the SEP uses on the outside edges. Outside edge refers to the TO and FRO beam edges farthest apart when displayed on a voltage-time trace. It then computes the angle by averaging the inside and outside measurements. In this way, it cancels out receiving system nonlinearities that can affect the SEP.

A DEP equivalent beam width is computed from the difference between the outside and inside angles and low pass filtered ( $\omega = 0.05$  radians/second). If a high level in-beam multipath condition occurs, one of these measurements will be shifted so that the raw beam width is lengthened. When the raw beam width exceeds the average beam width by 1  $\mu$ s, the presence of multipath is indicated. The angle computation is then bypassed for several scans while a count is made to determine whether the inside or outside angle is the most perturbed. If one beam edge is perturbed by multipath, the DEP switches to the SEP mode on the opposite edge until the multipath disappears. Any time that the raw beam width returns to within 1  $\mu$ s of the average beam width, the count is cleared and both inside and outside angles are used for the measurement. As with the other processors, a frame count is maintained to control the flag on the DEP angle data.

The DEP technique was designed to reduce serious multipath errors which may occur during azimuth curved approaches and the effect of shadowing by obstacles in the path of the beam.

#### 4. Split Gate Processor.

The splitgate tracker (figure 1c) finds the centroid of each beam by taking the difference of sums of four amplitudes (8  $\mu$ s apart) on each side of the peak amplitude. The computation of the difference of sums of four amplitudes is repeated about a sampling point shifted in the direction toward making the difference zero. When the sign of the difference of the sums changes (i.e., the sum on inside goes from greater to less than sum on the outside), an interpolation finds the mean point to 1/4  $\mu$ s. No beam width measurement is needed with this technique as a fixed number of samples is adequate for the normal range of beams encountered (1/2° to 4°).

Reference 3 indicates that this technique would show improved performance in both noise and high-level multipath relative to the DGP technique.

#### TECHNICAL APPROACH.

The four processing techniques were to be tested under the following conditions: (1) partial orbits, (2) constant glide-path approaches, (3) strong specular multipath conditions (using a flare elevation antenna), (4) shadowing under taxi maneuvers, (5) shadowing under takeoff maneuvers, and (6) using two different transmitting antenna beam widths. Due to nonavailability of the flare antenna, dynamic specular multipath (due to ground reflections) tests were not performed (static flare test data are available in reference 4). However, diffraction multipath data apparently occurred during the orbital flights. Diffraction multipath herein refers to a spreading interference pattern caused by the monitor pole located in the near field of the elevation antenna. Also, two different transmitter beam width sources were not available in order to test SEP beam width correction algorithms (reference 2). The object was to compare the three techniques

of SPGT, SEP, and DEP to the standard DGP technique. It was not considered necessary to perform mathematical comparisons as the data easily lends itself to observational comparisons. The data were compared for mean error differences, referred to as bias errors, and for standard deviation error differences, herein referred to as noise.

Some of this flight test data, with an analysis, are contained in reference 5. The sample data shown in this report are typical of all the flight data from a repeatability aspect.

#### FLIGHT TEST RESULTS.

The flight test data are shown in appendix A. The top of each plot indicates the type of flight pattern, the run number, and the date and time of the run. The y-axis indicates whether the data were relative to the azimuth or elevation unit and the processing technique used. The x-axis is either in degrees or nautical miles and always relative to the azimuth site. The two types of plots contained in the appendix are: the diagnostic plot, which shows both raw theodolite tracker data and raw MLS angle data; and the error plot, which is the difference between the tracker and MLS angles. The CALSPAN processor outputs a combination of four processing techniques (one of which was always the DGP), although eight combinations exist. The DEP technique is designed for use only with azimuth data, and the SEP technique only with elevation (primarily flare) data. However, the aircraft shadowing data also shows the SEP processing technique as used on the azimuth signals.

A description of the logic the multi-mode processor uses to generate flags is discussed in reference 6. Two types of flags are generated whenever the processor declares a piece of data invalid or missing. Frame flags are used to denote those areas where an approximate value is substituted for the unusable data. System flags

denote that an excess number of frame flags occurred and the receiver output is set to zero. However, the system flag operation observed in the flight test data did not always function as expected and might be due to software problems.

### 1. 3° Glidepath Centerline.

The azimuth data for the centerline approaches are shown in figures A-1 to A-8. The DGP and SPGT difference (error) plots (figures A-2 and A-4) are essentially the same except for two outliers on the SPGT error plot. Outliers, large extraneous angle excursions, are generally insignificant and are usually removed by the receiver software. The reason for these outliers is not known. The processor does not incorporate any slew rate limiter whereby the MLS data are flagged and an approximate value substituted for it. A slew rate limiter is generally designed to eliminate any angle change greater than 1° per second. For run 3, figures A-5 to A-8, the DGP is seen to be superior in both mean error and standard deviation error to the DEP data.

The elevation plots are shown in figures A-9 to A-16. The DGP error plot, figure A-10, and the SPGT plot, figure A-12, are essentially the same. The DGP plot, figure A-14, appears to have significantly less noise than the SEP data in figure A-16. However, the DGP bias and the SEP bias are about the same. The SEP mode, figure A-15, shows a large group of flags and an off-scale MLS angle occurring near the end of the run; whereas, the dwell gate processing is not flagged and appears normal.

### 2. 5° Glidepath, Centerline.

The azimuth data for the 5° centerline approaches are shown in figures A-17 to A-24. The SPGT errors (figure A-20) are essentially identical to the DGP errors (figure A-18), which is consistent with the 3° glide slope data. The DEP (figure A-24) shows a significantly higher noise

level and a slightly higher mean error than the DGP (figure A-22) data.

The elevation data appear in figures A-25 to A-32. Comparison of the DGP with the SPGT and SEP data shows the SPGT essentially identical to the DGP. The SEP is clearly noisier than the DGP but with essentially the same bias.

### 3. Orbits.

The azimuth orbits, figures A-33 to A-38, were flown at about 7 nautical miles (nmi) from the azimuth transmitter and at about 2.8° elevation angle. Here again, the DGP (figure 34) and the SPGT errors (figure A-36) are essentially the same. The DEP (figure A-38) error plot obviously has larger mean and standard deviation errors than the DGP (figure A-34) data.

Comparing the DGP (figure A-34) orbit data with any of the previous glide slope DGP data shows the noise on the orbits to be about twice that on the approaches. The scanning beam signal at the receiver input terminals was measured on previous projects at about -75 decibels per milliwatt (dBm) on a glide slope and about -77.5 dBm on an orbit. (Further investigations are expected in order to account for the difference in the noise levels.) Also, the data show large errors beyond the  $\pm 50^\circ$  azimuth angles. The loss of data from  $-56^\circ$  to  $-60^\circ$  might be due to the processing limit of the phase three receiver or to transmitter scanning errors. The large angle errors beyond  $+50^\circ$  might also be due to a limitation of the CALSPAN processing algorithms.

The elevation data for the orbits are shown in figures A-39 to A-44. The DGP (figure A-40) error plot and the SPGT (figure A-42) plot are almost identical. They also exhibit variations around  $-8.6^\circ$  ( $+3^\circ$  to  $-20^\circ$ ), which are typical of multipath. The SEP error plot is shown in figure A-44. Observational comparison of the SEP data within and outside the

multipath region shows the standard deviation to be about equal. The SEP data does not show the same coverage as the DGP or SPGT. This may be due to a combination of the transmitter power being reduced in azimuth and that SEP requires 15 to 20 dB more signal than DGP or SPGT.

The source of this multipath is probably the elevation monitor antenna. The MLS angle from the elevation unit to the monitor pole is  $-10^\circ$ . The angle from the elevation site to the midpoint of the multipath is about  $-10.4^\circ$  ( $-8.6^\circ$  from the azimuth site), assuming the aircraft is 7 nmi from the azimuth site. The elevation angle of the monitor horn is  $1.86^\circ$  and the aircraft was at  $3.2^\circ$ . However, there is a 2-foot lightning rod (3/8 inch diameter) on top of the horn. Reference 7 indicates that these conditions could cause diffraction, especially since the monitor antenna is in the near field of the elevation antenna.

#### 4. Shadowing-Takeoff Maneuvers.

For these tests a Convair 880 would takeoff in front of the azimuth transmitter when the MLS receiver equipped Aerocommander was about 2-1/2 nmi away and on a constant glidepath approach. The data are shown in figures A-45 to A-52. They show that the Convair 880 is shadowing the Aerocommander at about the 2.3 nmi mark. The DGP (figure A-46) and the SPGT error plot (figure A-48) show practically identical errors in the shadow region. The DEP (figure A-50) and SEP (figure A-52) plots show significantly larger errors than the DGP (figure A-46). (The SEP data (figures A-51 and A-52) has a large run of frame flags centered around the shadowing region (2.2 to 2.7 nmi). However, SEP is not intended to be used for azimuth signals.)

#### 5. Shadowing-Taxiing Maneuvers.

For these tests, the Convair 880 was taxiing off the runway when the Aerocommander was about 2-1/2 nmi away and on

an approach. The tail of the 880 was probably most responsible for blocking the azimuth transmitter signals. The data for all four processing techniques are shown in figures A-53 to A-60. In the shadow region, the DGP (figure A-53) appears to have slight improvement over the SPGT (figure A-55) data. Again, the DEP (figure A-59) and SEP (figure A-60) data appear significantly noisier than the DGP (figure A-54). The data were flagged throughout the shadow region. The MLS data in the flagged region was set to zero for DEP and SEP, which would indicate system flags rather than frame flags should have occurred.

## SUMMARY AND CONCLUSIONS

### SINGLE-EDGE PROCESSING.

Diffraction multipath conditions apparently occurred during the orbital flights of September 27, 1979. The type of multipath produced by the monitor antenna would generate distortions on both sides of the elevation beam, although the one side would probably exhibit larger perturbations than the other side. Figures A-39 to A-44 show this condition in the region of  $-20^\circ$  to  $+3^\circ$ . By visual observation, the SEP data in figure A-44 show the ratio of the standard deviation within the multipath region to that outside the region to be about the same. This same ratio is about two for the DGP (figure A-40) and the SPGT (figure A-42) error plots. Therefore, the data for this one flight show that the SEP technique has possibilities of reducing the effects of multipath for elevation signals. However, it is clearly noisier overall (under normal flight conditions) than the DGP and SPGT techniques. However, this processor was designed to perform significantly better than the other three techniques for strong elevation signals exhibiting specular multipath conditions.

### SPLIT-GATE PROCESSING.

The SPGT technique functions like a derivative processor in that it determines the approximate location of the beam peak, and then interpolates to find the mean point within  $1/4$  s. According to the theoretical report cited in reference 3, this technique should have a slight improvement over the DGP technique under specular multipath conditions and noise performance. However, this was not observed on figures A-40 and A-42, which apparently exhibited some diffraction multipath. Essentially, the same errors for both the DGP and SPGT are shown in the shadowing test data of figures A-45 and A-47. The noise performance for both the SPGT and DGP techniques were approximately the same.

### DWELL-GATE PROCESSING.

The DGP technique is presently used in most TRSB angle receivers and the one against which all the flight data were compared. Considering both noise and bias errors for the particular flight conditions, none of the other three techniques showed any improvement; i.e., both noise and bias error improvements over the DGP technique.

### DUAL-EDGE PROCESSING.

The dual-edge processor had a significantly higher noise level than the other three techniques for the glideslope approaches and orbits. These large errors were not expected. However, it is assumed that changes in the DEP algorithm might improve its performance. This technique was designed to detect multipath; then use a SEP technique on the opposite side of the beams. The SEP technique selects only one edge of the beam and is only intended for use with elevation signals. However, by comparing

the frame flag occurrence in figures A-49, A-51, A-57, and A-59, the DEP technique can be seen to perform better than the SEP technique. This would indicate the DEP technique has the ability to detect multipath conditions and to switch to the opposite side of the beams. However, shadowing is a diffraction multipath condition and not a specular multipath condition which the DEP technique was designed for. (There are several disadvantages to this technique which are described in reference 2.) Essentially, the same errors for both the DGP and SPGT are shown in the shadowing test data of figures A-45 and A-47.

### AIRCRAFT SHADOWING.

The shadowing tests exhibited very large bias errors, particularly when the shadowing aircraft was turning in front of the azimuth antenna. These errors reached  $0.07^\circ$  for the aircraft taking off and  $0.8^\circ$  for the aircraft taxiing. These error levels indicate that such shadowing should be avoided by operating procedures when an aircraft is nearing the touchdown region (a theoretical analysis of aircraft shadowing is discussed in reference 8).

### RECOMMENDATIONS

It is recommended that:

1. The DEP algorithms be investigated and modified for noise improvements.
2. All four techniques should be flight tested under normal conditions (approaches and orbits), specular multipath conditions, and using two azimuth transmitters having different beam widths.

## REFERENCES

1. Luciani, V. J., NAFEC Range Instrumentation System, FAA-NA-79-32, February 1980.
2. Beneke, J., et al., TRSB Multimode Digital Processor, Final Report, FAA-RD-78-84, April 1978.
3. Kelly, R. J. and La Berge, E. F. C., Comparison Study of MLS Airborne Signal Processing Techniques, Presented at NAECON 1978, Dayton, Ohio, May 16-18, 1978.
4. Wightman, C. W., Flare Pole Tests of the MLS Multimode Digital Processor, CALSPAN Technical Note-15, June 1978.
5. Wightman, C. W., Flight Test Data for Multimode Digital Processor, CALSPAN Technical Note-16, December 1979.
6. CALSPAN Corporation, Microwave Landing System Multimode Digital Processor, Instruction Manual, August 1979.
7. Evans, J. E., MLS Multipath Studies, Phase 3, Volume I: Overview and Propagation Model Validation/Refinement Studies, Final Report, FAA-RD-79-21, April 25, 1979.
8. Capon, J., Multipath Parameter Computations for the MLS Simulation Computer Program, FAA-RD-76-55, April 8, 1979.

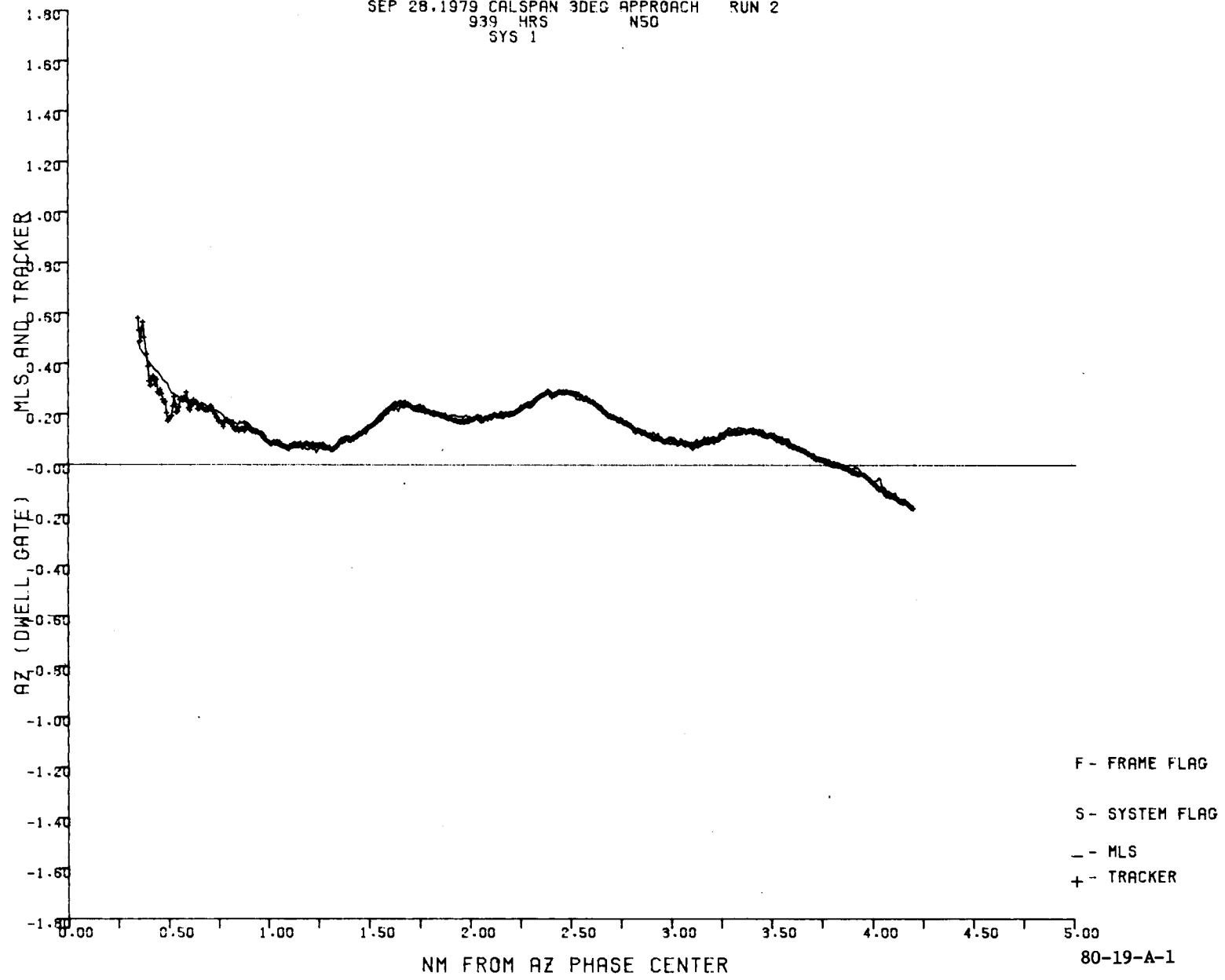
APPENDIX A

FLIGHT DATA

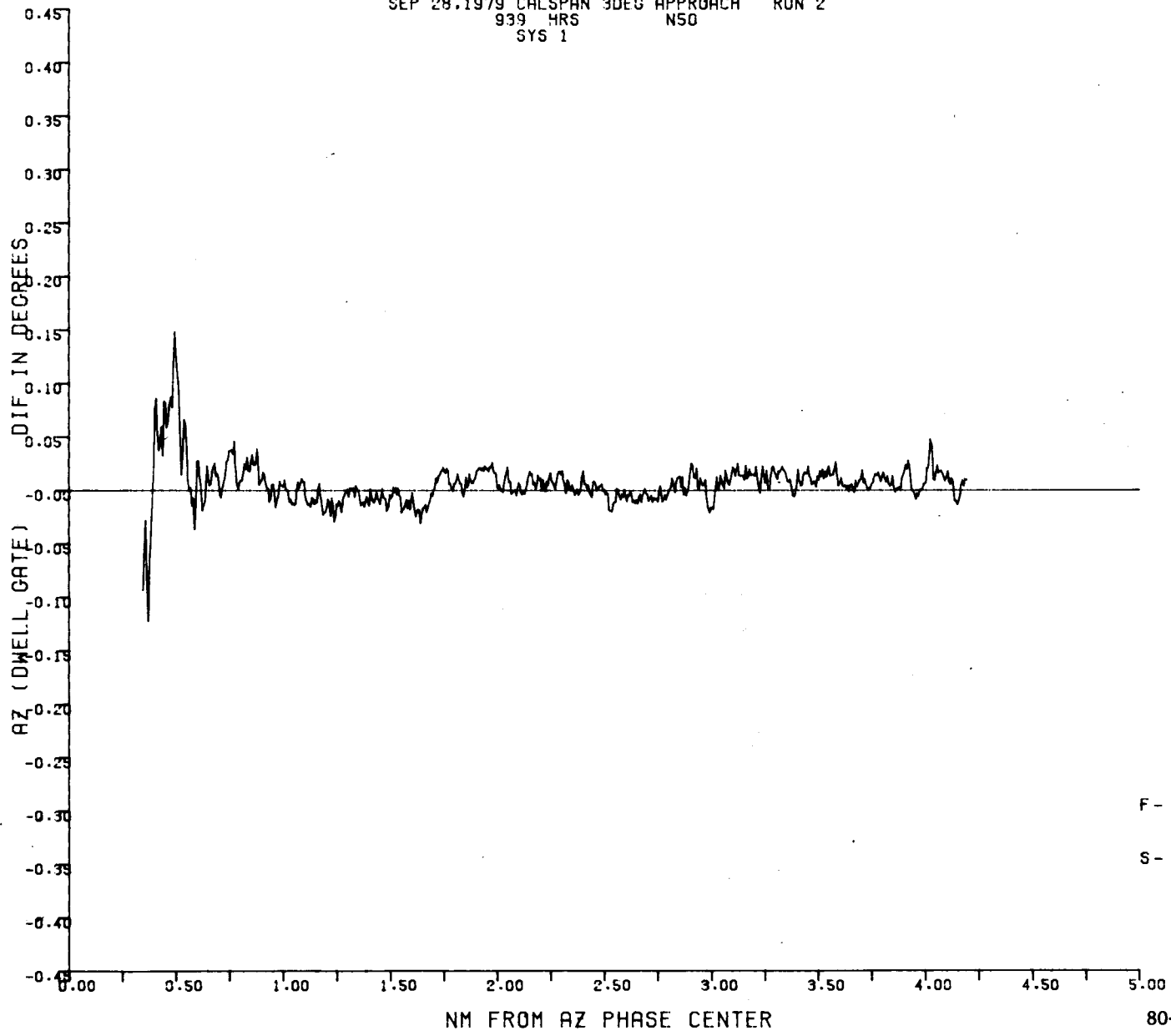
<u>Type of Pattern</u>	<u>Page No.</u>
3° Glideslope	A-1 to A-16
5° Glideslope	A-17 to A-32
Orbits	A-33 to A-44
Shadowing	
Take-Off Maneuvers	A-45 to A-52
Taxiing Maneuvers	A-53 to A-60

SEP 28.1979 CALSPAN 3DEG APPROACH RUN 2  
939 HRS N50  
SYS 1

I-A-1



SEP 28.1979 CALSPAN 3DEG APPROACH RUN 2  
939 HRS NSO  
SYS 1



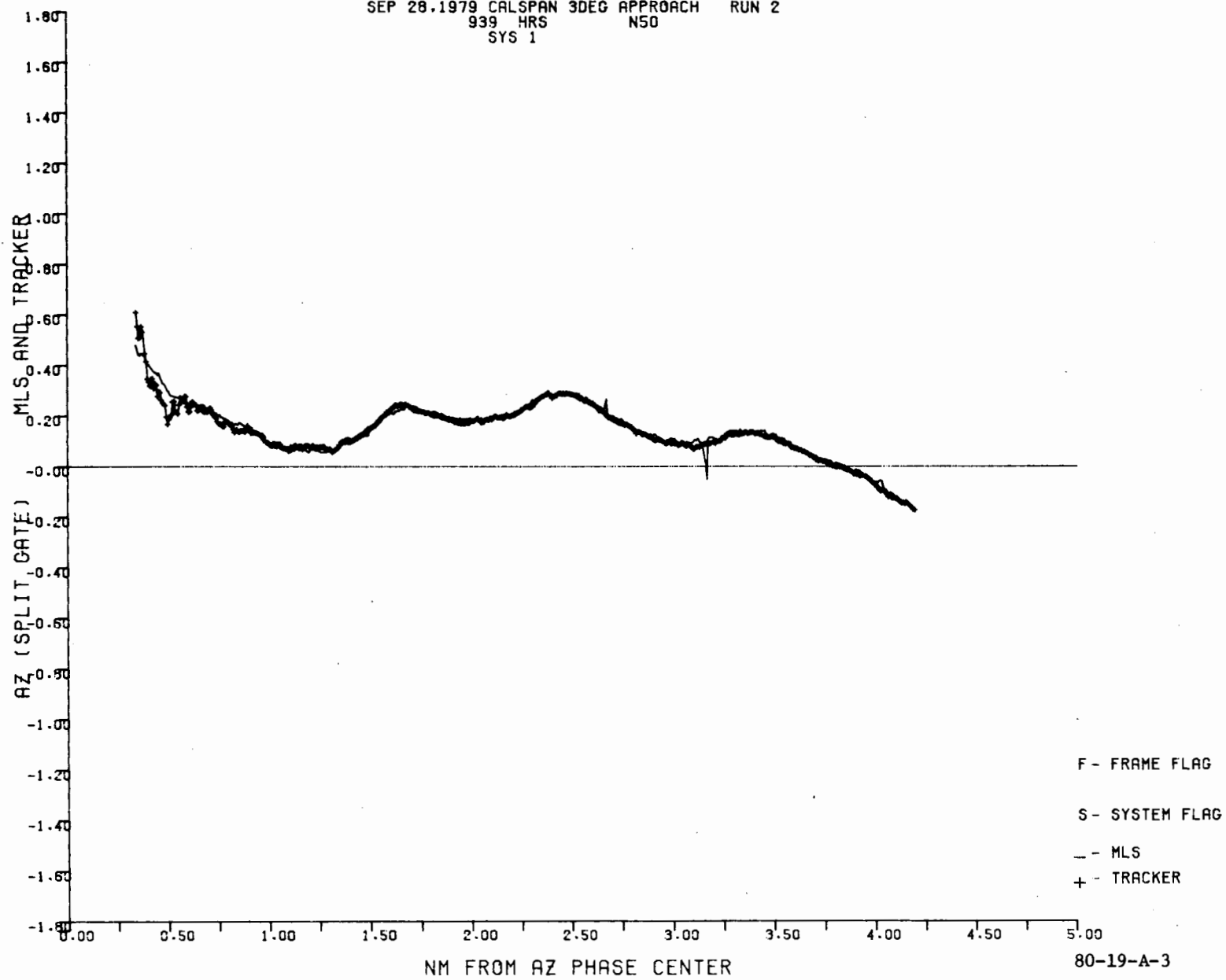
F - FRAME FLAG

S - SYSTEM FLAG

80-19-A-2

A-2

SEP 28.1979 CALSPAN 3DEG APPROACH RUN 2  
939 HRS N50  
SYS 1

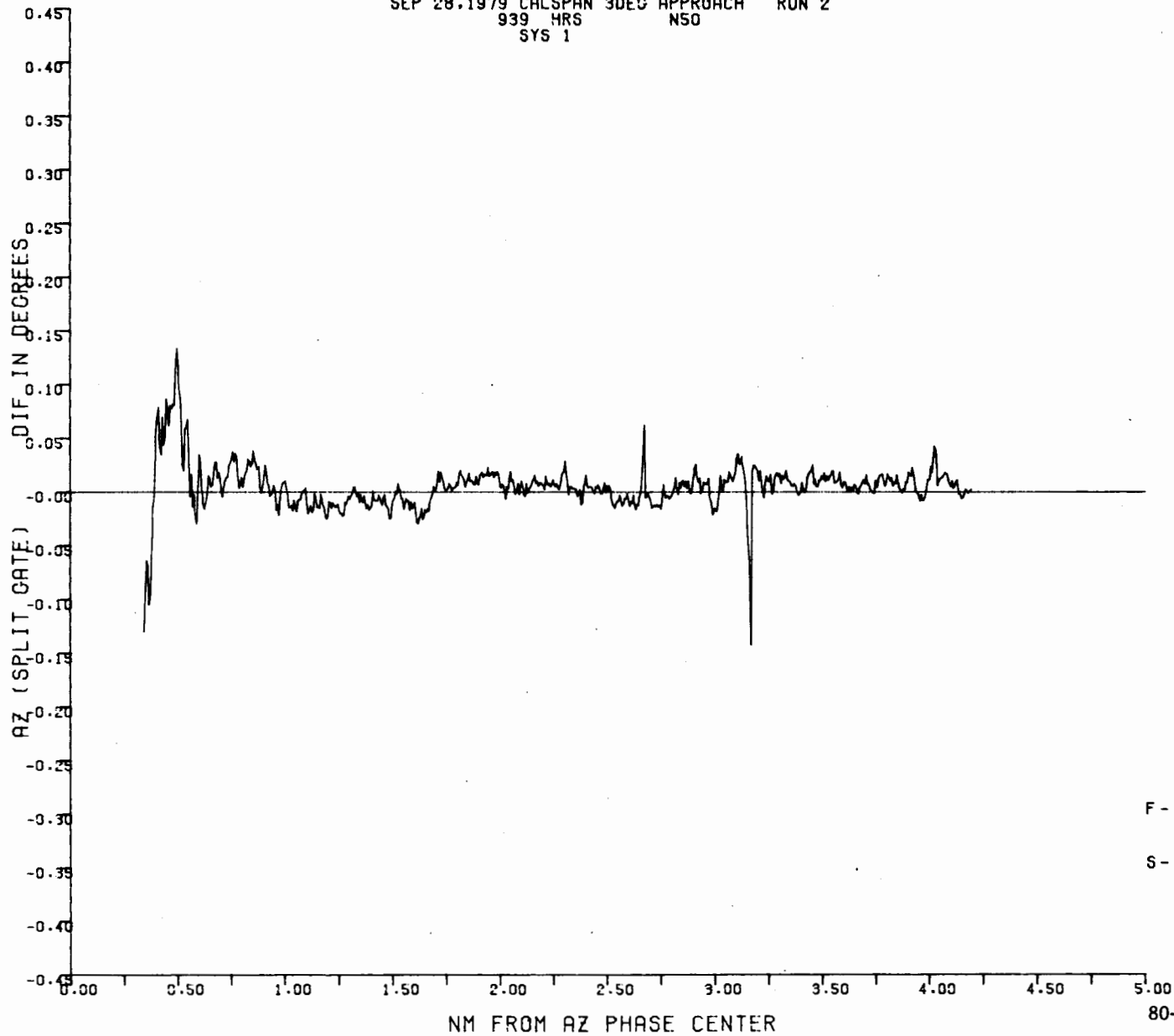


A-3

80-19-A-3

SEP 28.1979 CALSPAN 3DEG APPROACH RUN 2  
939 HRS N50  
SYS 1

A-4

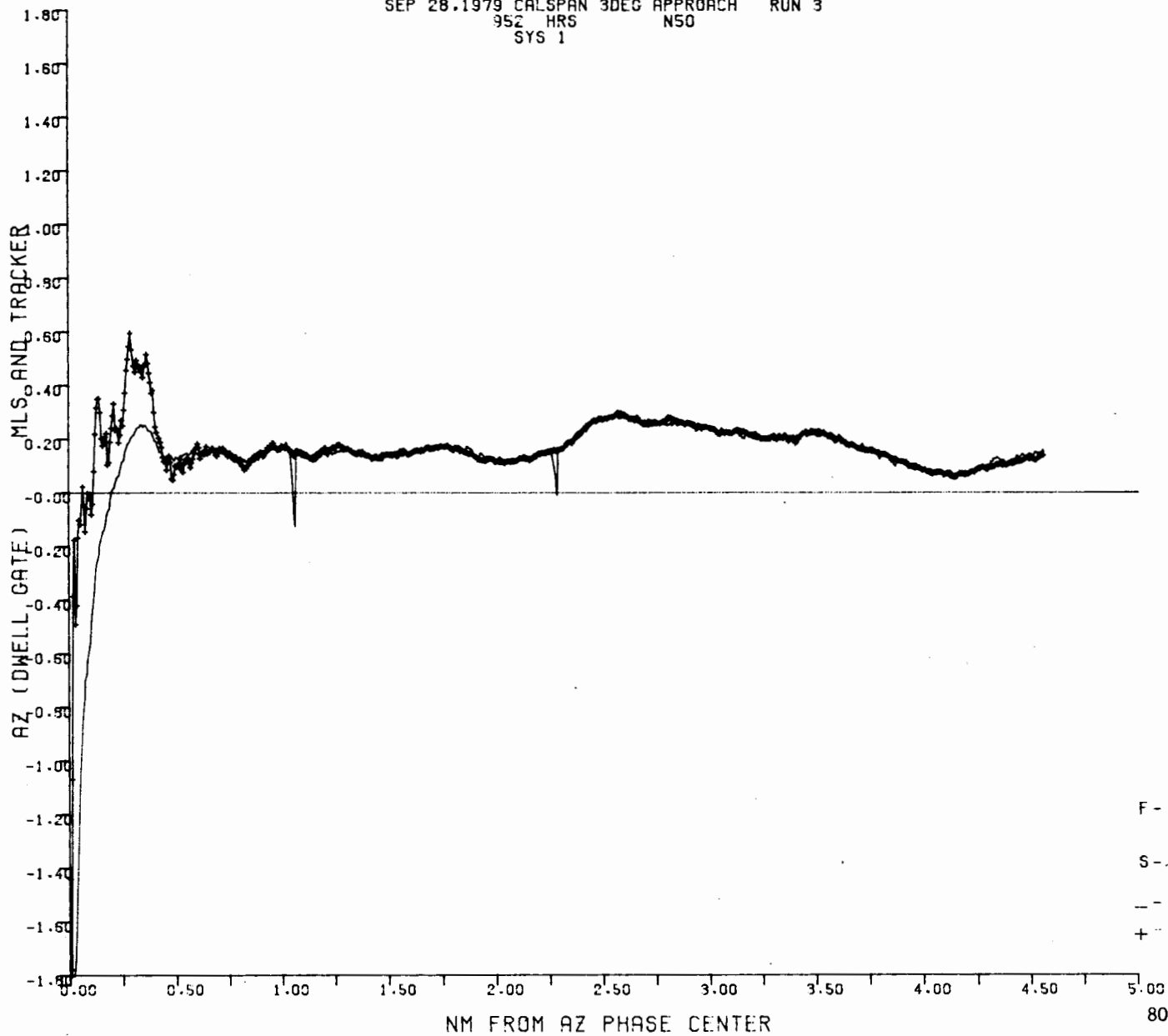


F - FRAME FLAG  
S - SYSTEM FLAG

80-19-A-4

SEP 28.1979 CALSPAN 3DEG APPROACH RUN 3  
952 HRS N50  
SYS 1

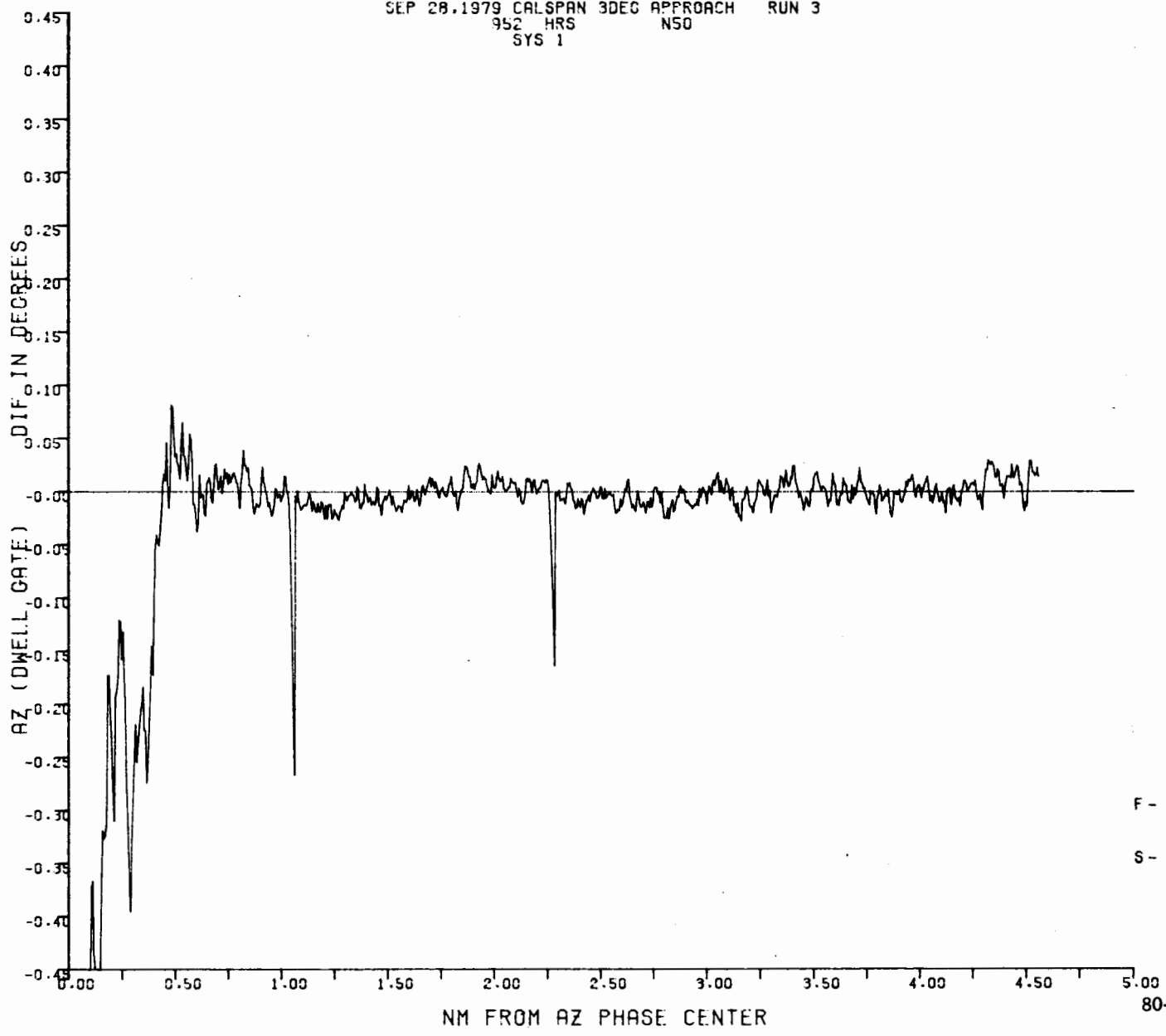
A-5



80-19-A-5

SEP 28.1979 CALSPAN 3DEC APPROACH RUN 3  
952 HRS NS0  
SYS 1

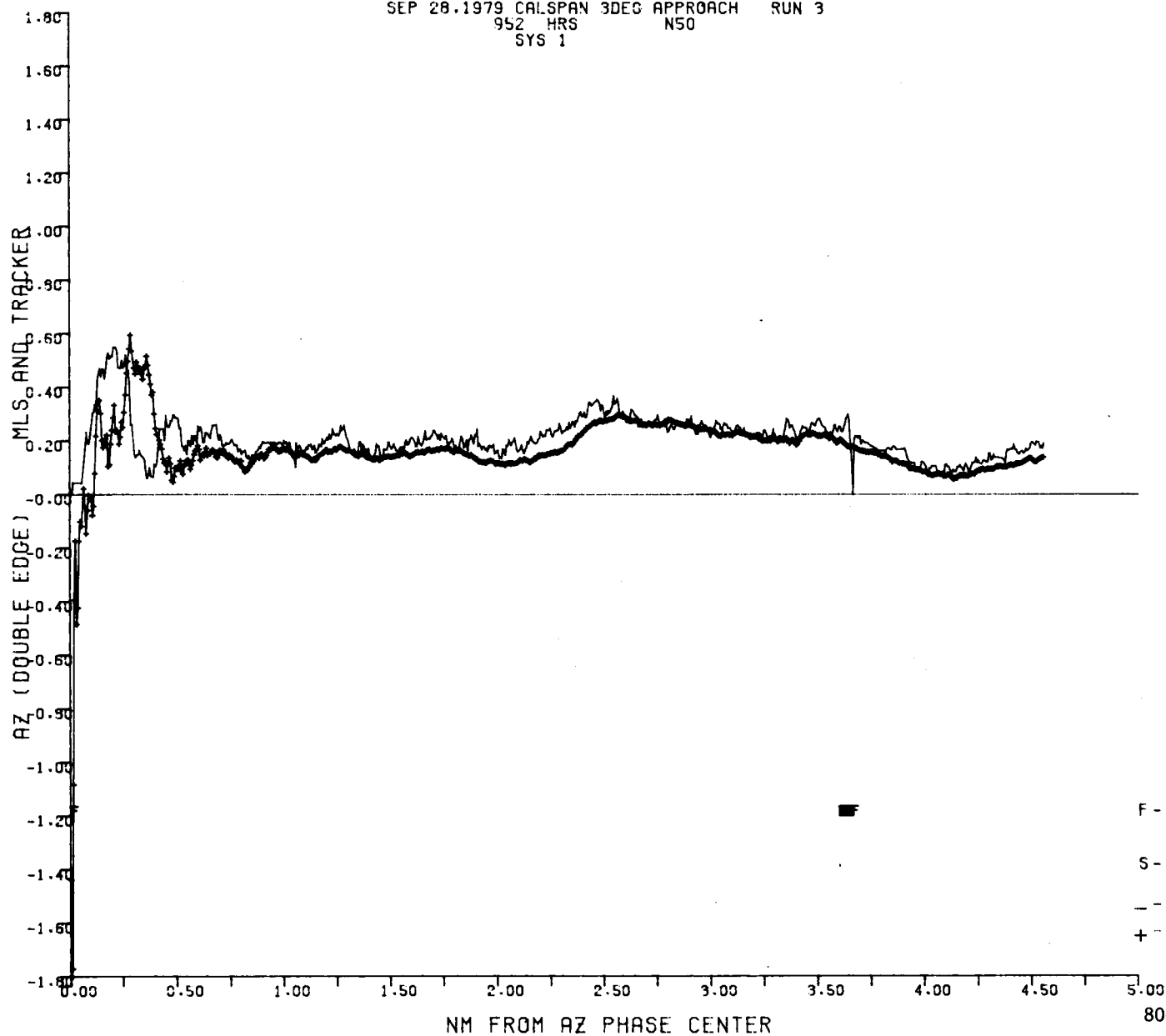
A-6



F - FRAME FLAG  
S - SYSTEM FLAG

80-19-A-6

SEP 28.1979 CALSPAN 3DEG APPROACH RUN 3  
952 HRS N50  
SYS 1

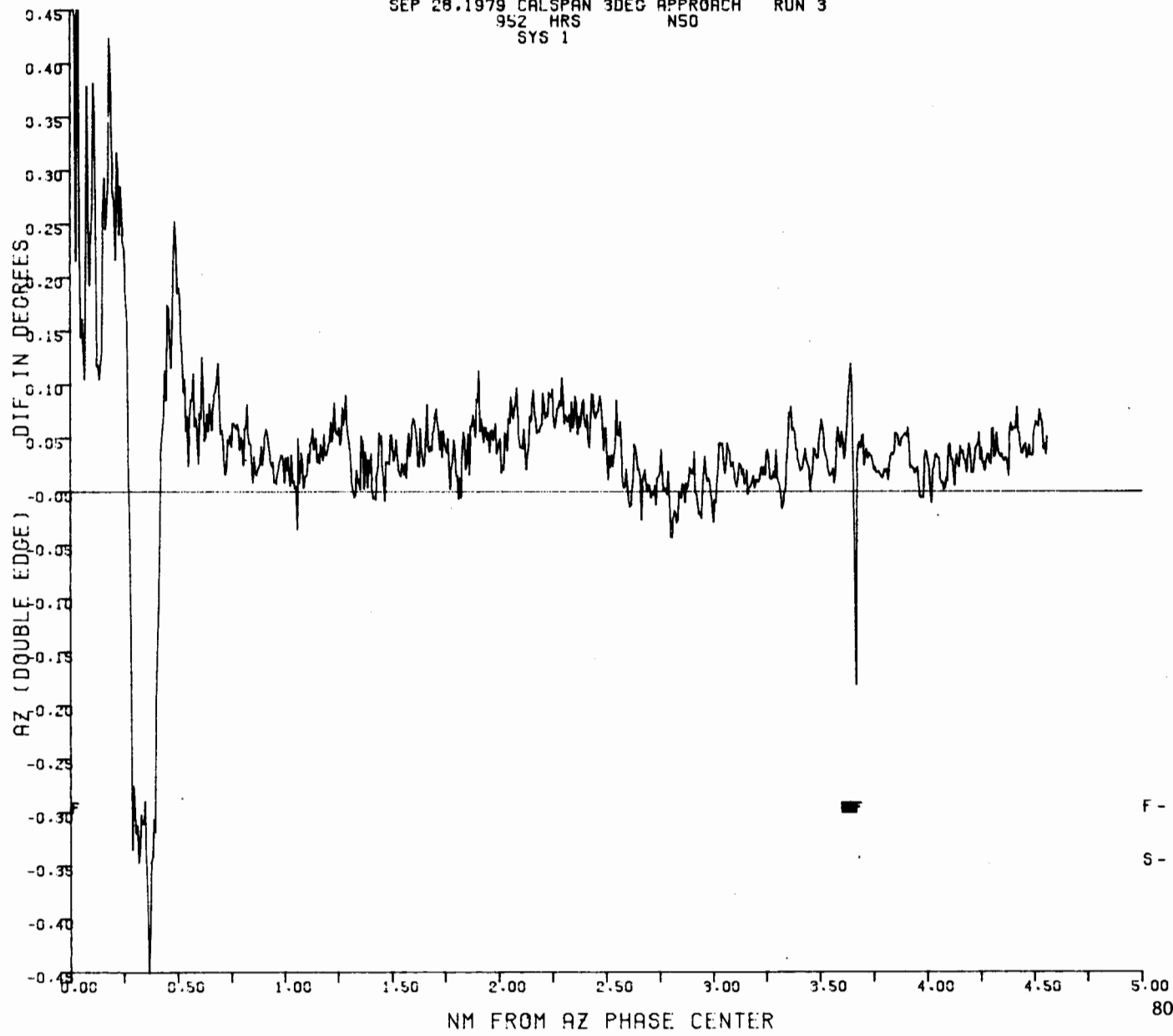


A-7

F - FRAME FLAG  
S - SYSTEM FLAG  
- - MLS  
+ - TRACKER

SEP 28.1979 CALSPAN 3DEG APPROACH RUN 3  
952 HRS NSO  
SYS 1

A-8

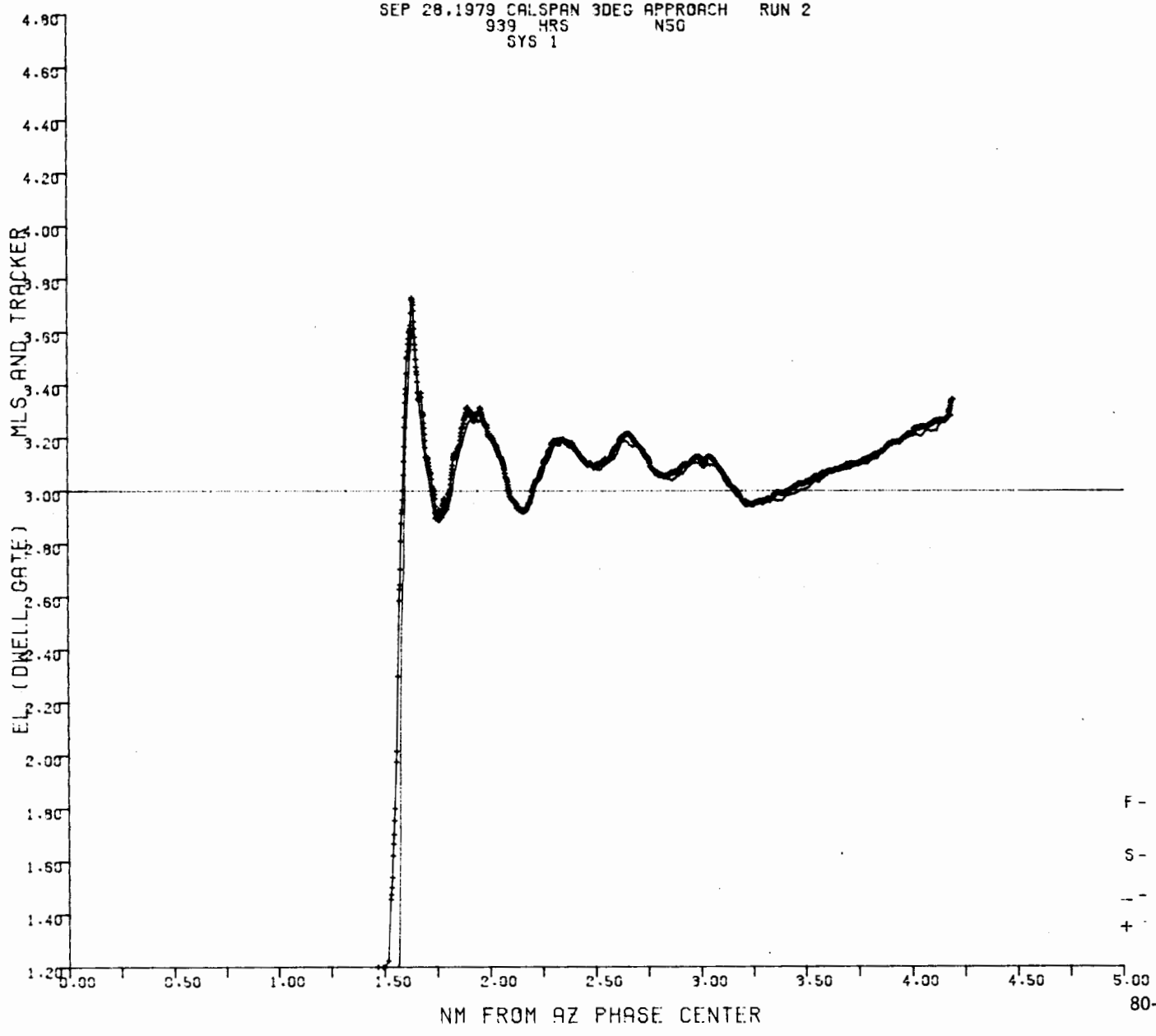


F - FRAME FLAG  
S - SYSTEM FLAG

80-19-A-8

SEP 28.1979 CALSPAN 3DEG APPROACH RUN 2  
939 HRS NSG  
SYS 1

A-9

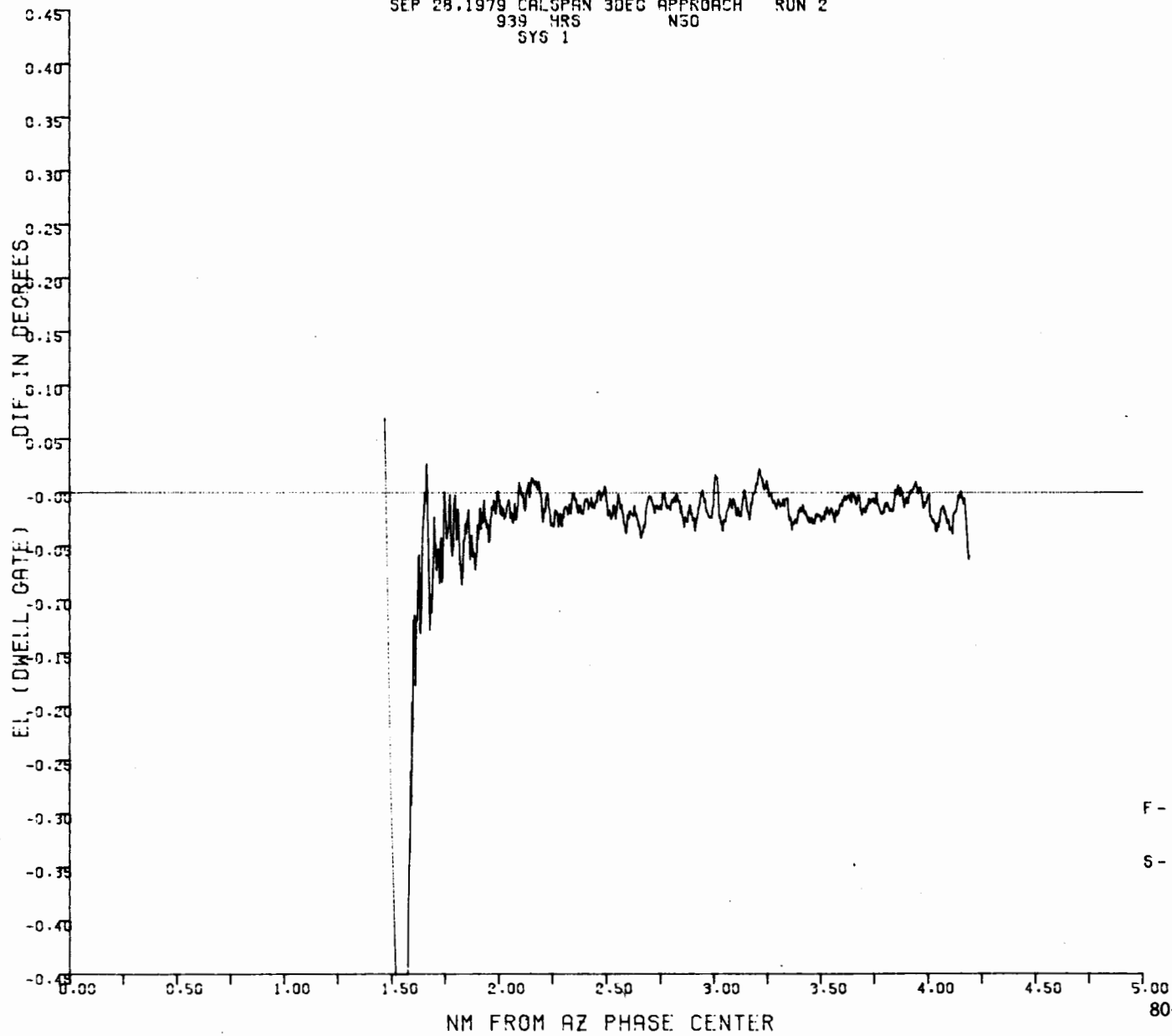


F - FRAME FLAG  
S - SYSTEM FLAG  
- - MLS  
+ TRACKER

80-19-A-9

SEP 28, 1979 CALSPAN 3DEC APPROACH RUN 2  
939 HRS N50  
SYS 1

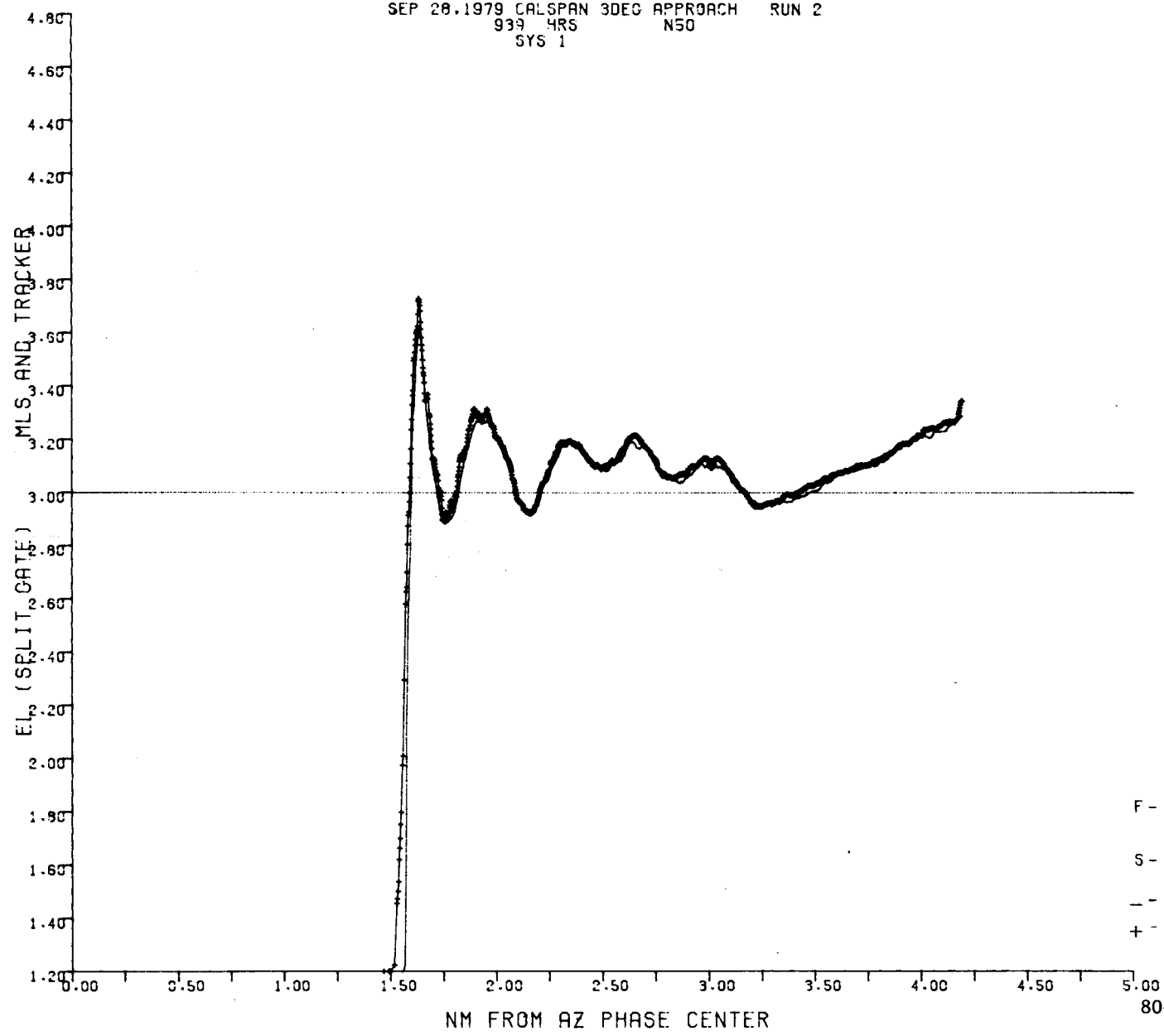
A-10



F - FRAME FLAG  
S - SYSTEM FLAG

80-19-A-10

SEP 28.1979 CALSPAN 3DEG APPROACH RUN 2  
939 HRS N50  
SYS 1

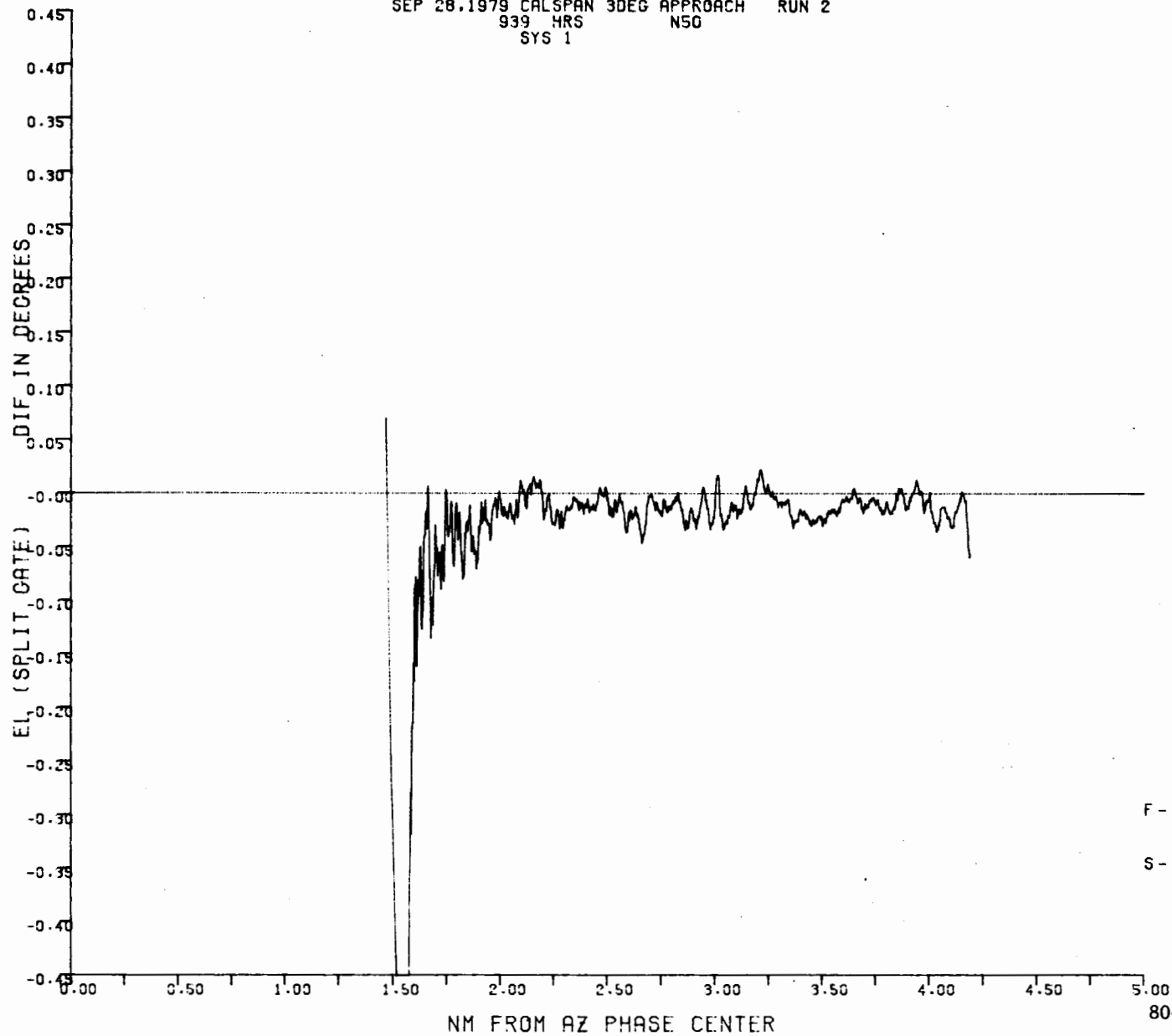


A-11

F - FRAME FLAG  
S - SYSTEM FLAG  
- - MLS  
+ - TRACKER

80-19-A-11

SEP 28.1979 CALSPAN 3DEG APPROACH RUN 2  
939 HRS N50  
SYS 1



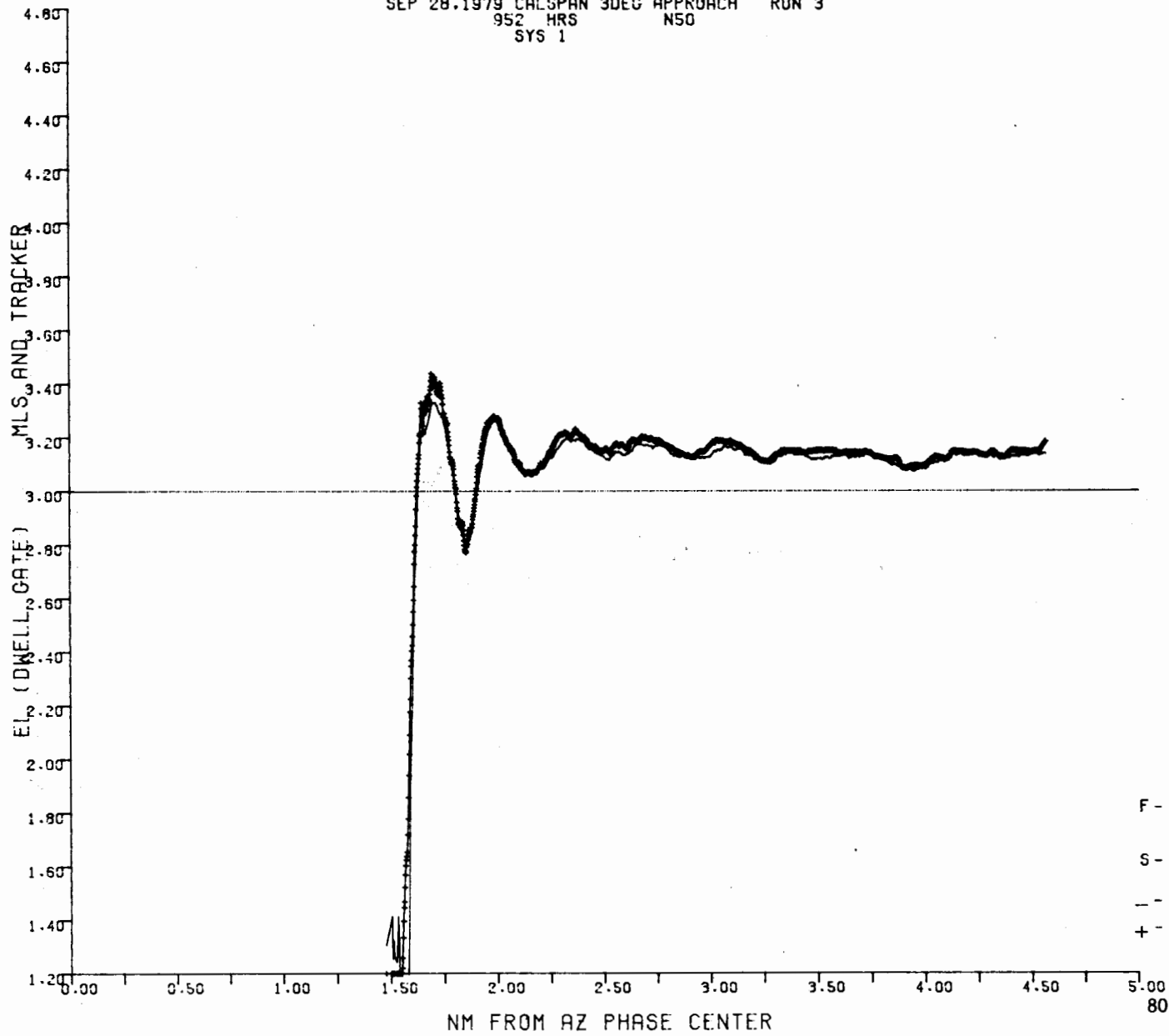
A-12

F - FRAME FLAG  
S - SYSTEM FLAG

80-19-A-12

A-13

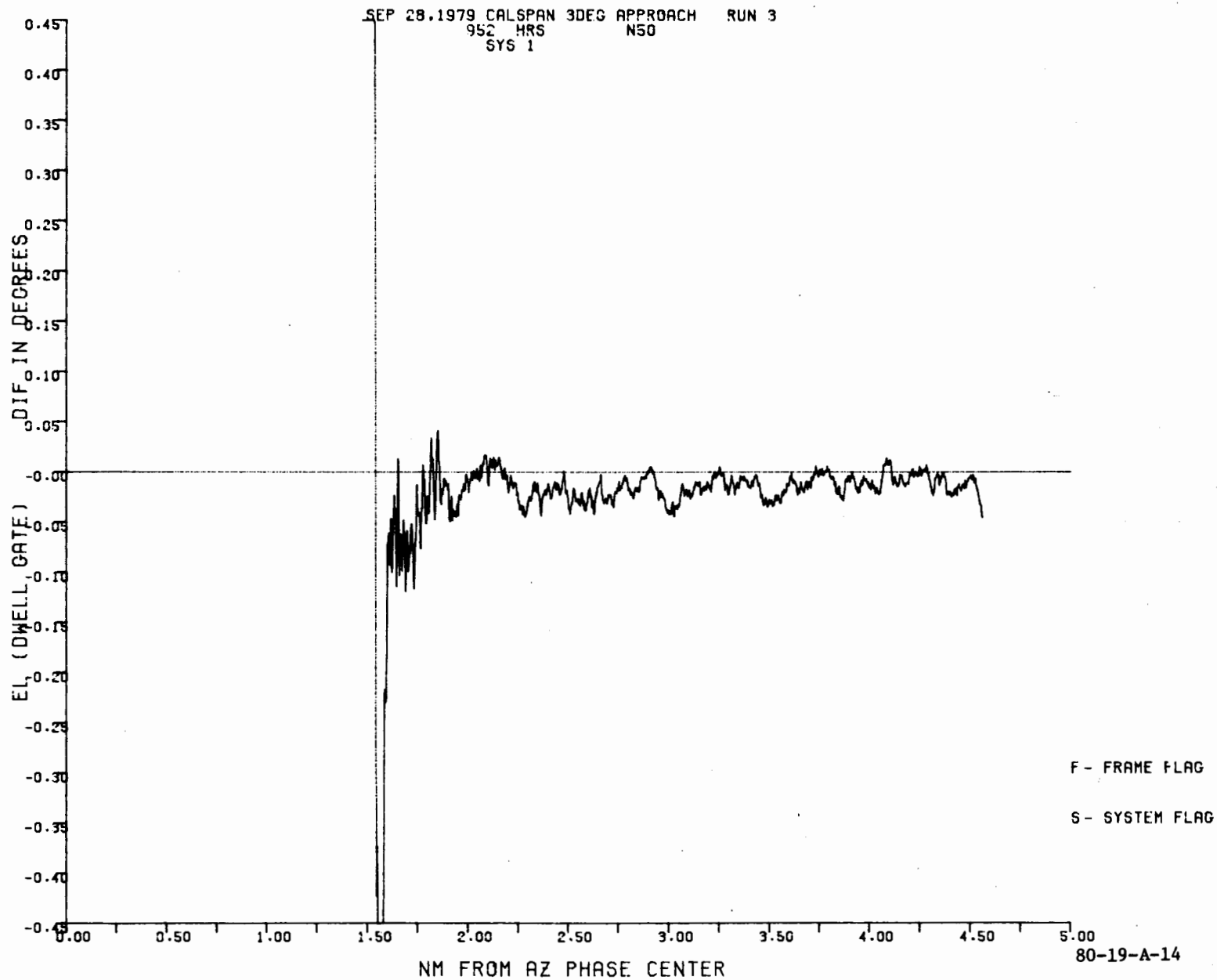
SEP 28.1979 CALSPAN 3DEG APPROACH RUN 3  
952 HRS N50  
SYS 1



F - FRAME FLAG  
S - SYSTEM FLAG  
- - - MLS  
+ - TRACKER

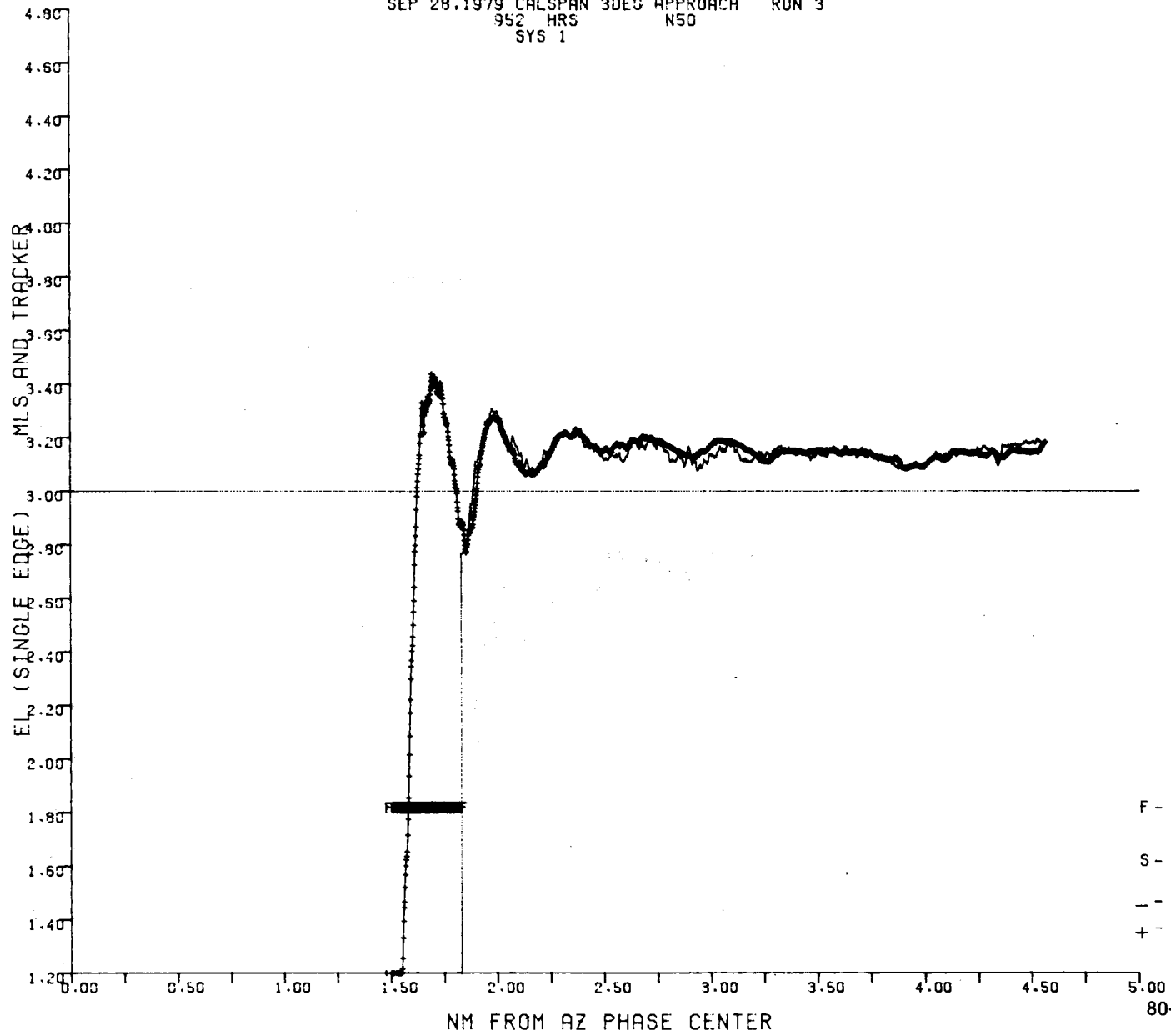
80-19-A-13

A-14



SEP 28, 1979 CALSPAN 3DEG APPROACH RUN 3  
952 HRS N50  
SYS 1

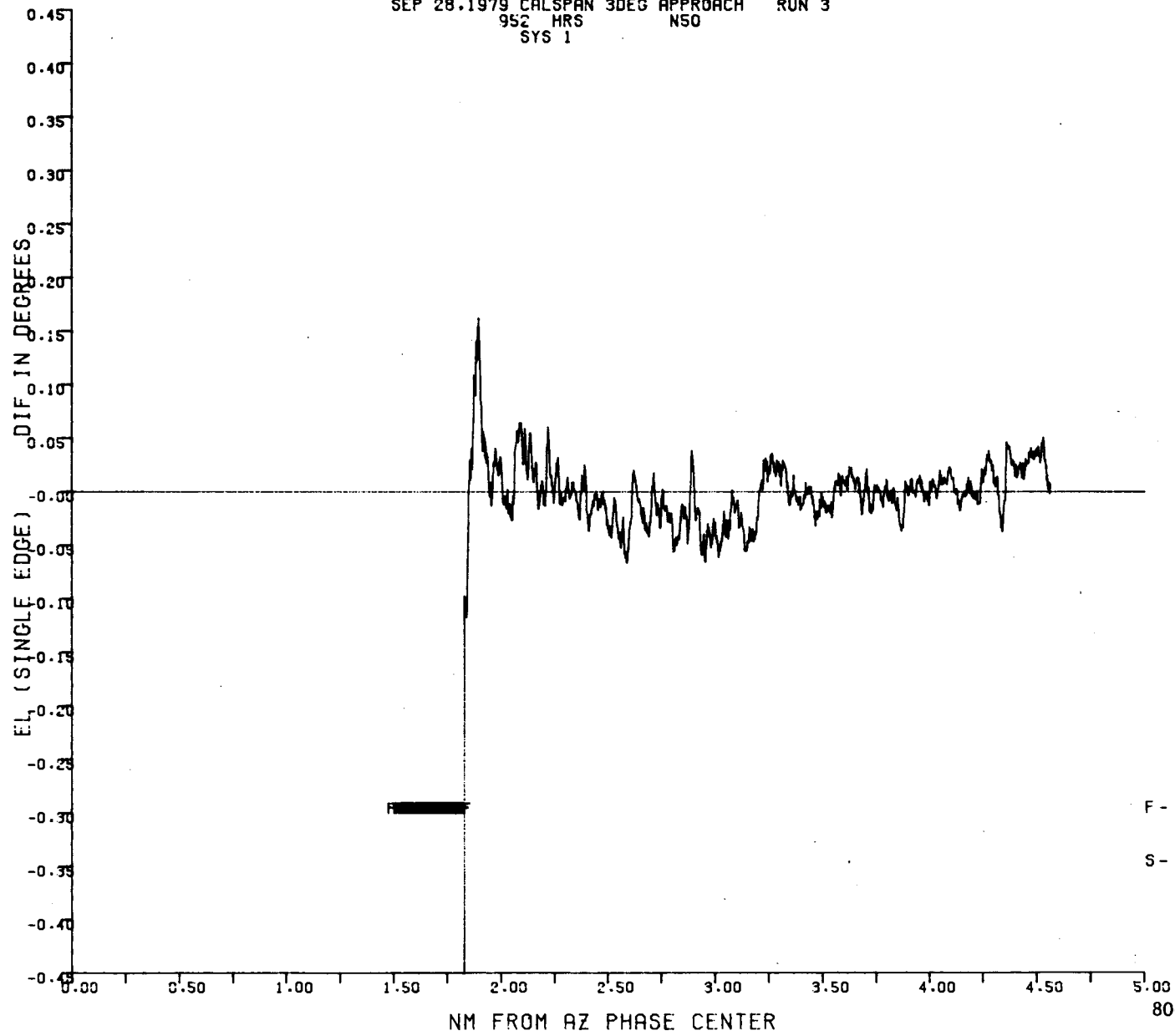
A-15



80-19-A-15

SEP 28.1979 CALSPAN 3DEG APPROACH RUN 3  
952 HRS NSO  
SYS 1

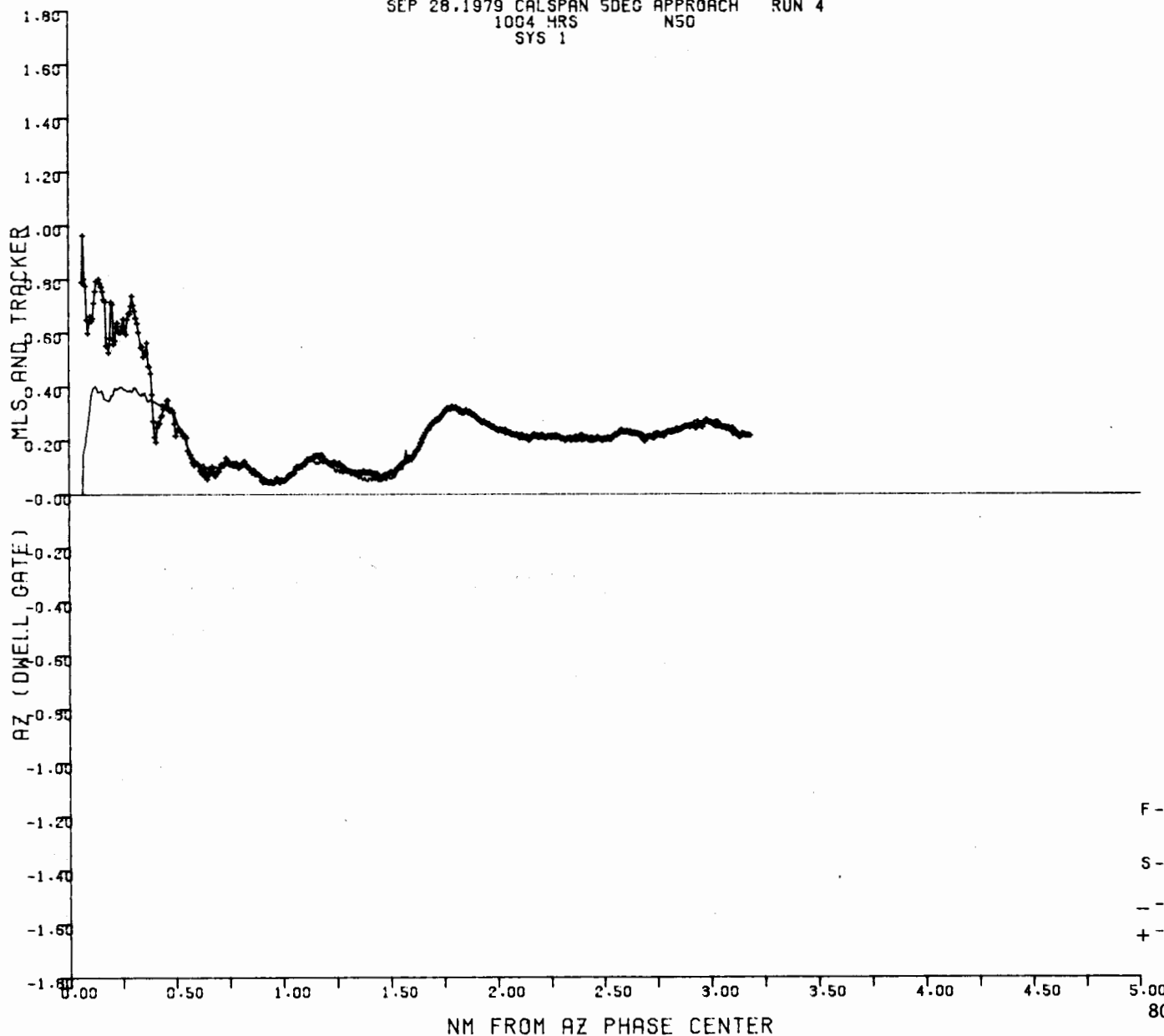
91-V



80-19-A-16

SEP 28.1979 CALSPAN 5DEG APPROACH RUN 4  
1004 HRS N50  
SYS 1

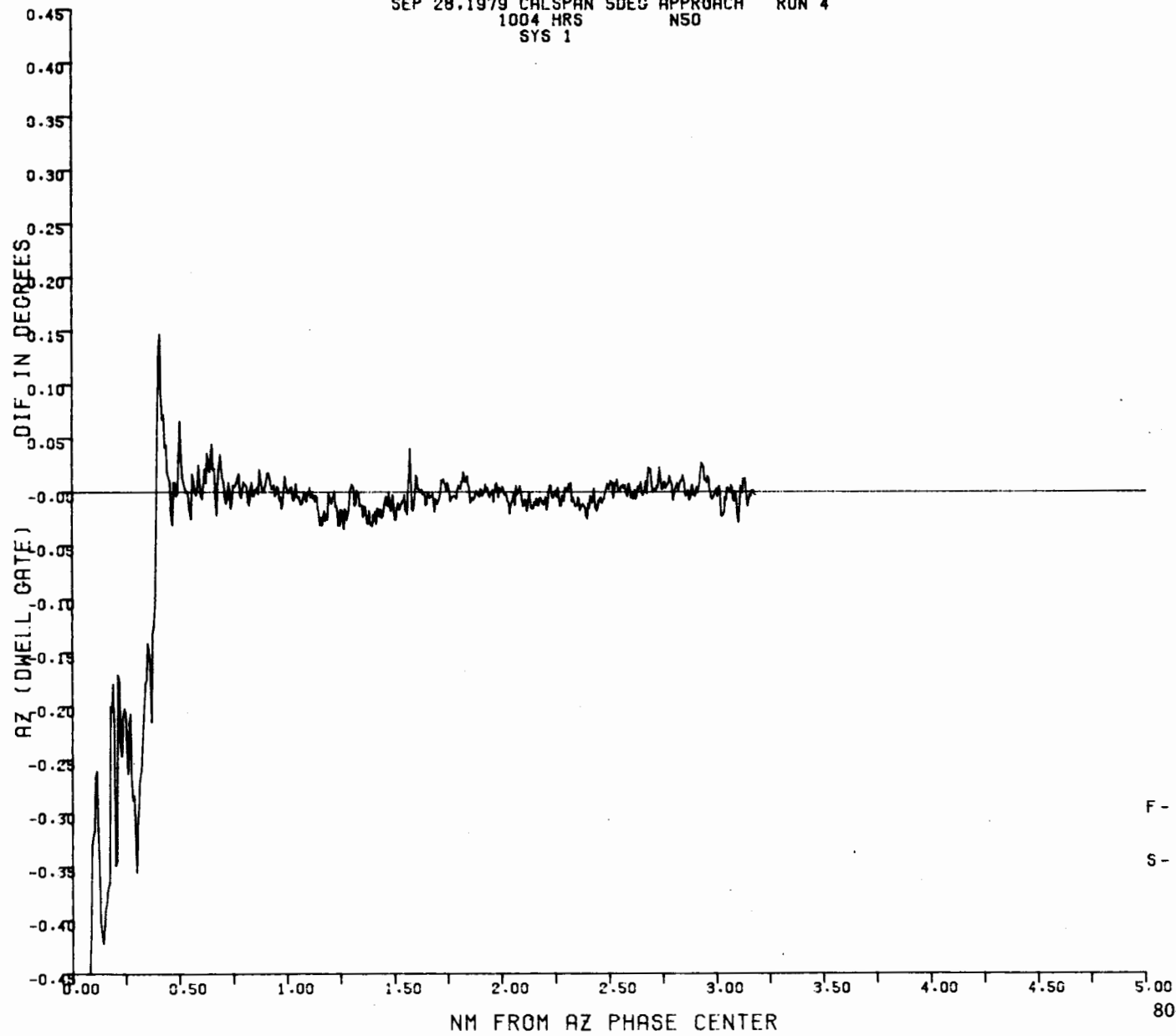
A-17



80-19-A-17

SEP 28.1979 CALSPAN SDEG APPROACH RUN 4  
1004 HRS NSO  
SYS 1

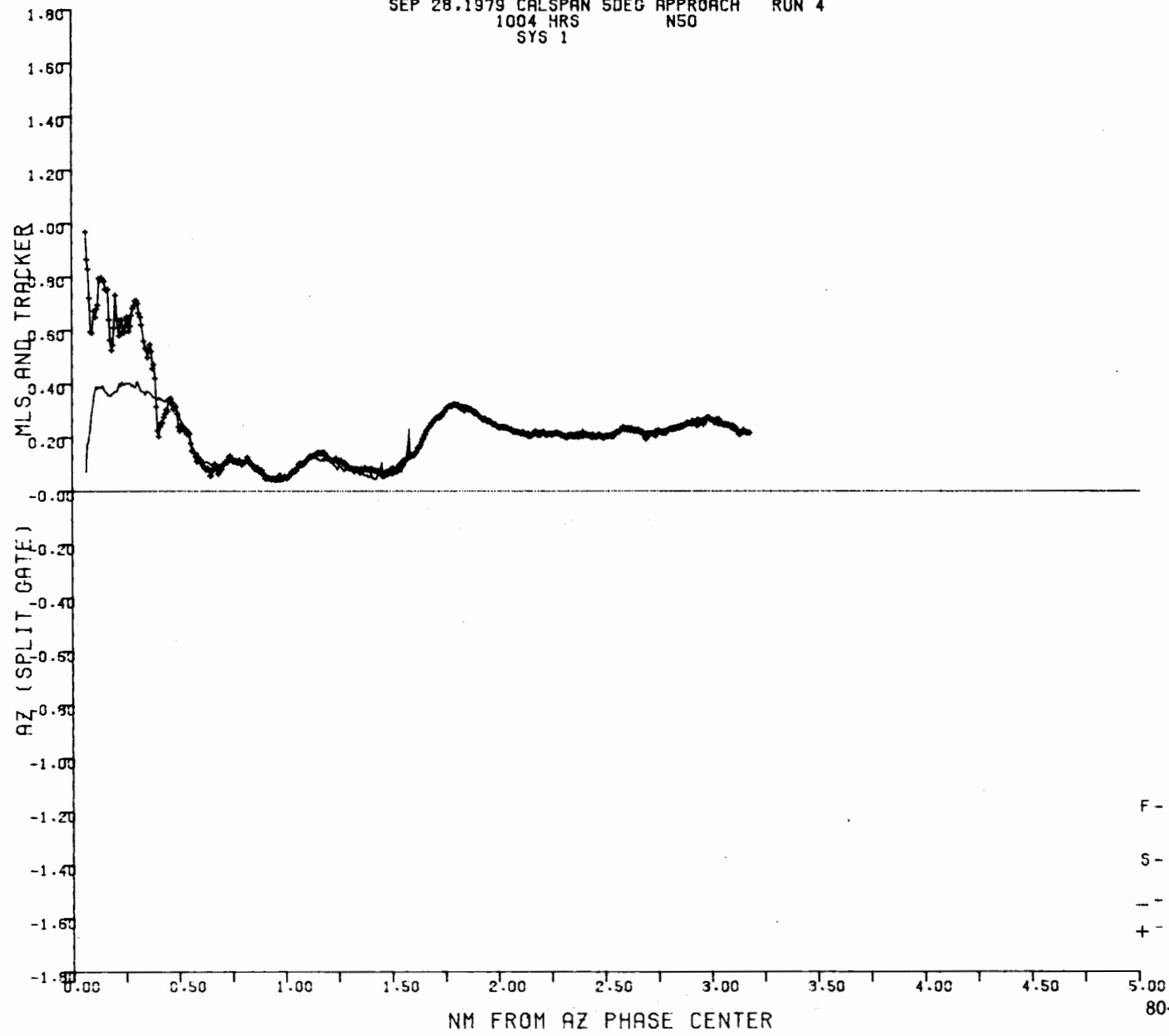
A-18



F - FRAME FLAG  
S - SYSTEM FLAG

80-19-A-18

SEP 28.1979 CALSPAN SDEG APPROACH RUN 4  
1004 HRS N50  
SYS 1

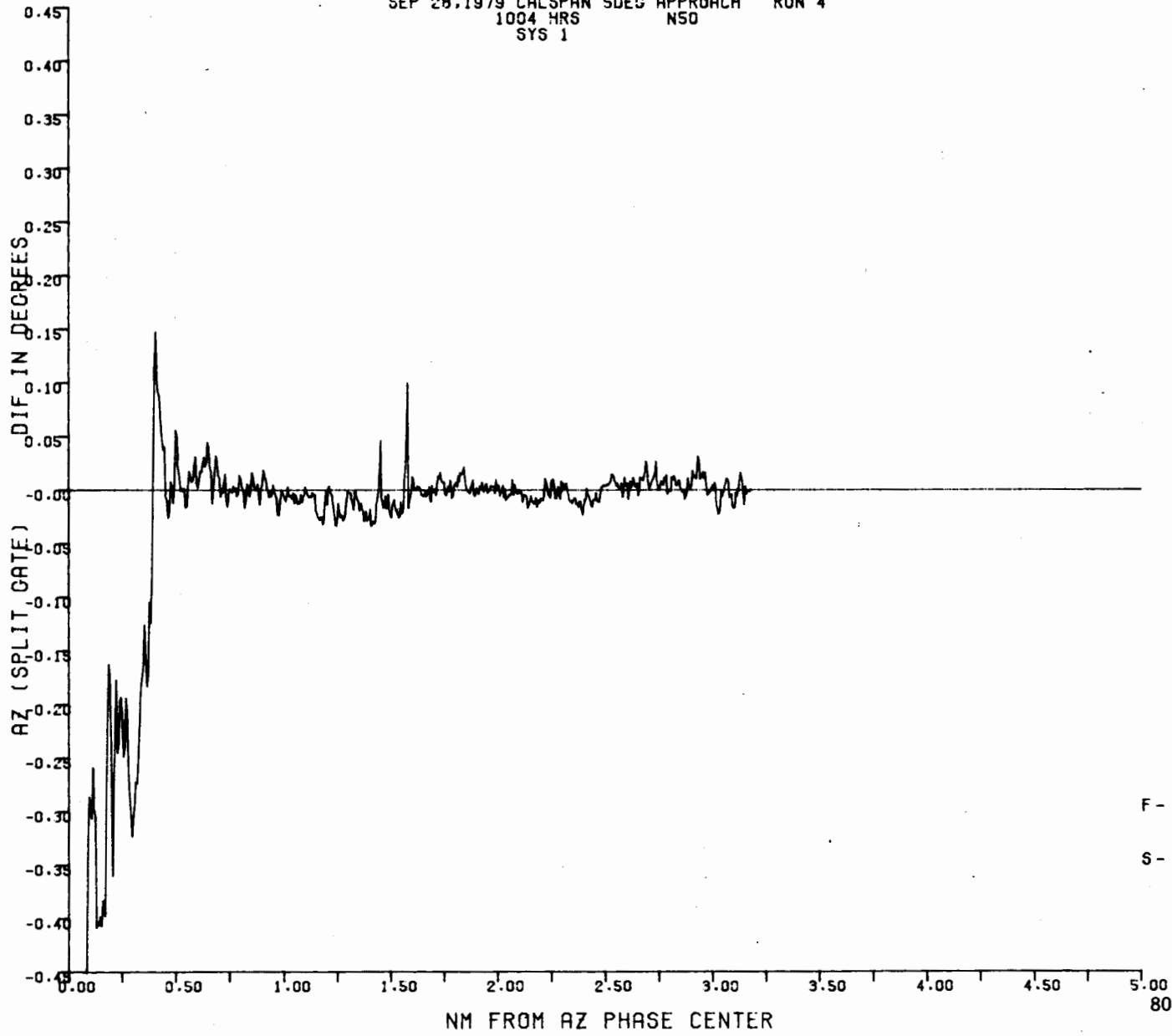


A-19

80-19-A-19

SEP 28.1979 CALSPAN SDEG APPROACH RUN 4  
1004 HRS NSO  
SYS 1

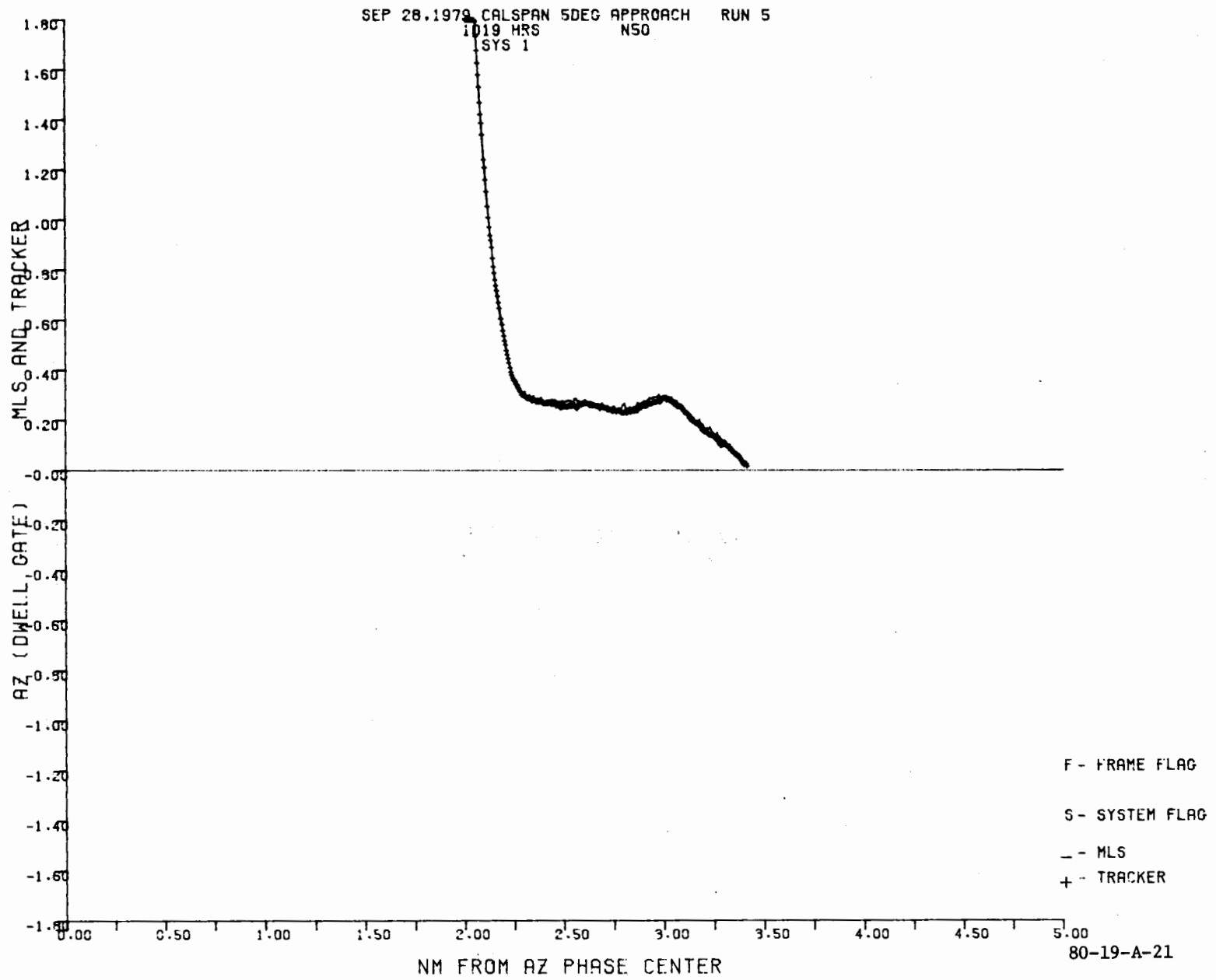
A-20



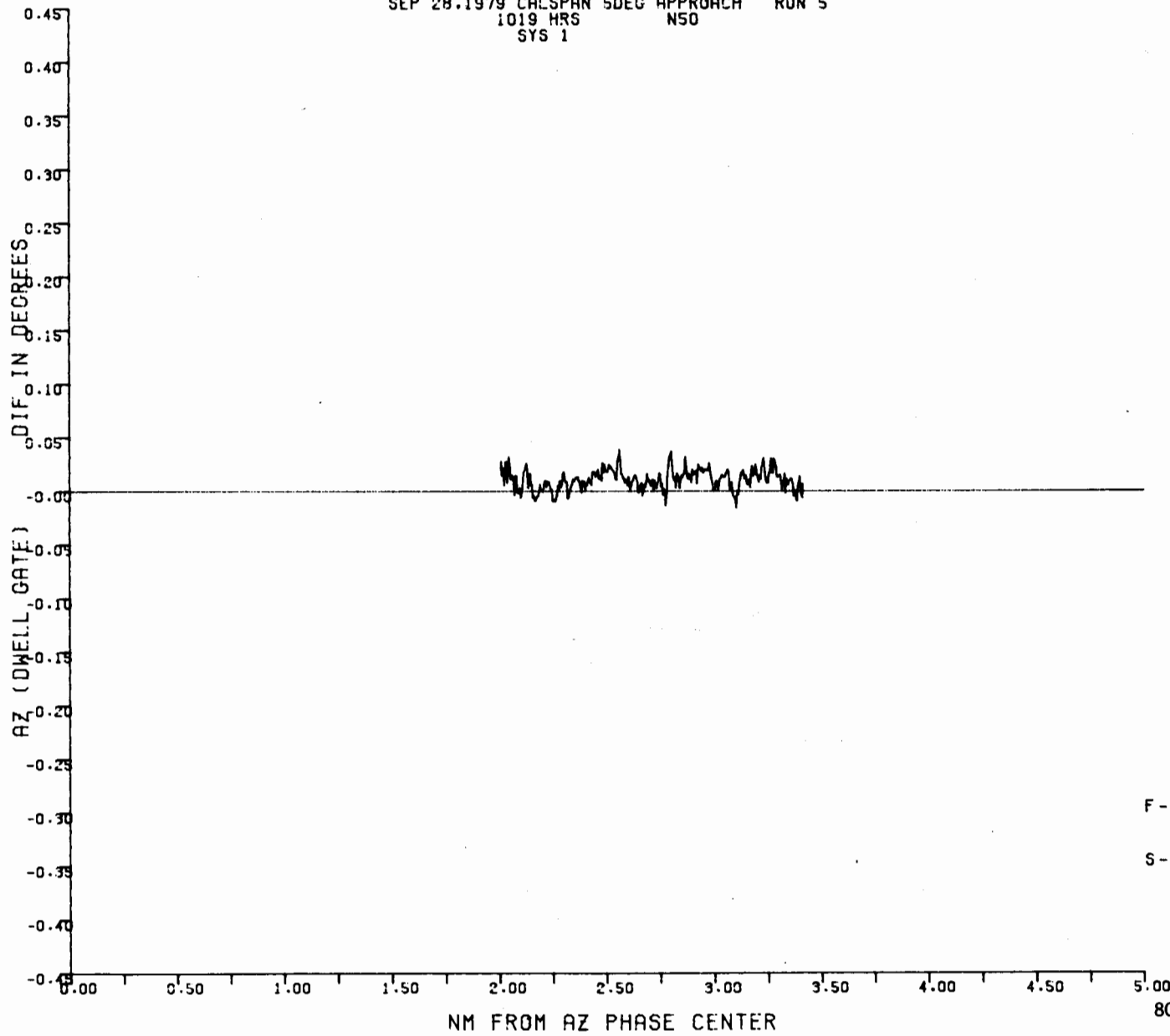
F - FRAME FLAG  
S - SYSTEM FLAG

80-19-A-20

A-21



SEP 28.1979 CALSPAN 5DEG APPROACH RUN 5  
1019 HRS N50  
SYS 1



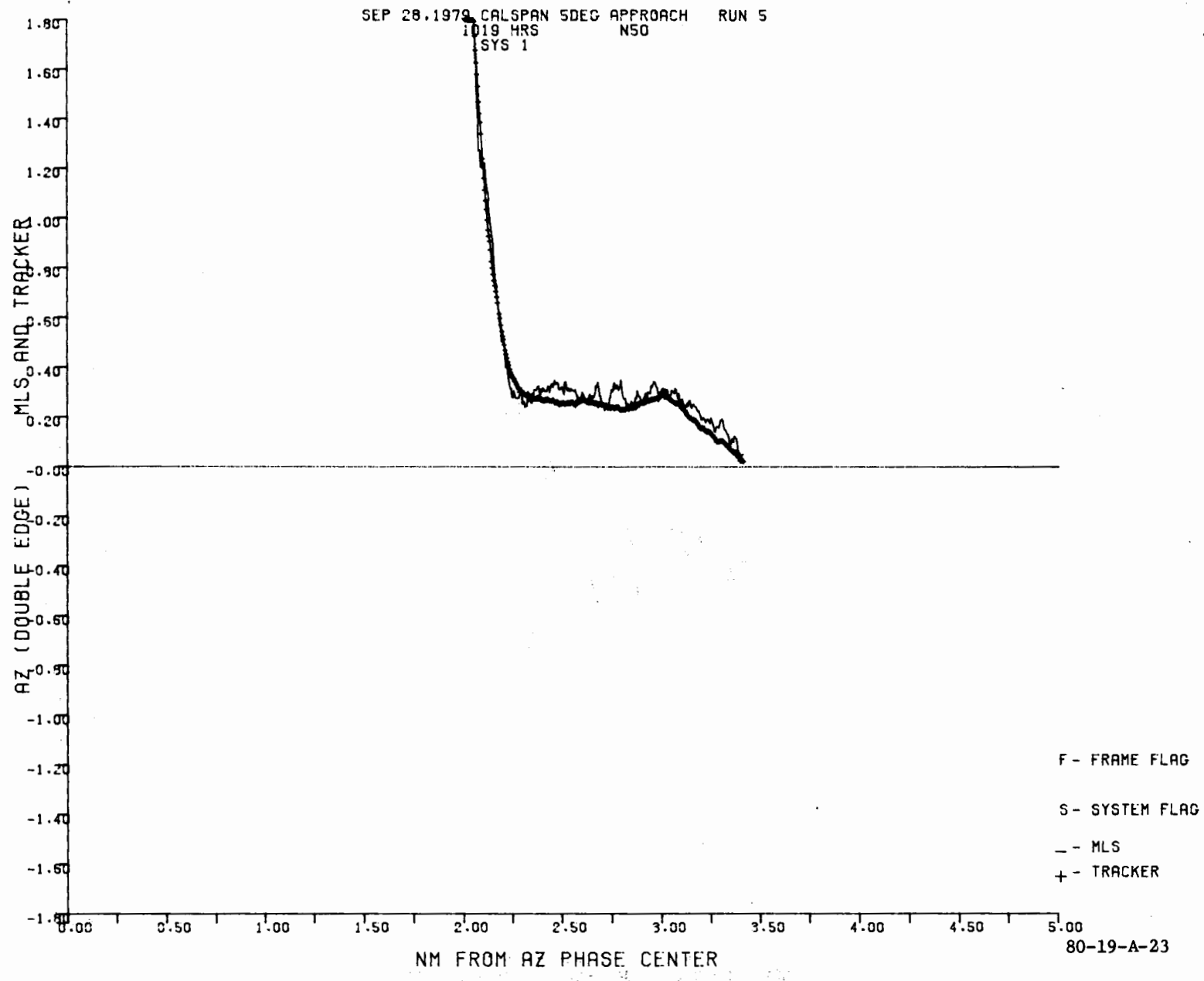
F - FRAME FLAG

S - SYSTEM FLAG

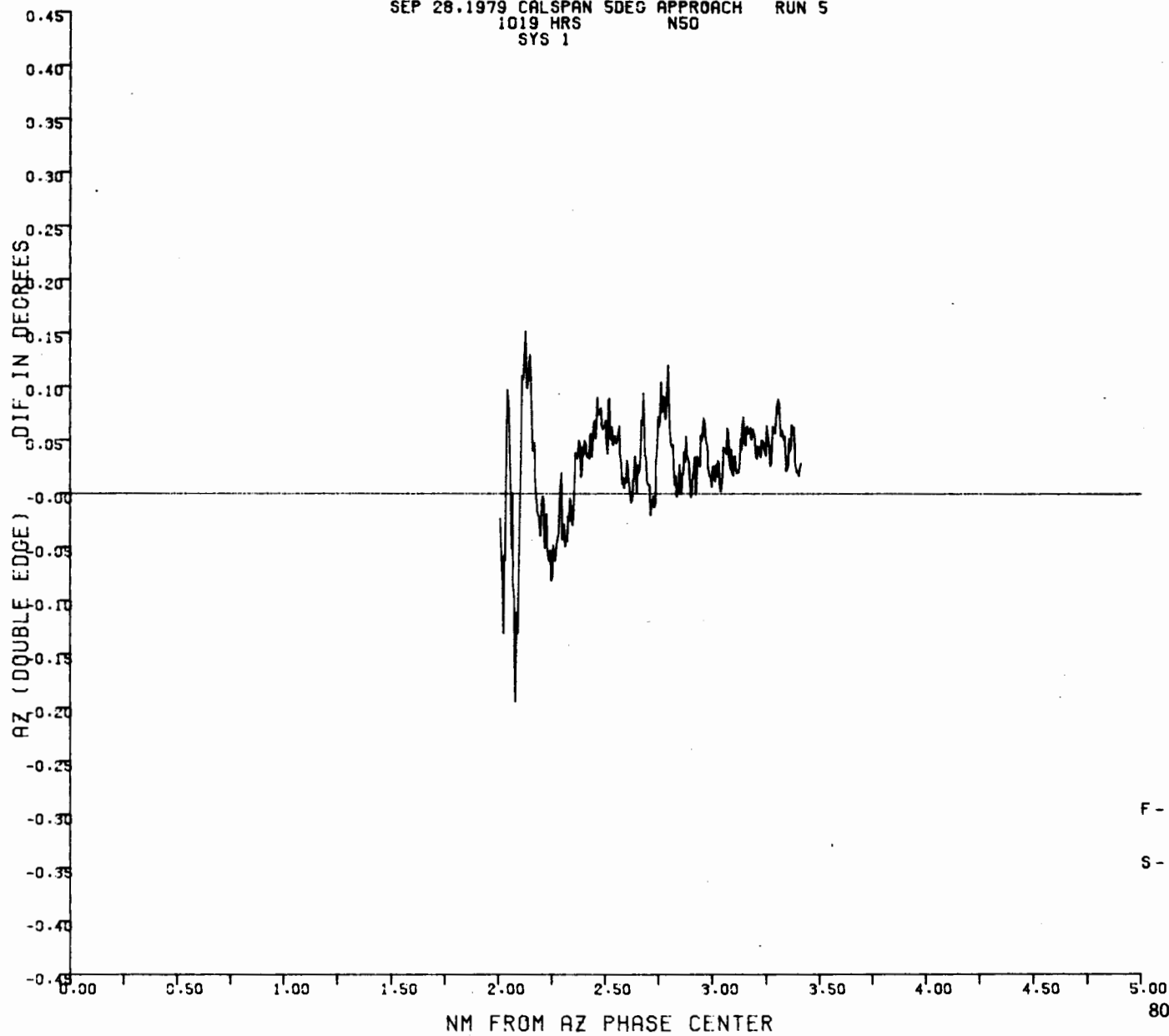
A-22

80-19-A-22

A-23



SEP 28.1979 CALSPAN SDEG APPROACH RUN 5  
1019 HRS N50  
SYS 1



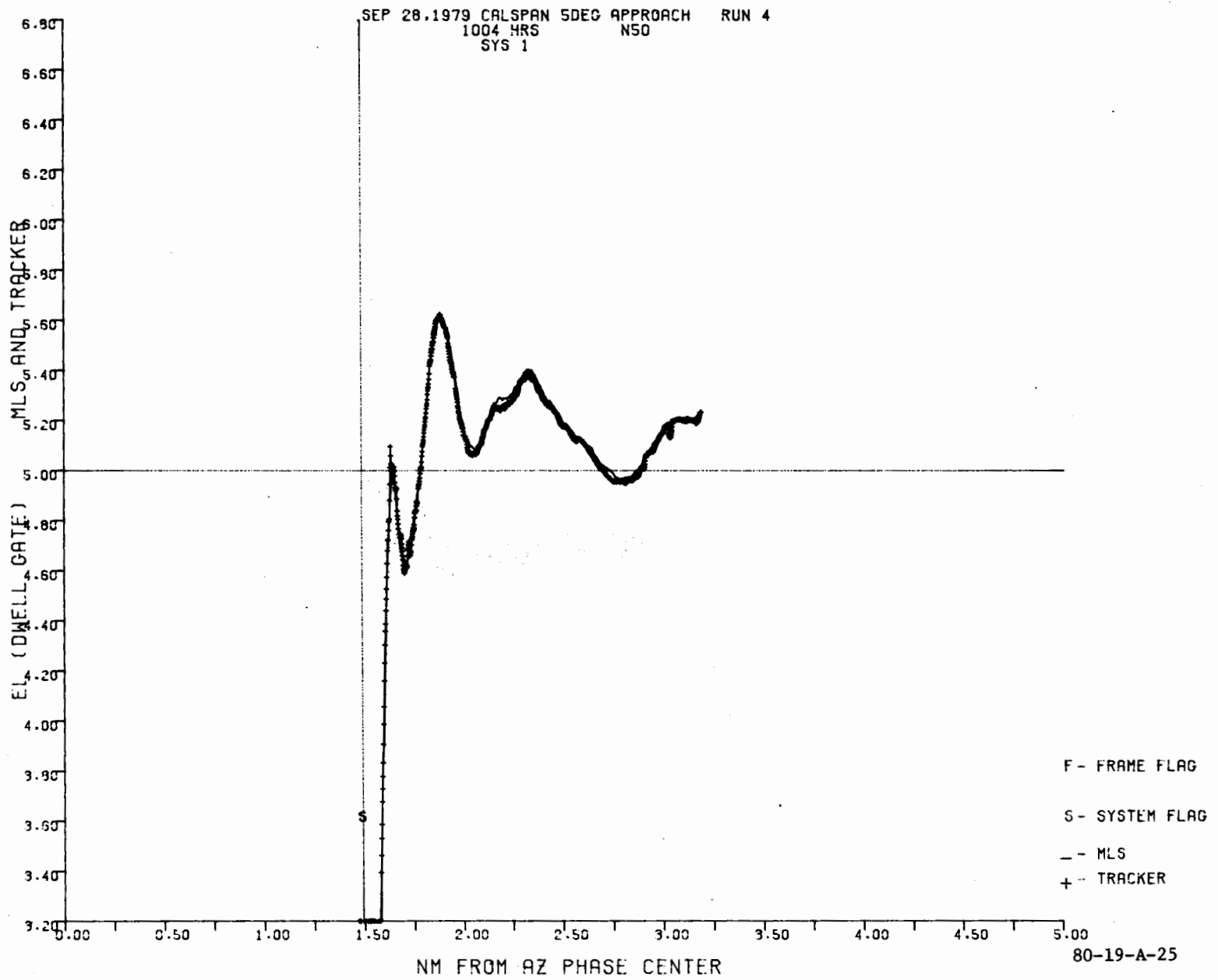
A-24

F - FRAME FLAG

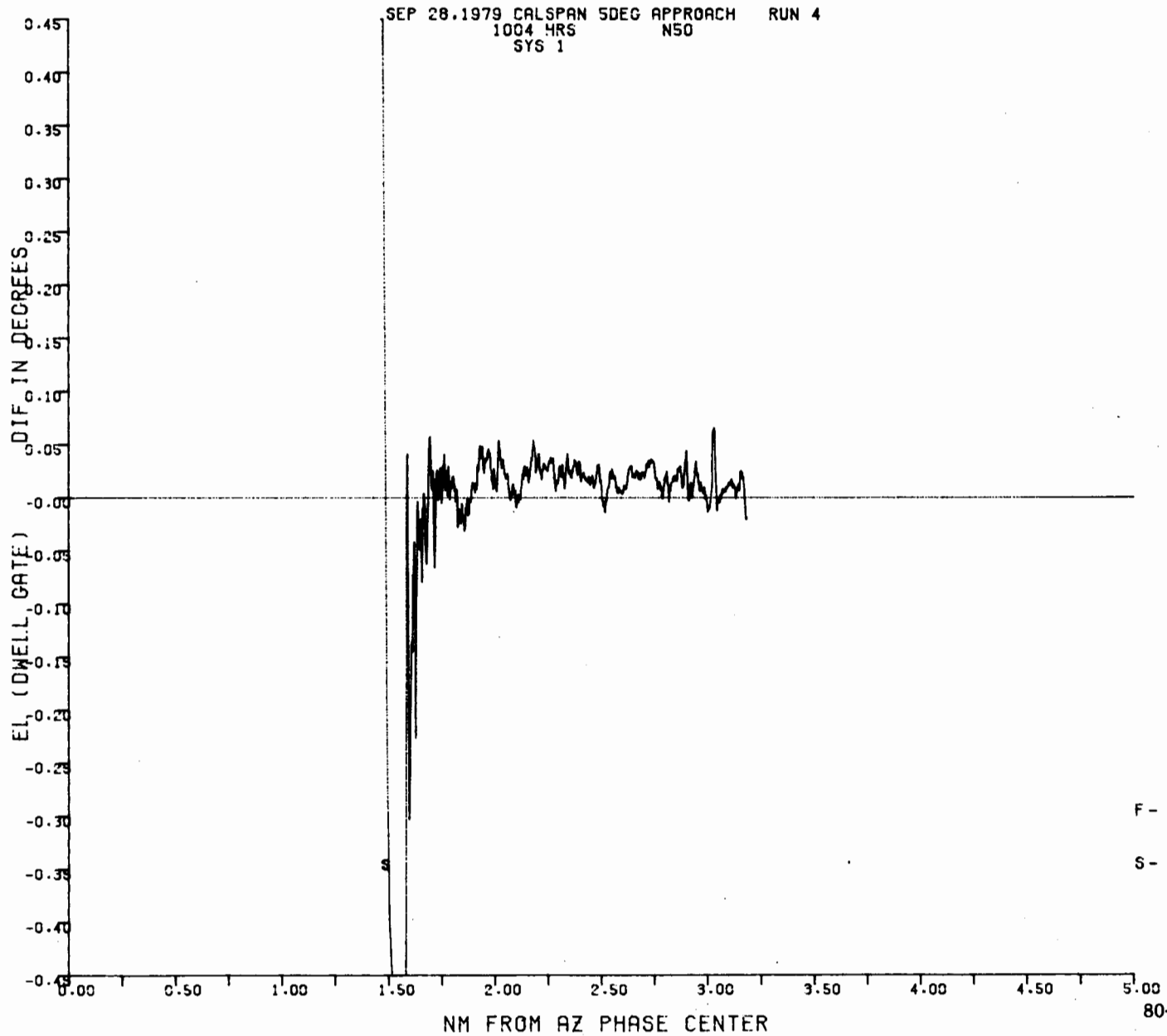
S - SYSTEM FLAG

80-19-A-24

A-25

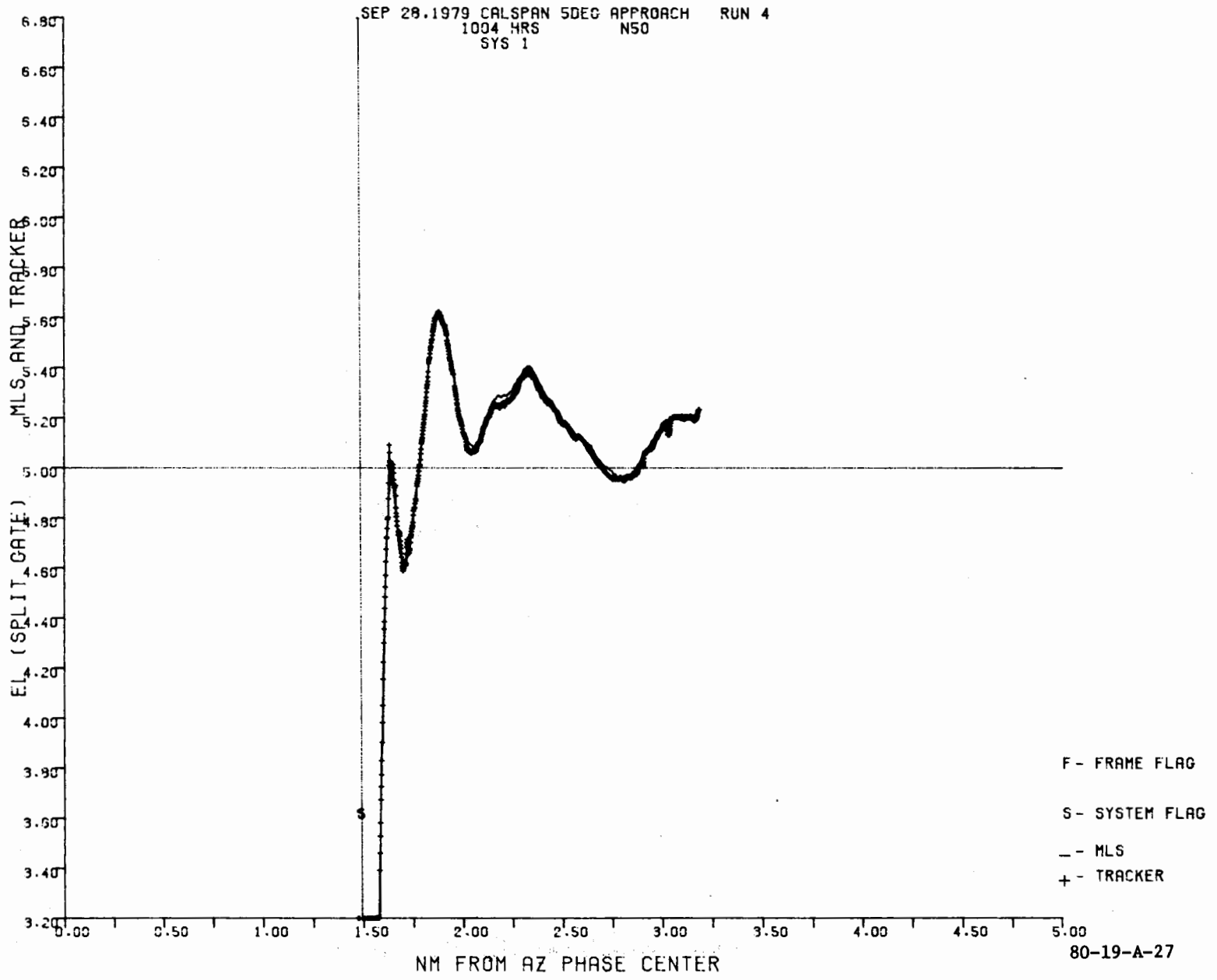


A-26

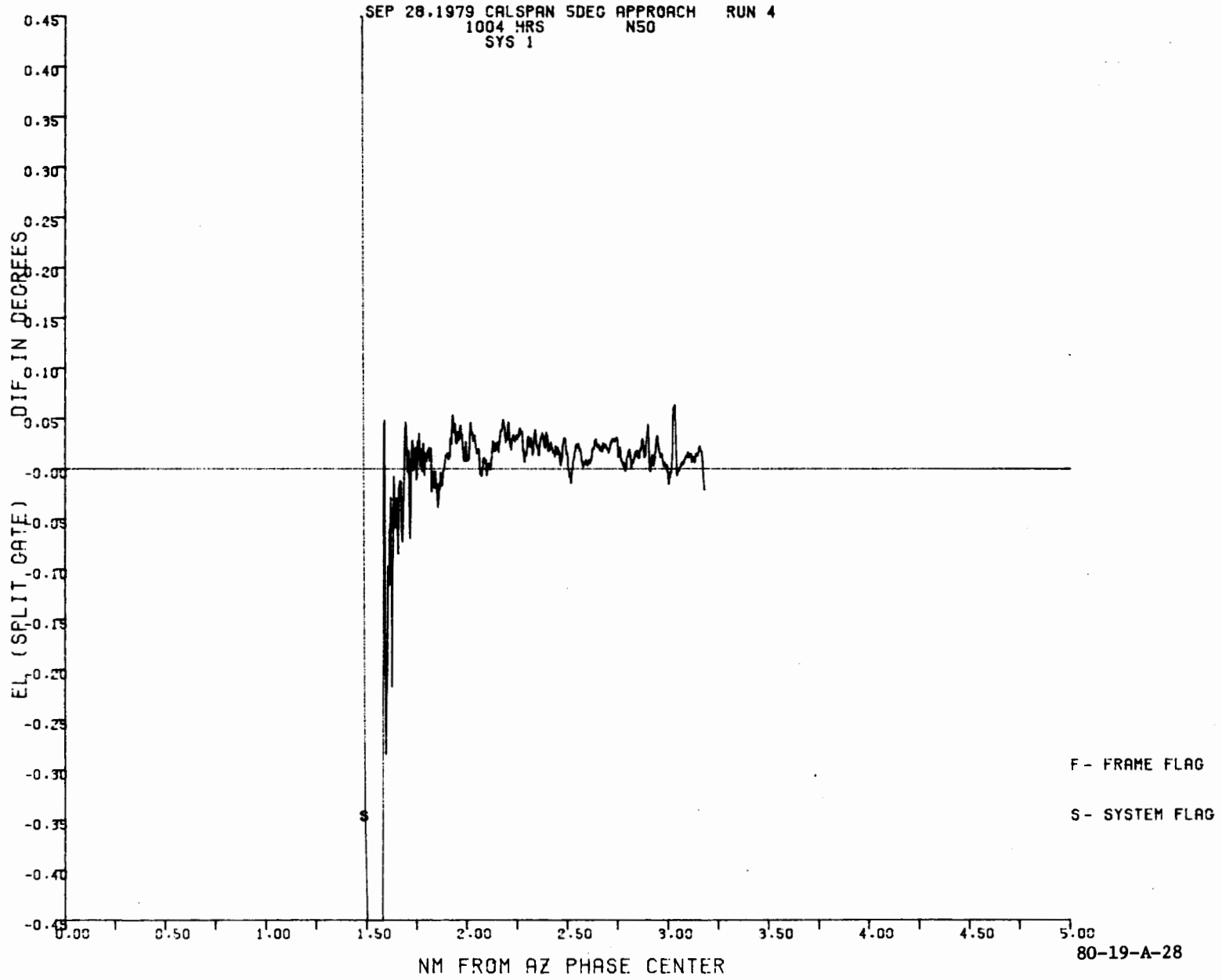


80-19-A-26

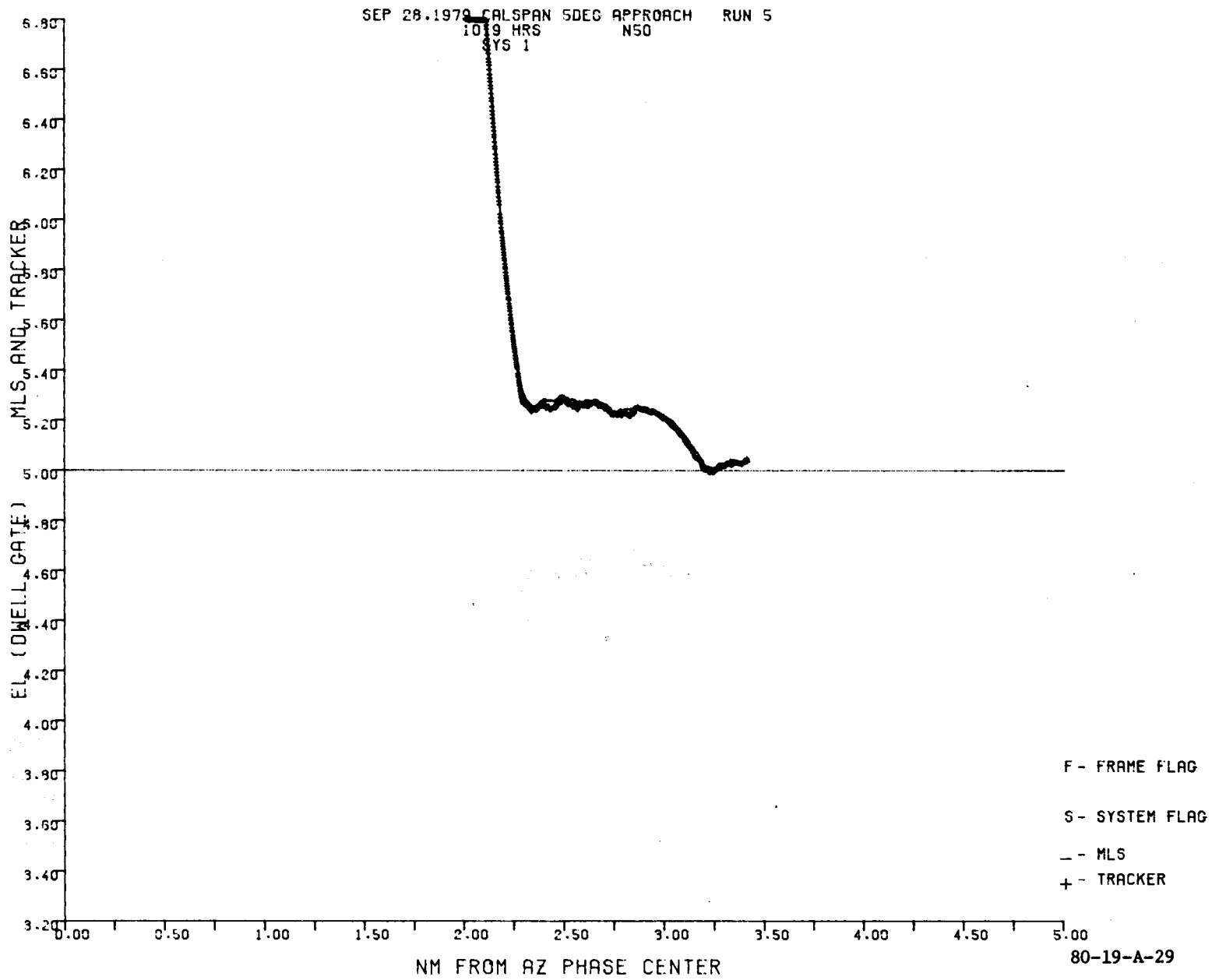
A-27



A-28

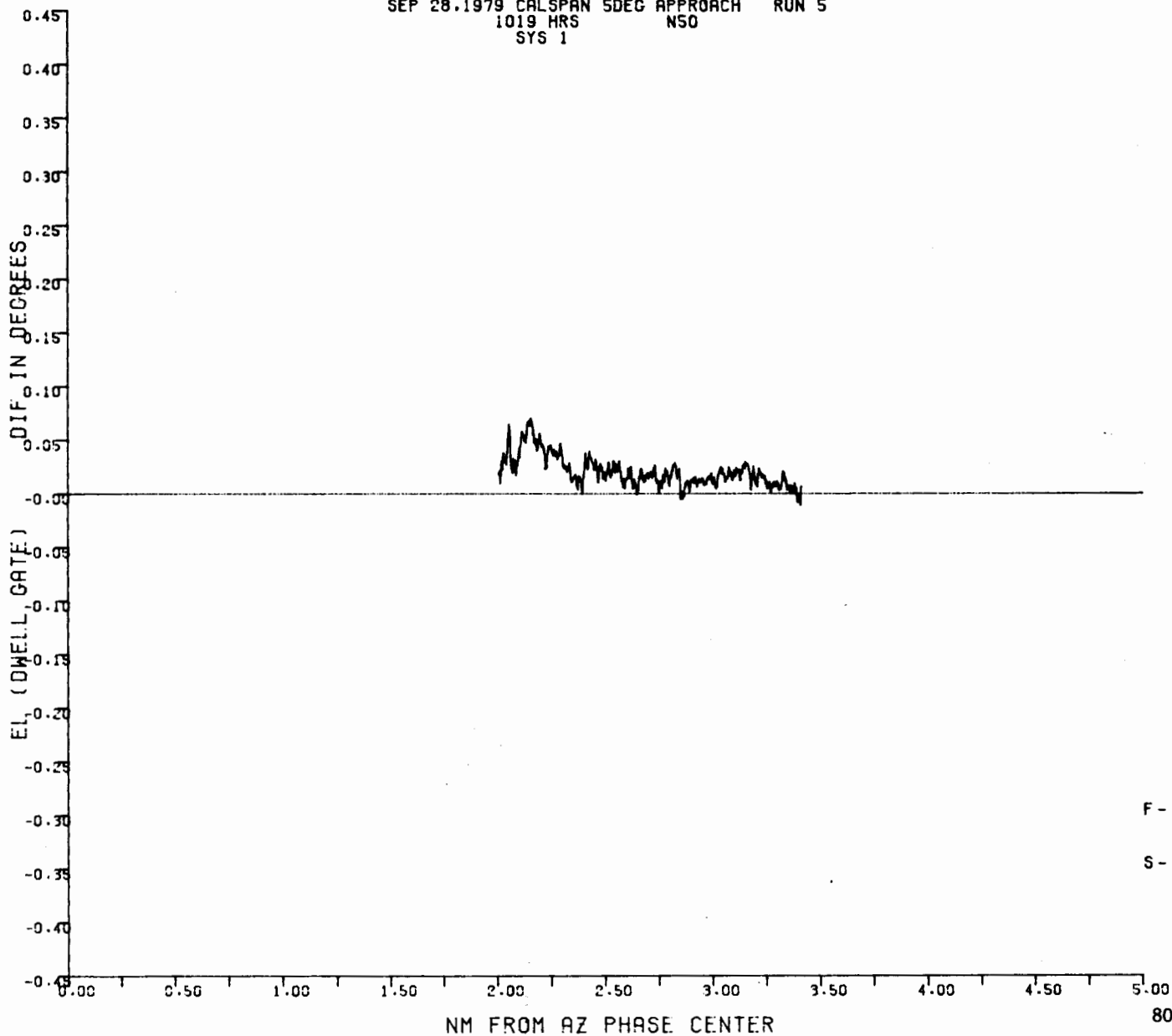


A-29



SEP 28.1979 CALSPAN SDEC APPROACH RUN 5  
1019 HRS NSO  
SYS 1

A-30

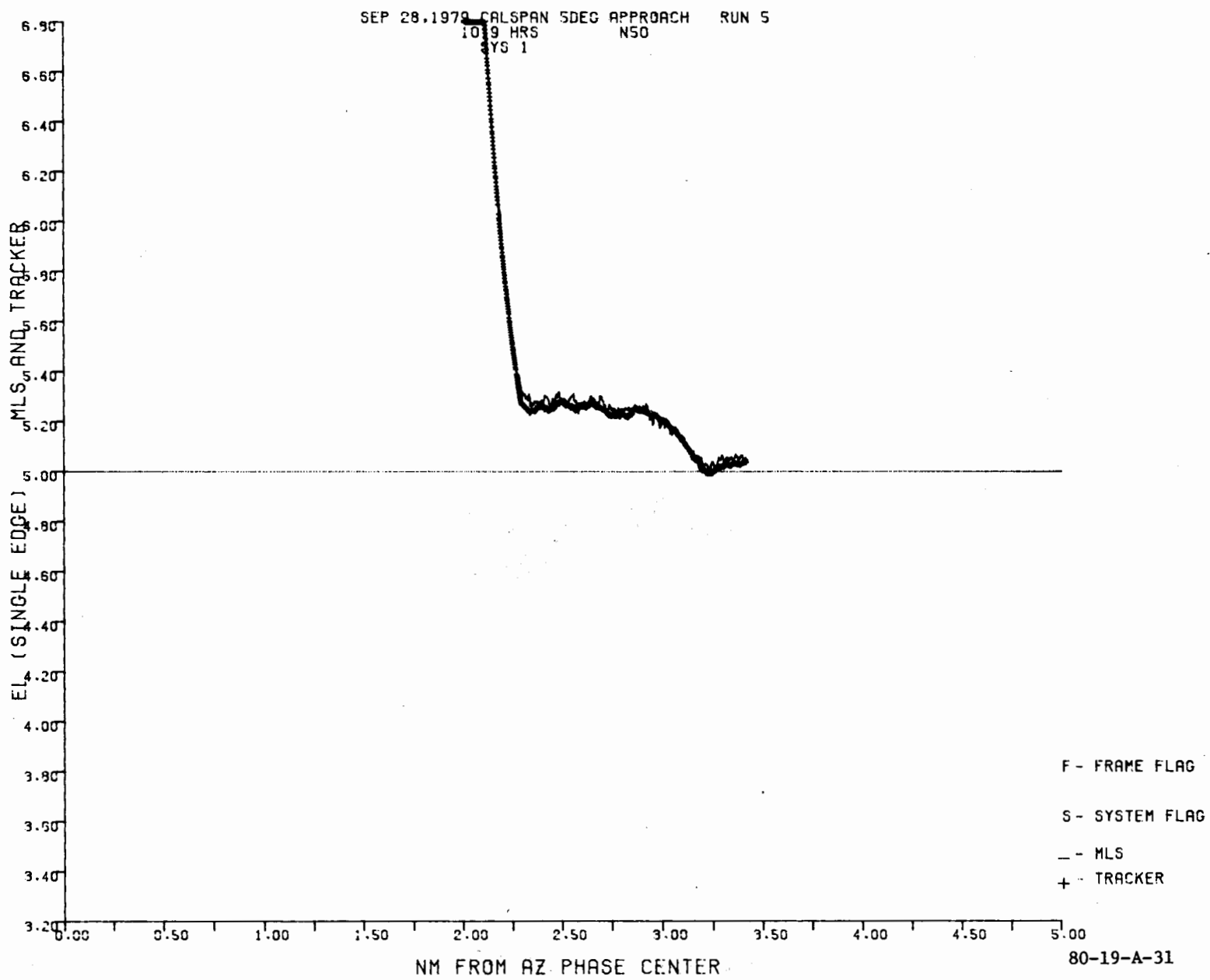


F - FRAME FLAG

S - SYSTEM FLAG

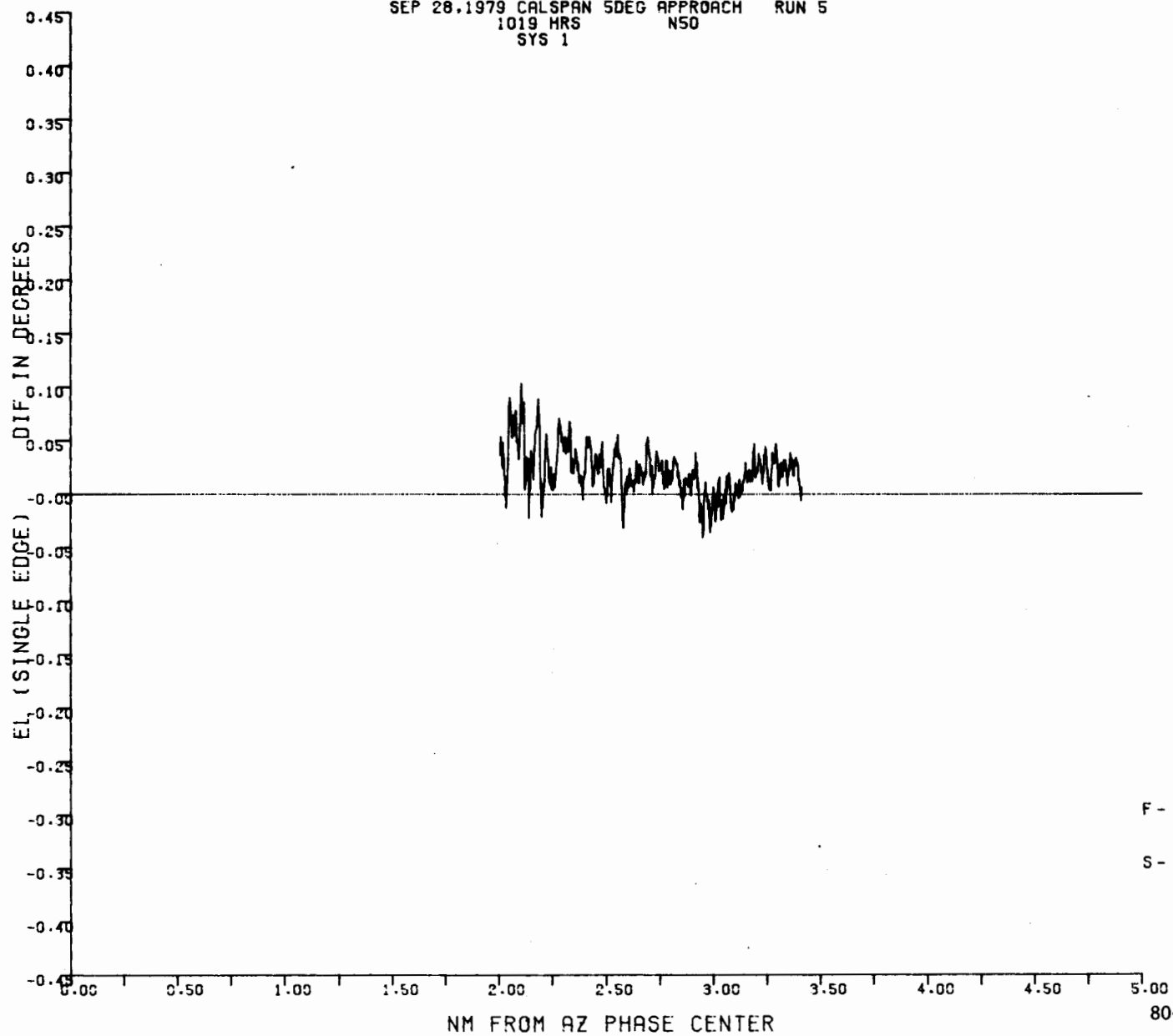
80-19-A-30

A-31



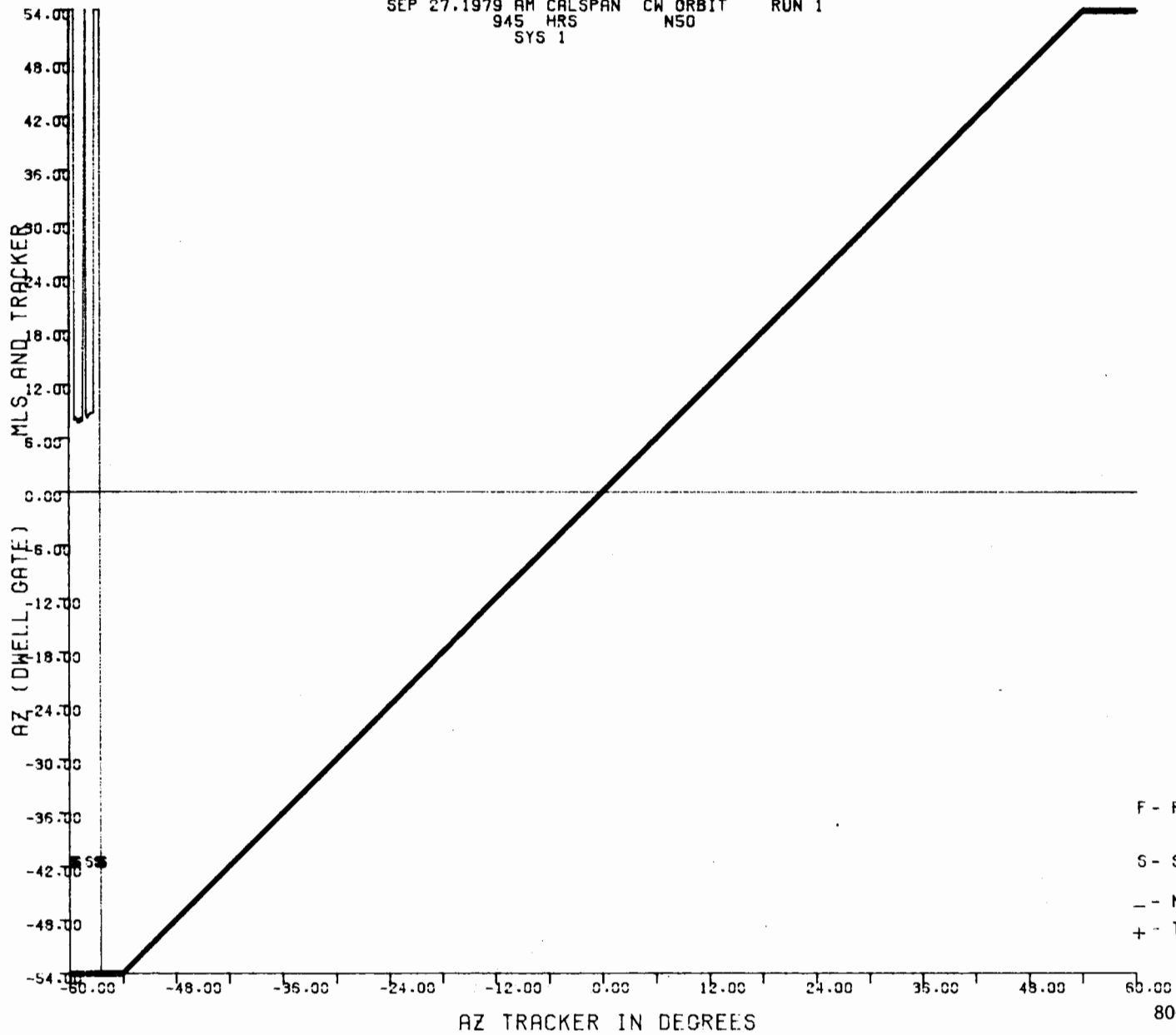
SEP 28.1979 CALSPAN SDEG APPROACH RUN 5  
1019 HRS N50  
SYS 1

A-32



80-19-A-32

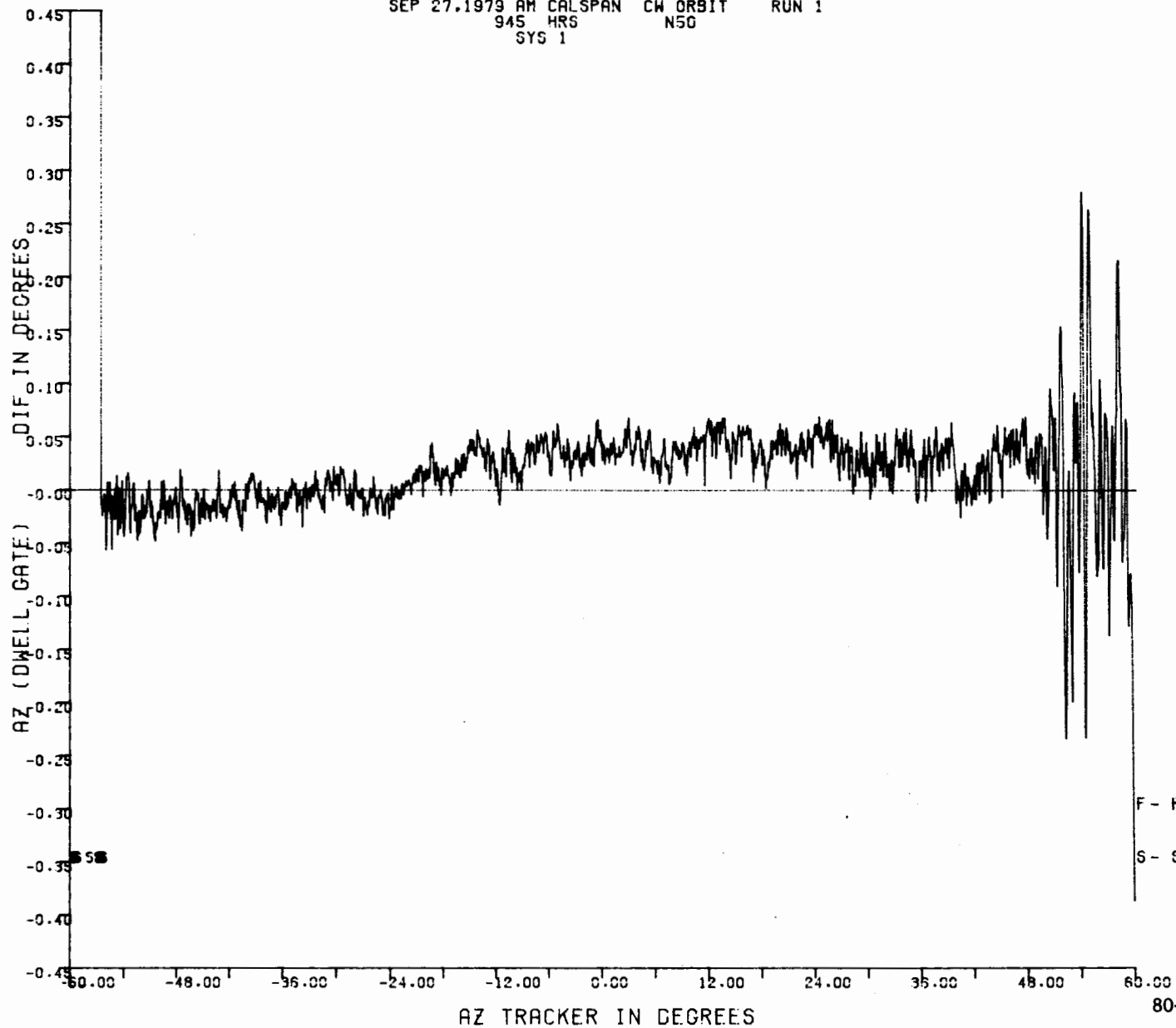
SEP 27.1979 AM CALSPAN CW ORBIT RUN 1  
945 HRS NSO  
SYS 1



A-33

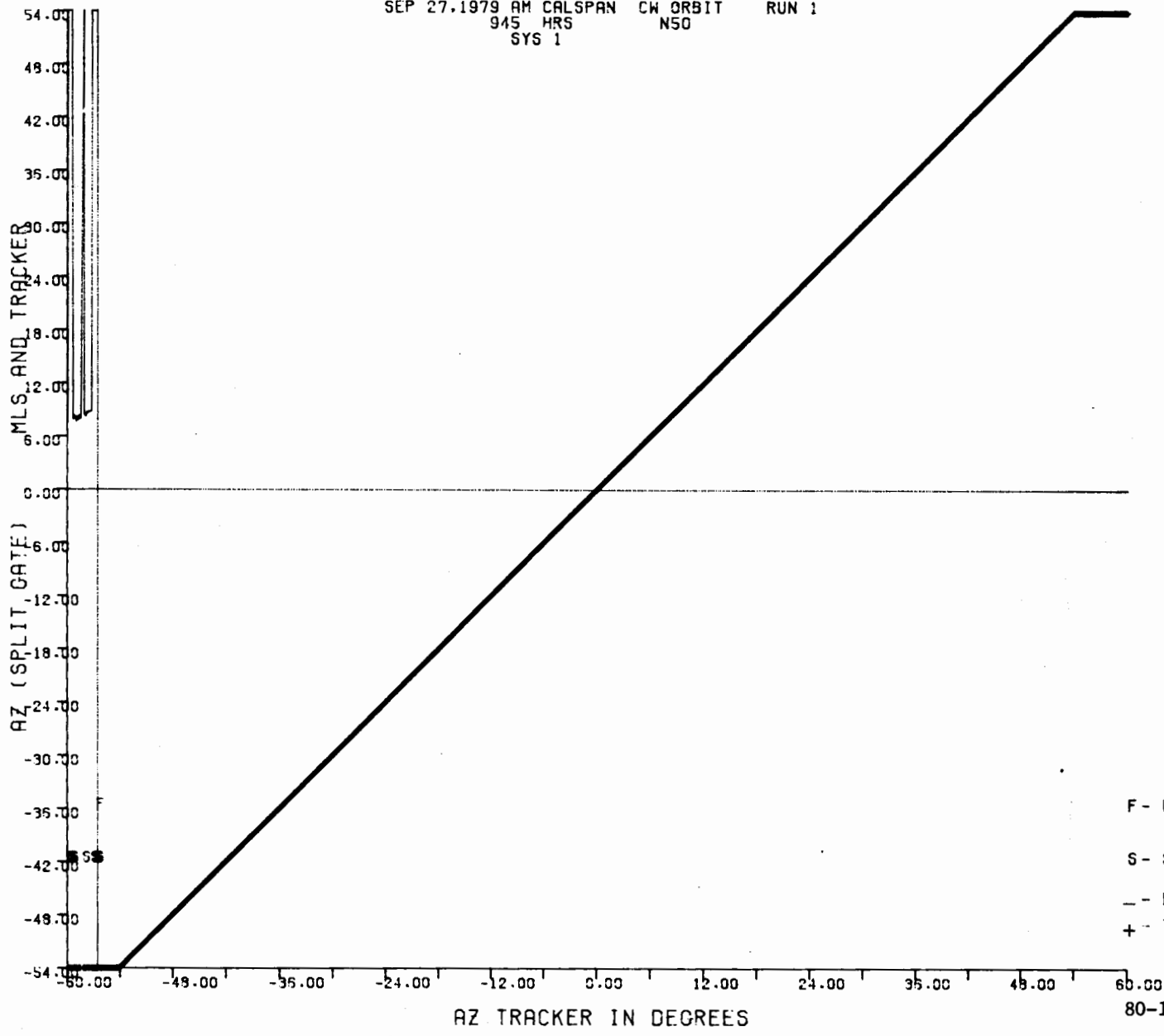
SEP 27.1979 AM CALSPAN CW ORBIT RUN 1  
945 HRS NSG  
SYS 1

A-34



80-19-A-34

SEP 27.1979 AM CALSPAN CW ORBIT RUN 1  
945 HRS N50  
SYS 1



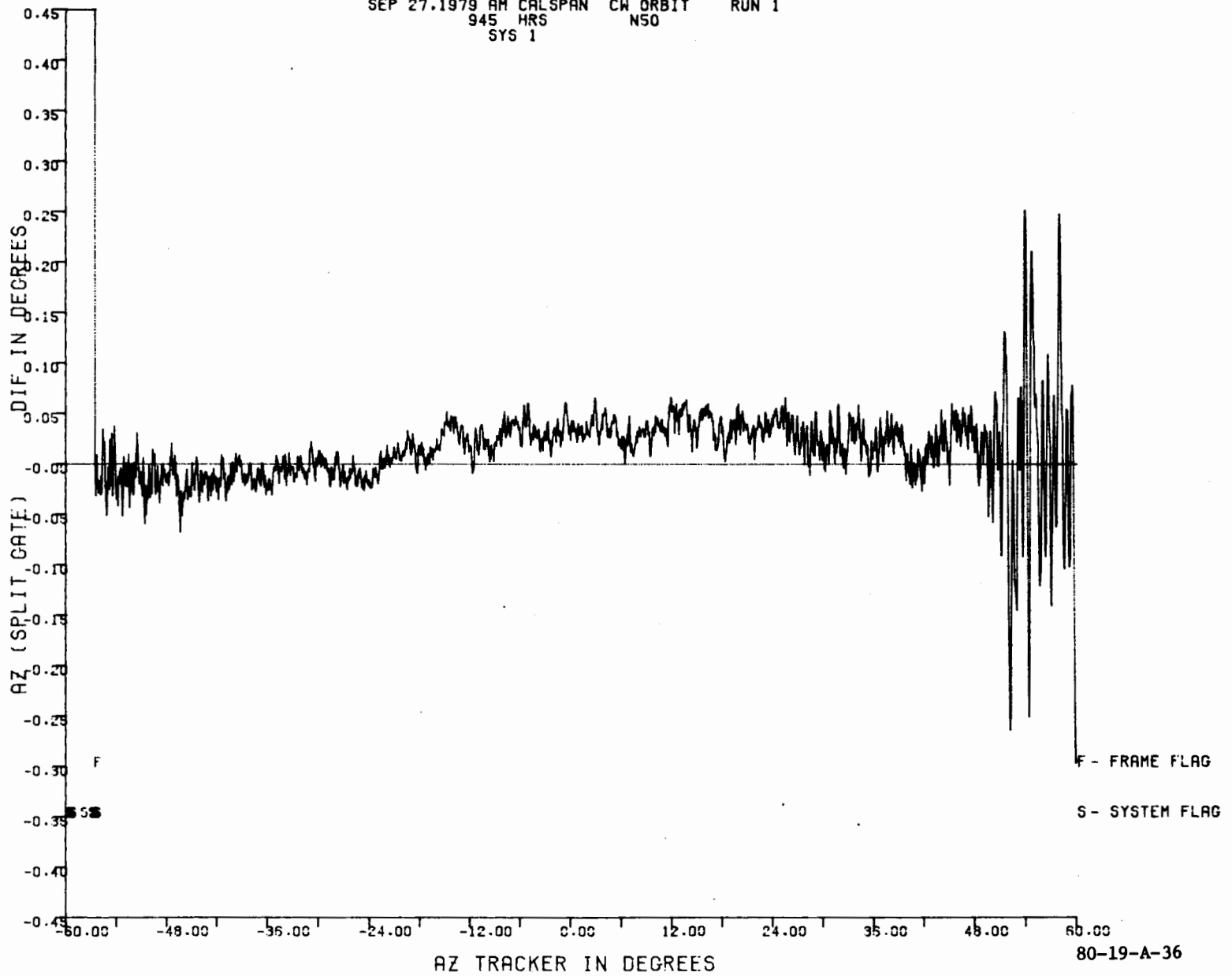
F - FRAME FLAG  
S - SYSTEM FLAG  
- - MLS  
+ - TRACKER

A-35

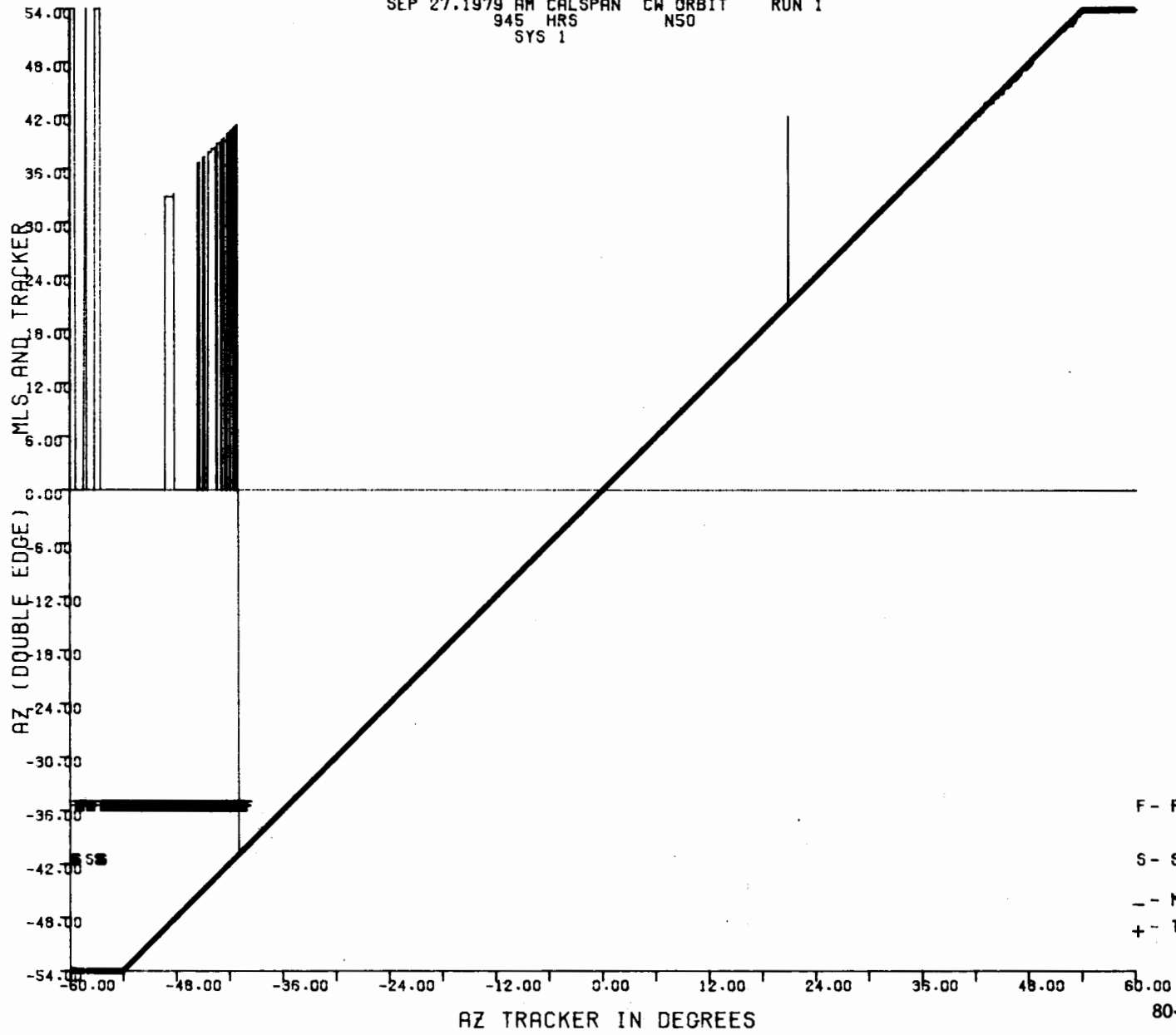
80-19-A-35

SEP 27.1979 AM CALSPAN CW ORBIT RUN 1  
945 HRS N50  
SYS 1

A-36



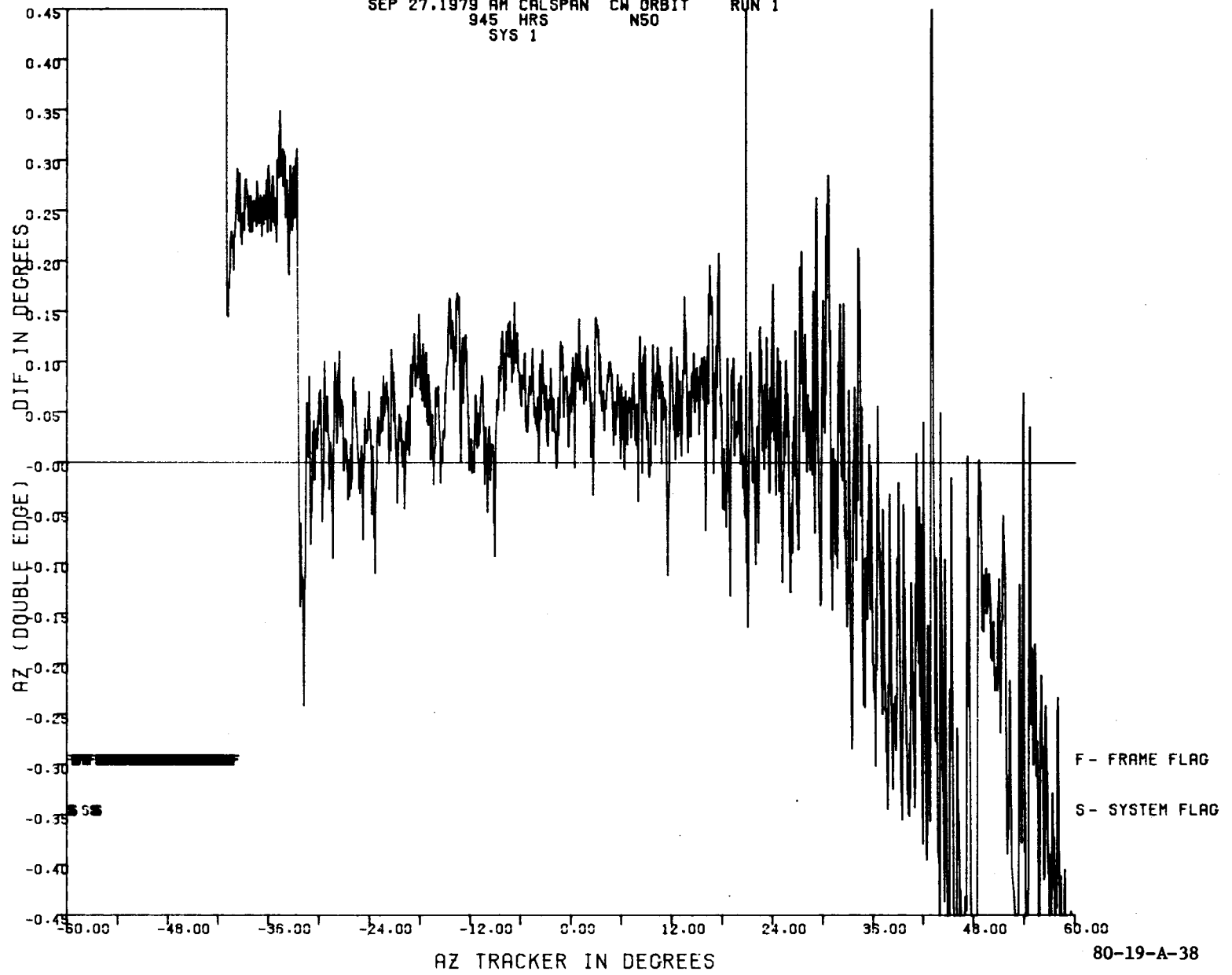
SEP 27.1979 AM CALSPAN CW ORBIT RUN 1  
945 HRS N50  
SYS 1



A-37

80-19-A-37

SEP 27.1979 AM CALSPAN CW ORBIT RUN 1  
945 HRS N50  
SYS 1

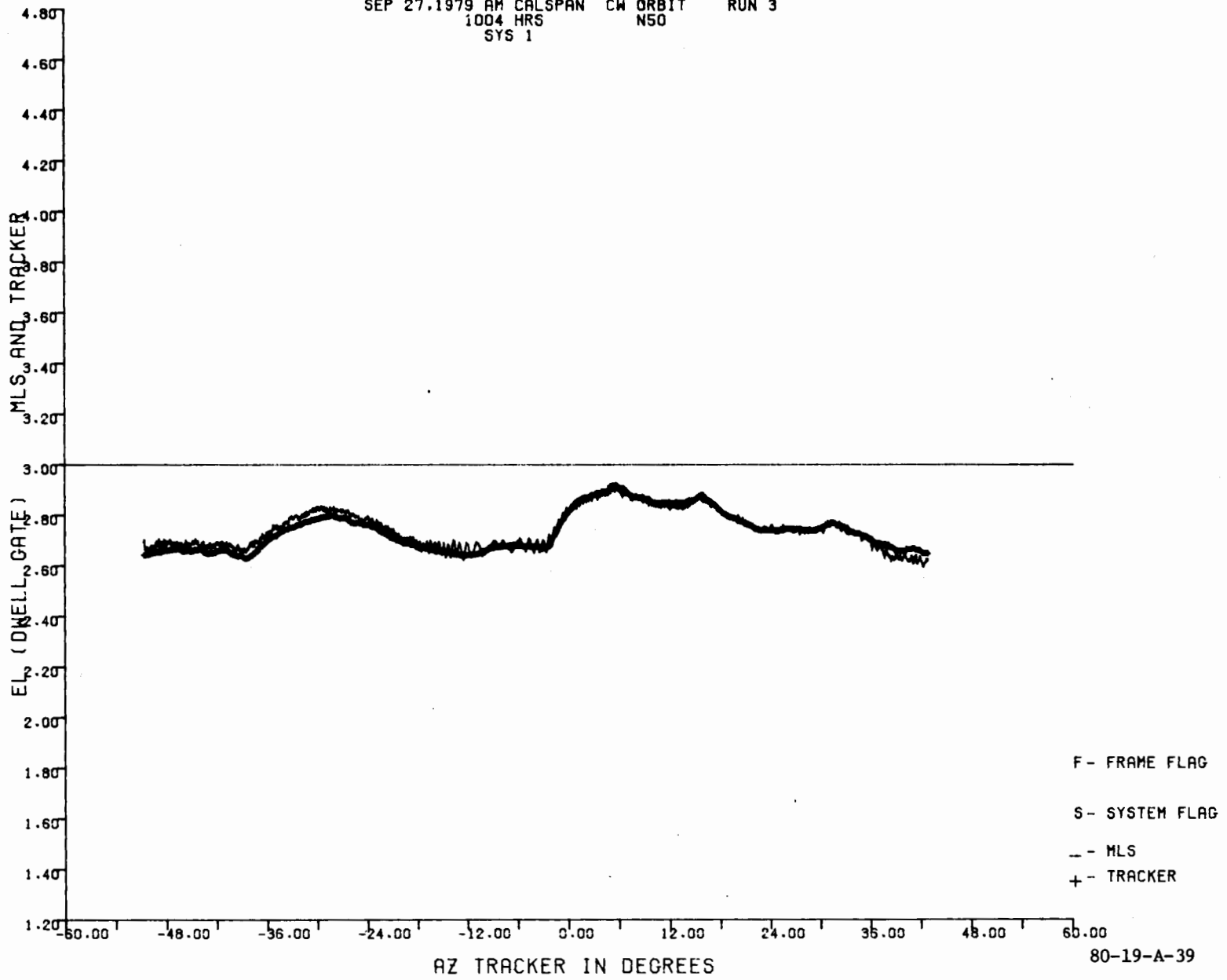


A-38

80-19-A-38

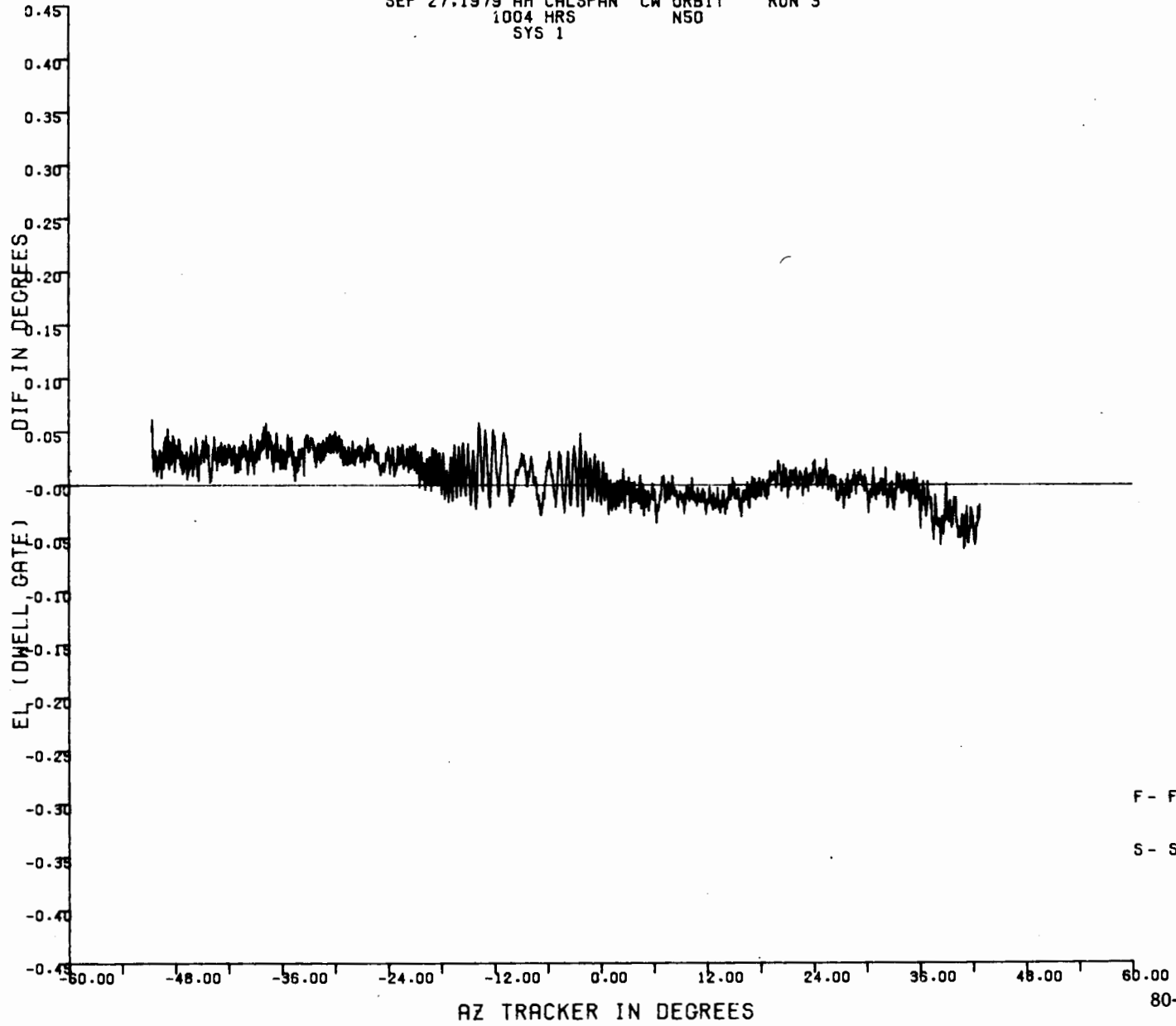
SEP 27.1979 AM CALSPAN CW ORBIT RUN 3  
1004 HRS N50  
SYS 1

A-39



SEP 27.1979 AM CALSPAN CW ORBIT RUN 3  
1004 HRS NSO  
SYS 1

A-40

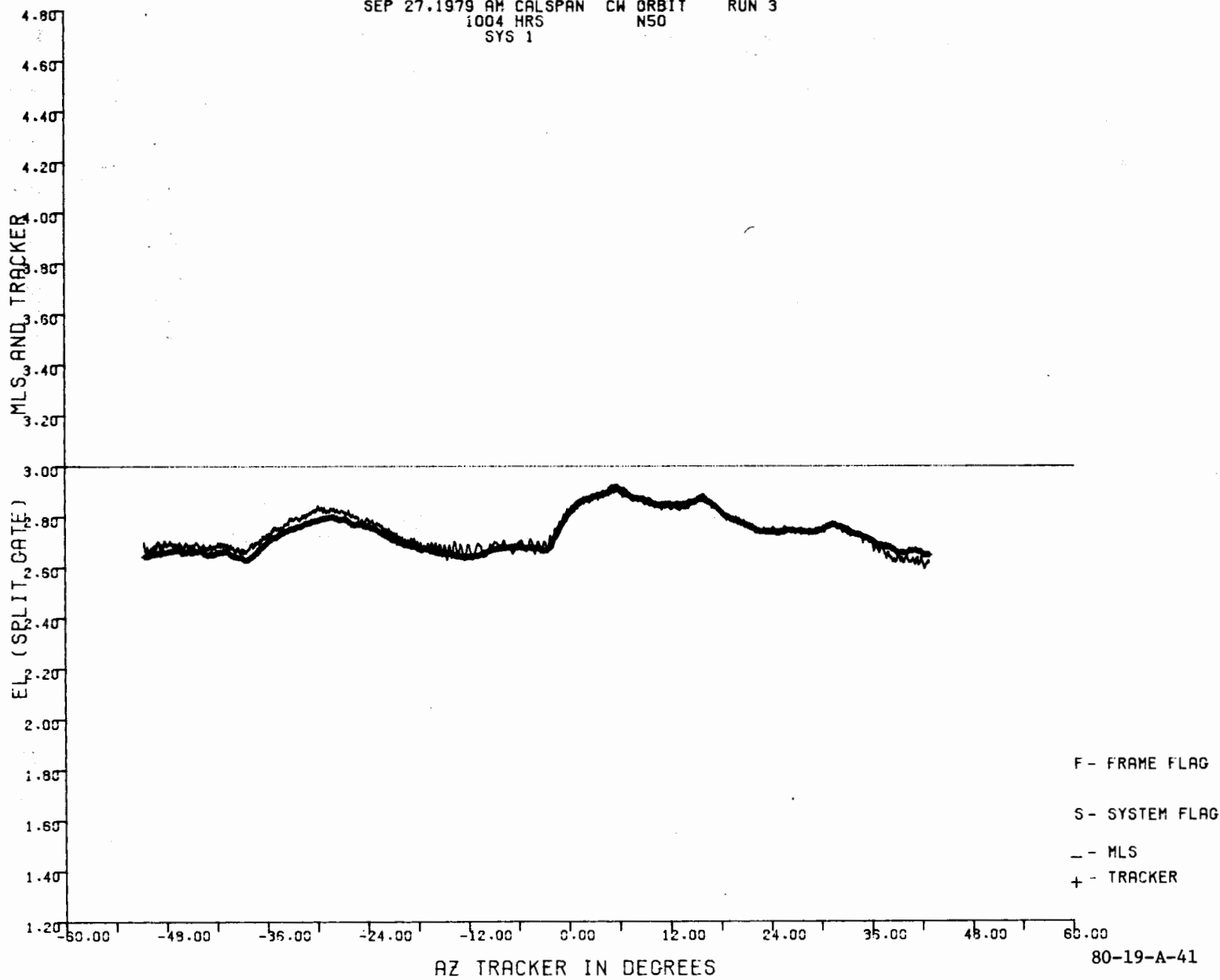


F - FRAME FLAG  
S - SYSTEM FLAG

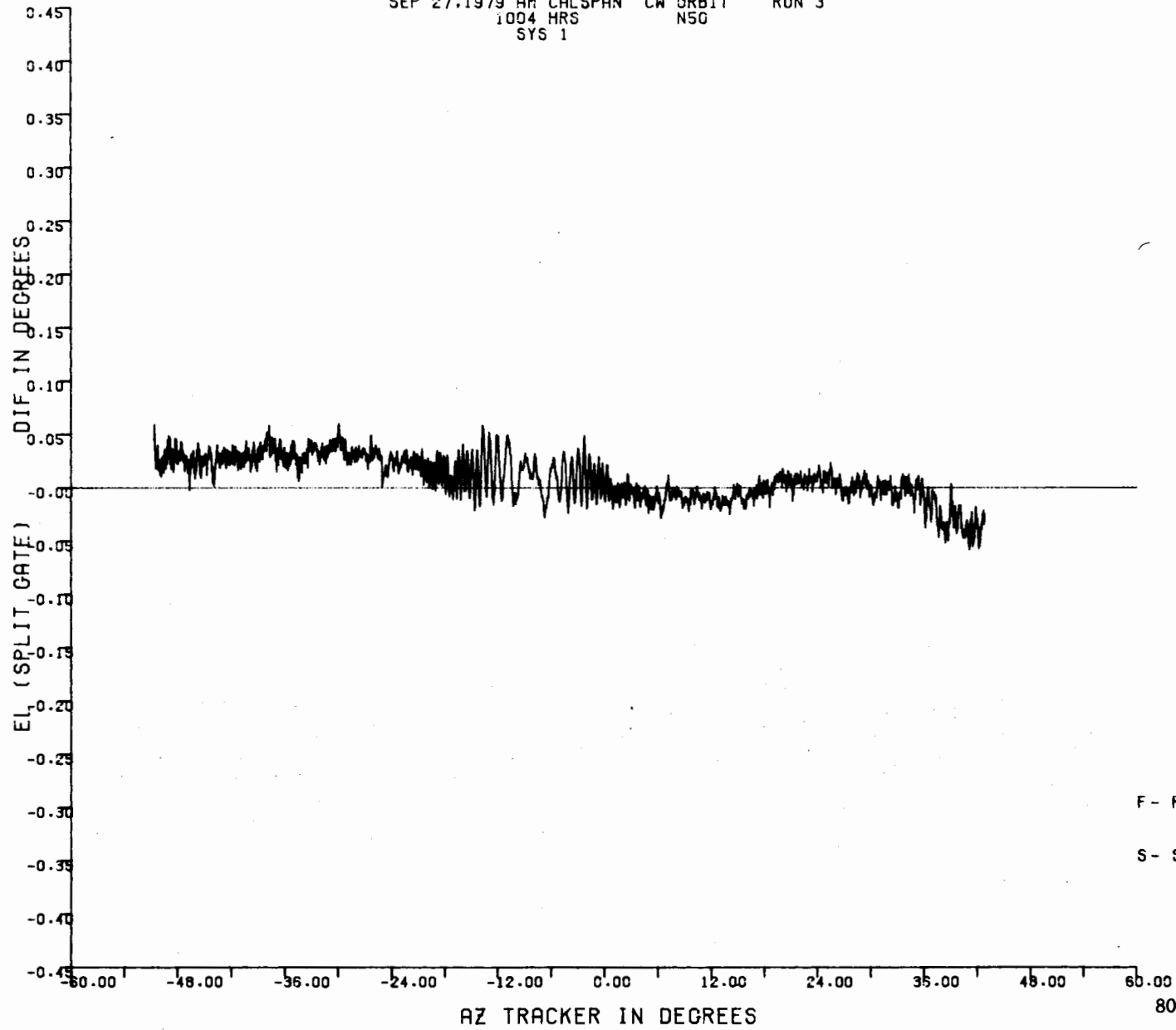
80-19-A-40

SEP 27.1979 AM CALSPAN CW ORBIT RUN 3  
1004 HRS N50  
SYS 1

A-41



SEP 27.1979 AM CALSPAN CW ORBIT RUN 3  
1004 HRS N50  
SYS 1



A-42

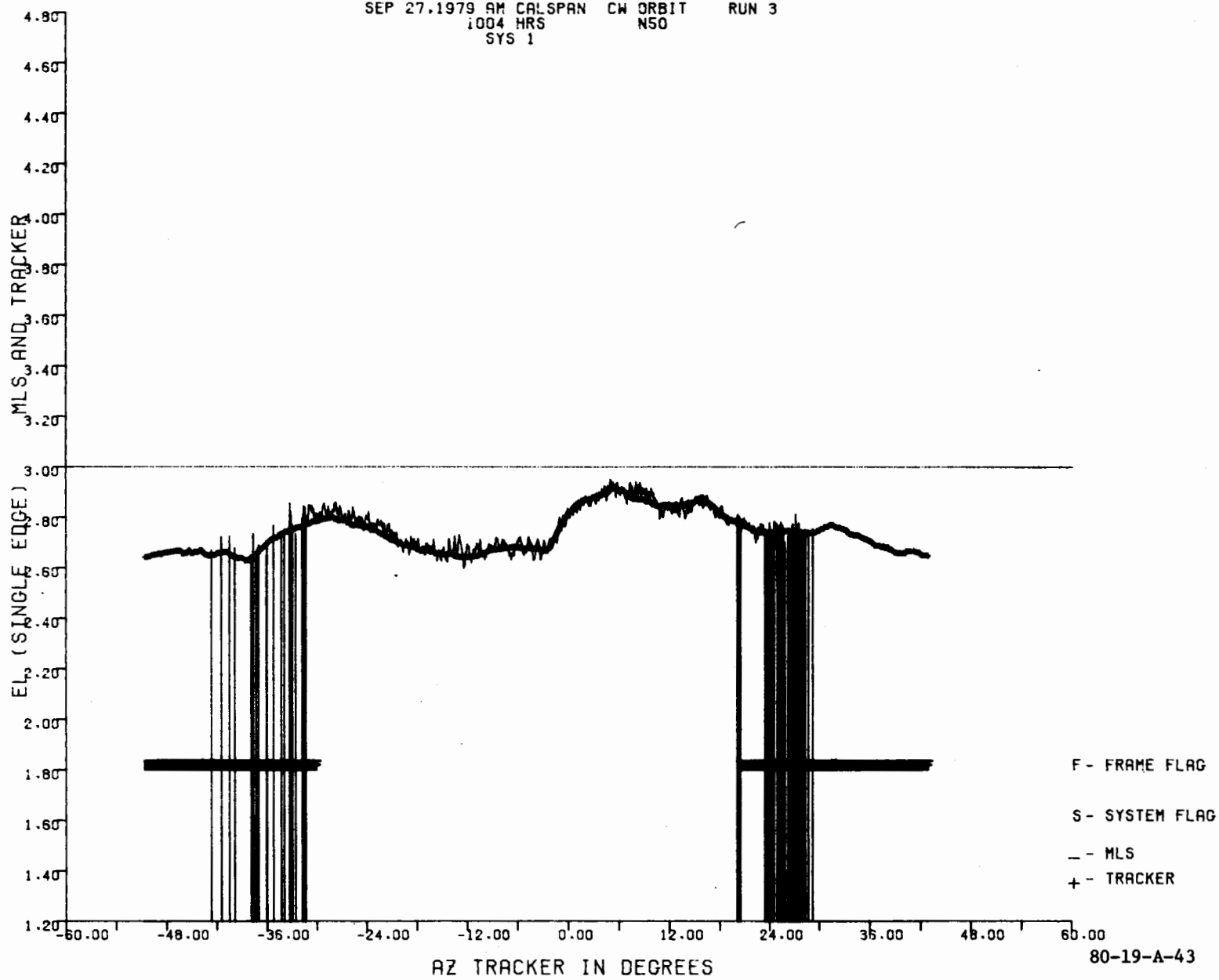
F - FRAME FLAG

S - SYSTEM FLAG

80-19-A-42

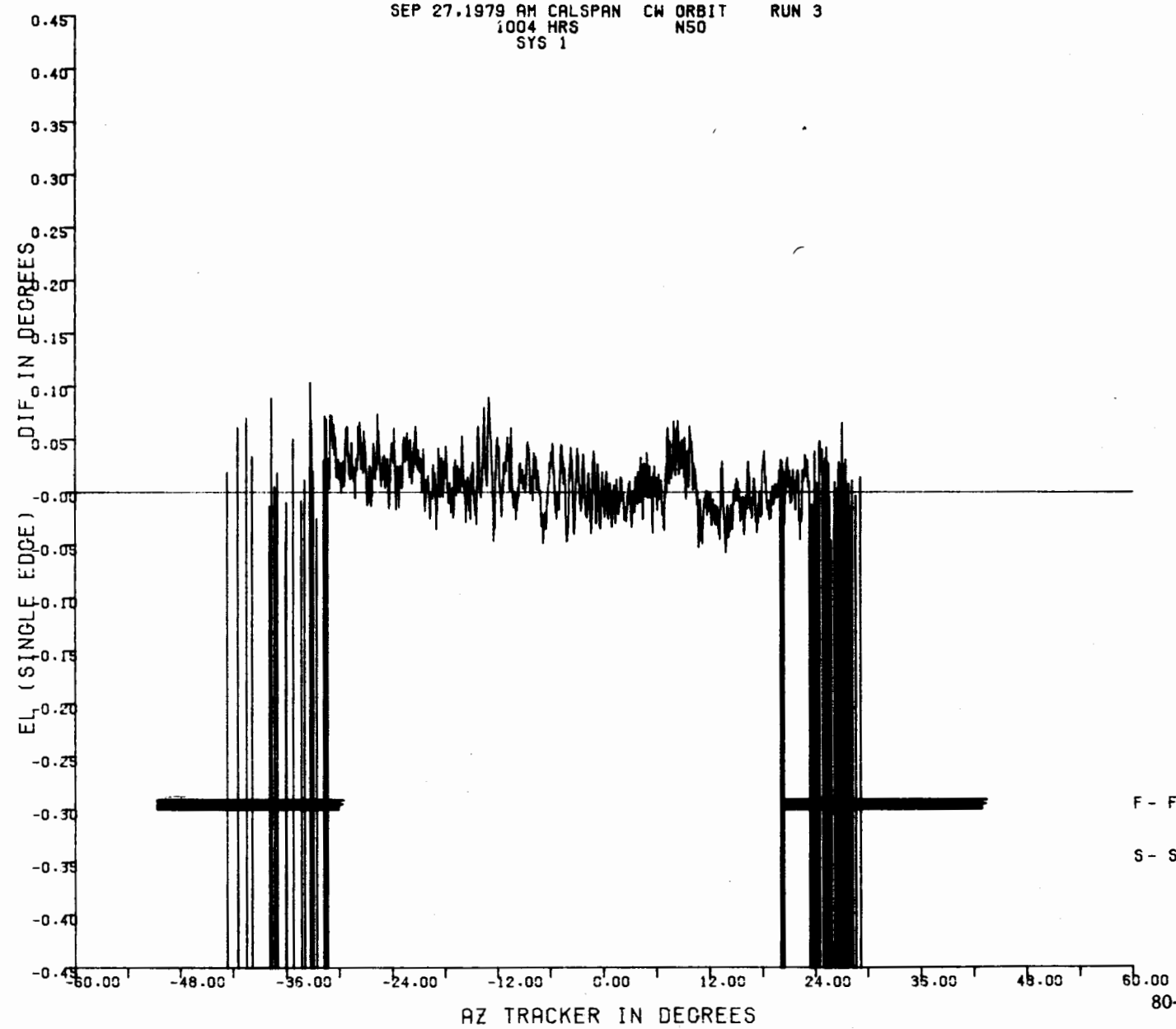
SEP 27.1979 AM CALSPAN CW ORBIT RUN 3  
1004 HRS N50  
SYS 1

A-43



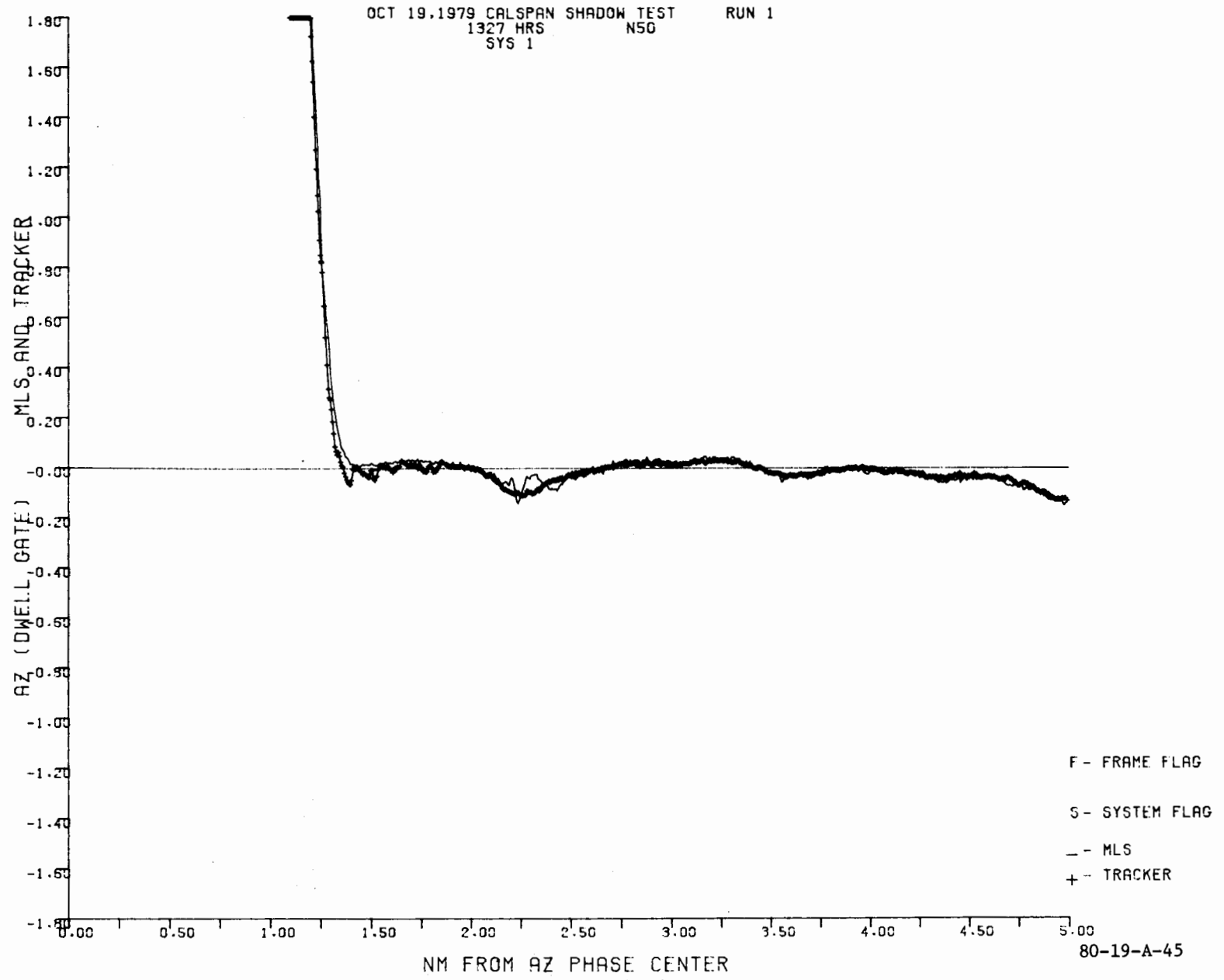
SEP 27.1979 AM CALSPAN CW ORBIT RUN 3  
1004 HRS N50  
SYS 1

77-A

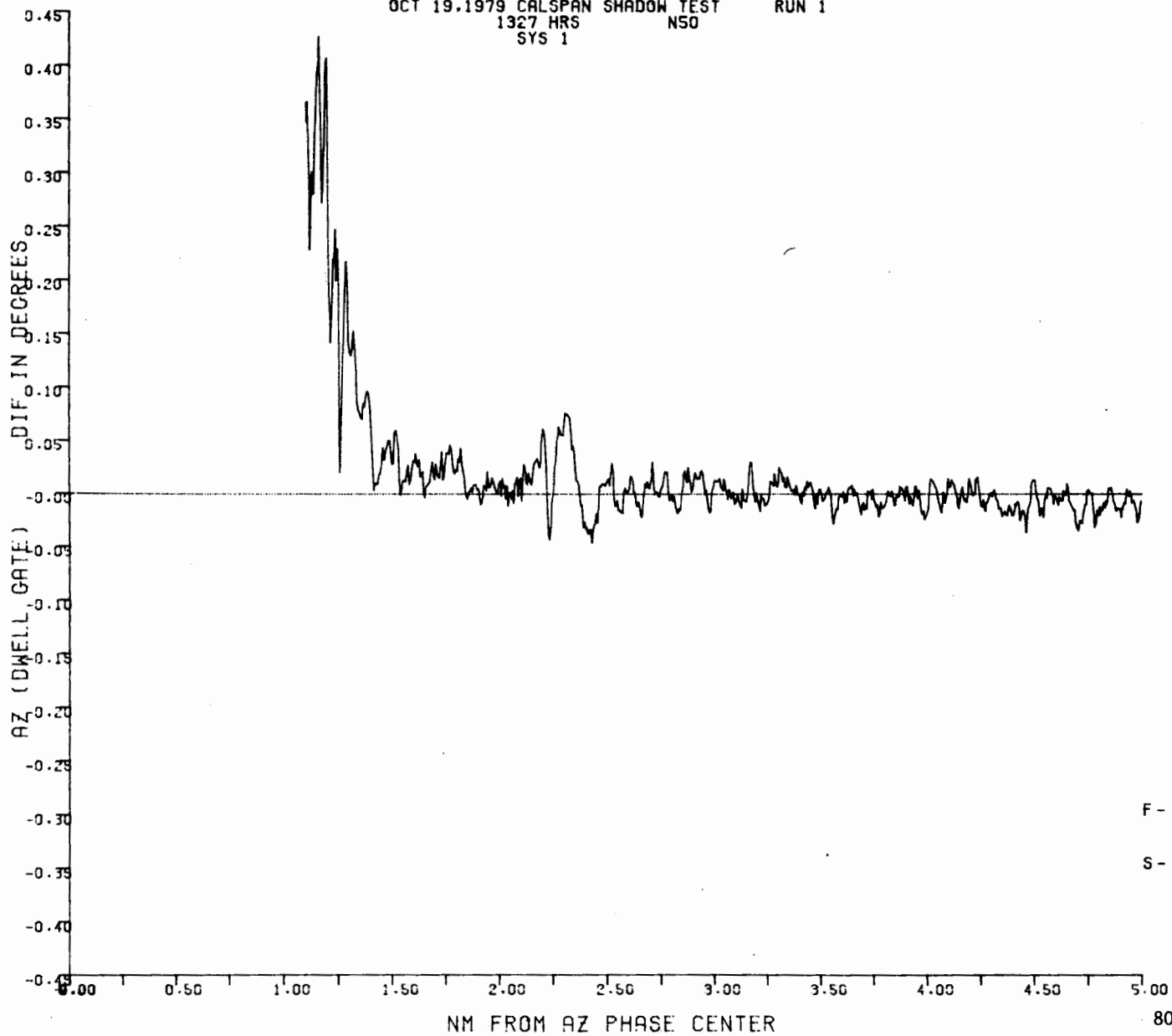


F - FRAME FLAG  
S - SYSTEM FLAG

A-45



OCT 19.1979 CALSPAN SHADOW TEST RUN 1  
1327 HRS NSO  
SYS 1



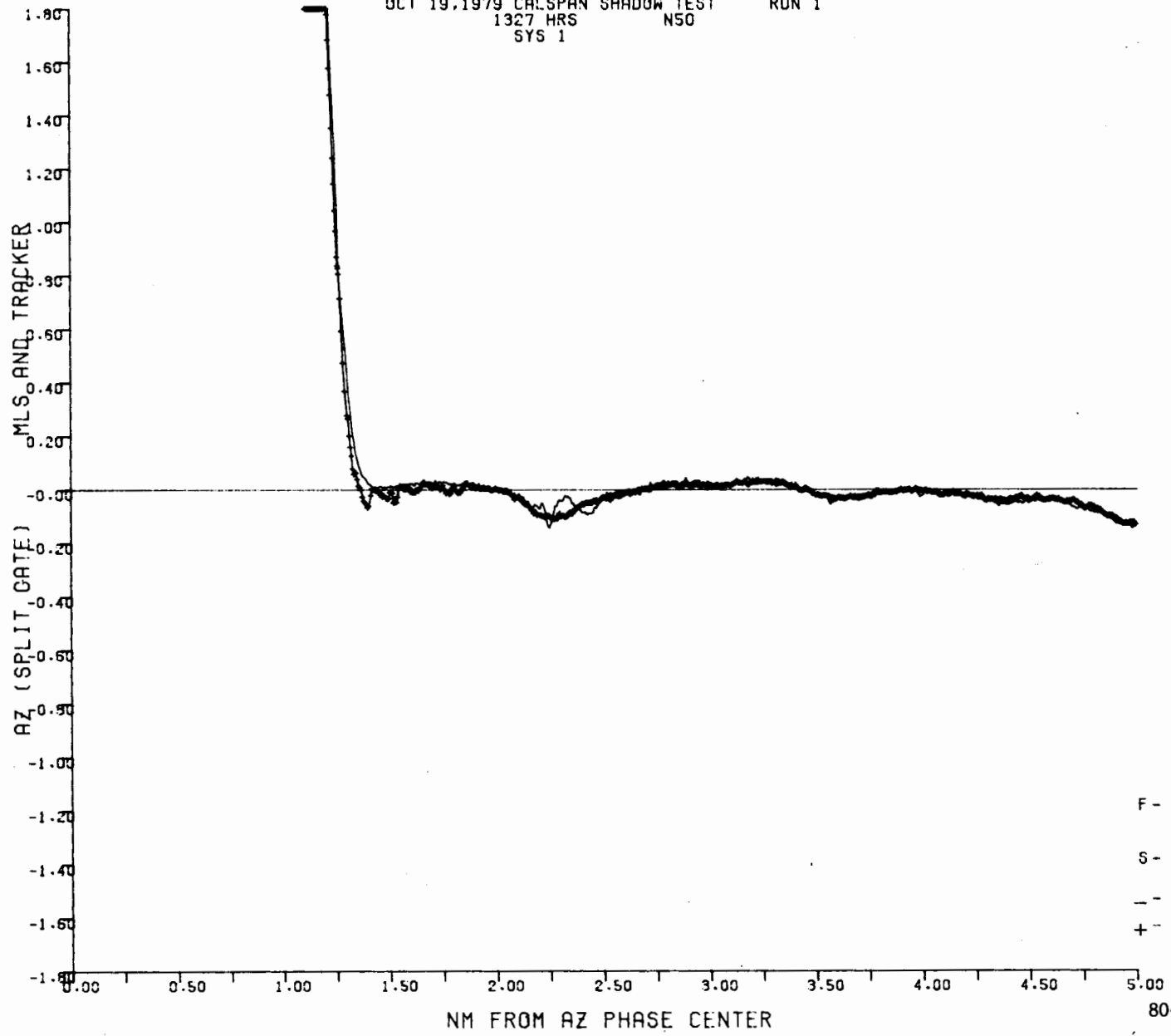
A-46

F - FRAME FLAG  
S - SYSTEM FLAG

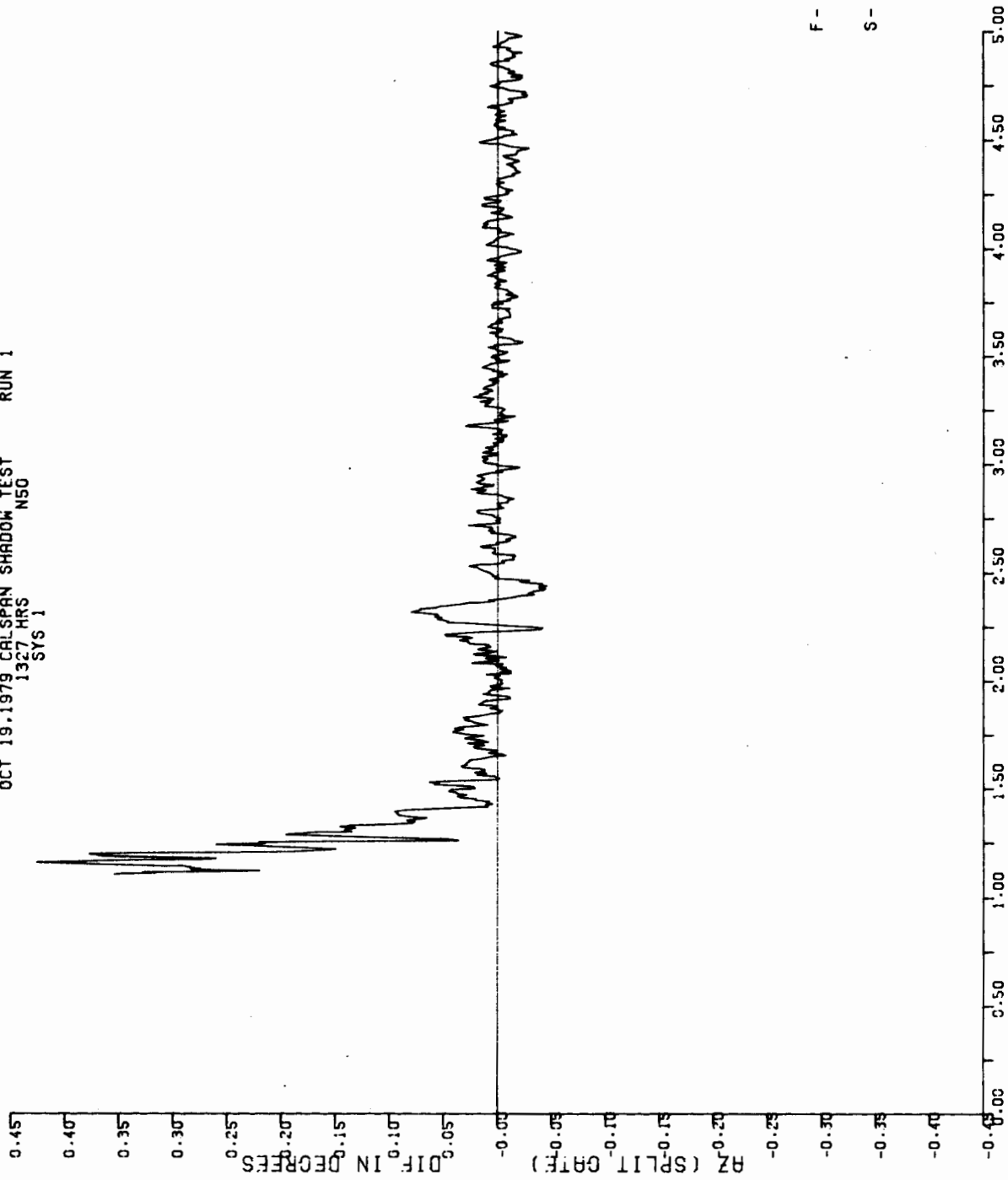
80-19-A-46

OCT 19, 1979 CALSPAN SHADOW TEST RUN 1  
1327 HRS NSO  
SYS 1

A-47



OCT 19.1979 CALSPAN SHADOW TEST RUN 1  
1327 HRS NSO  
SYS 1

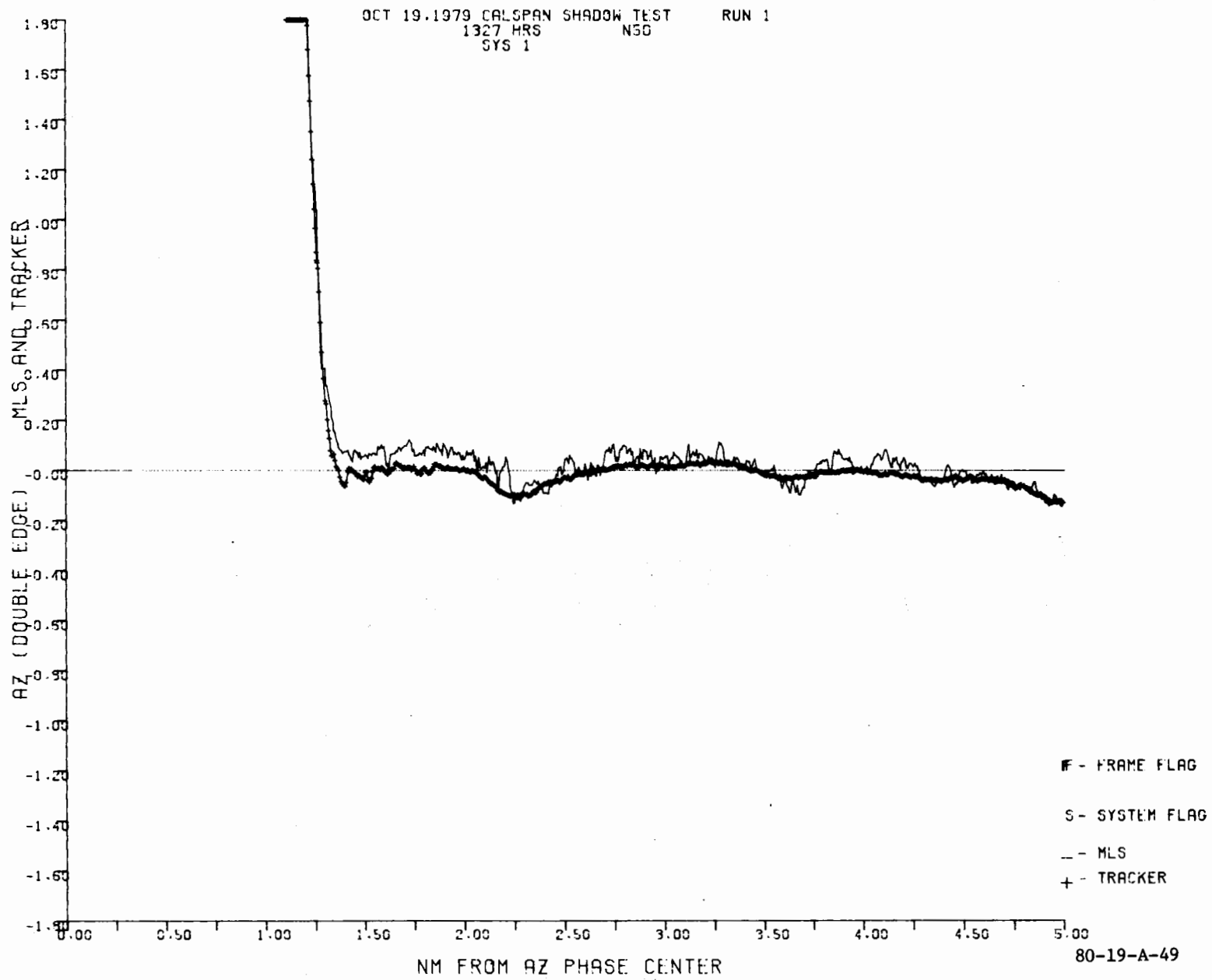


F - FRAME FLAG  
S - SYSTEM FLAG

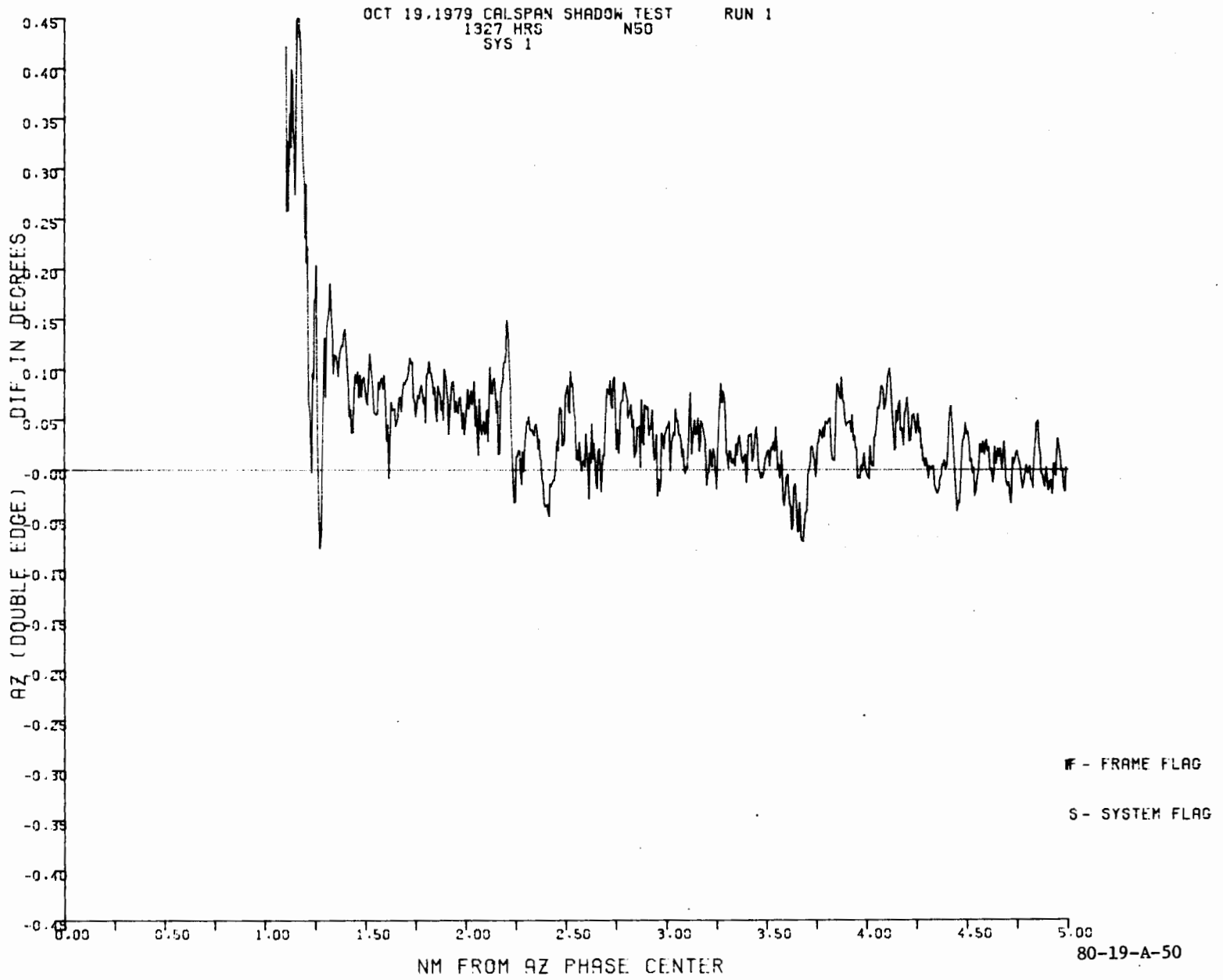
80-19-A-48

NM FROM AZ PHASE CENTER

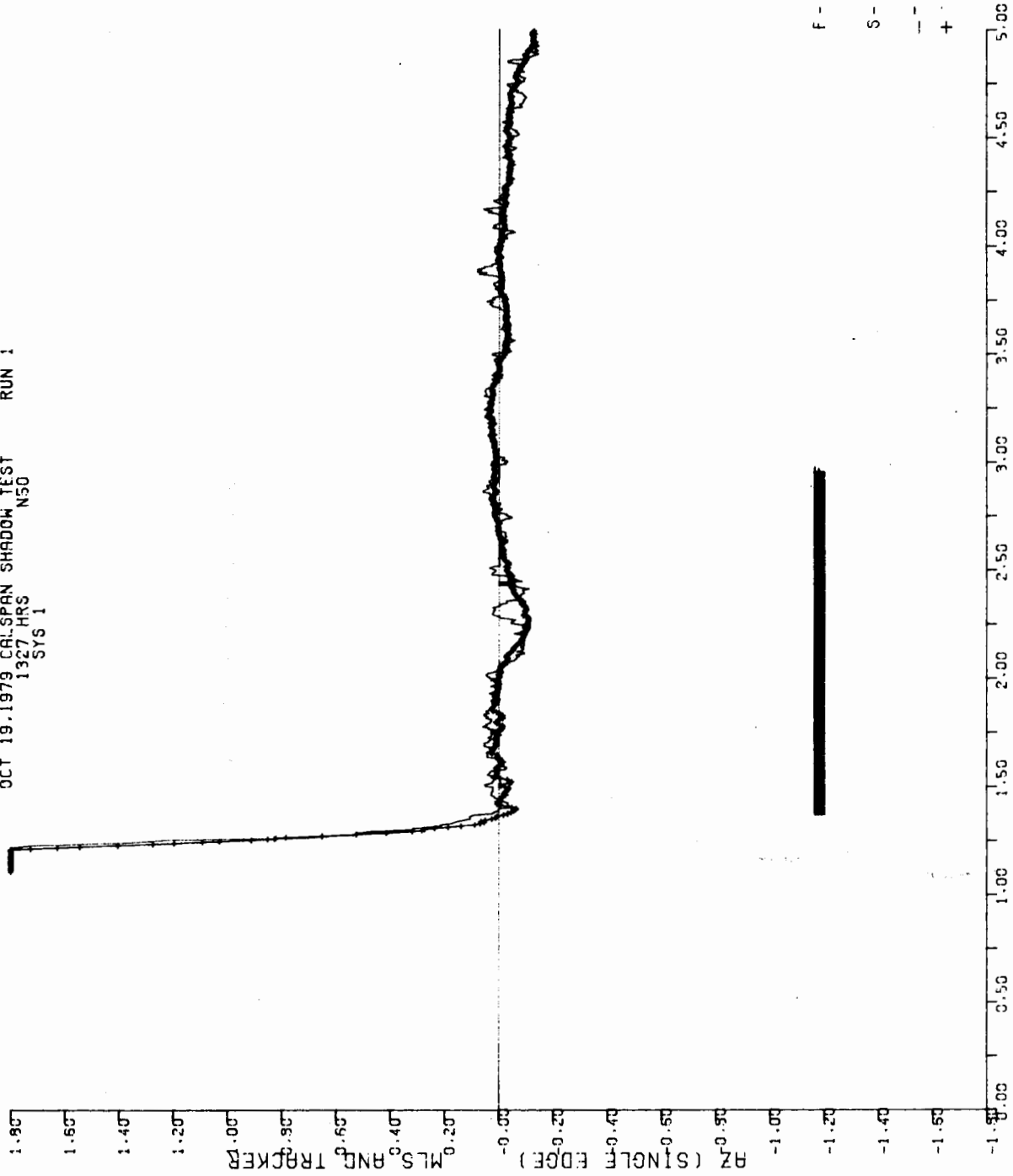
A-49



A-50

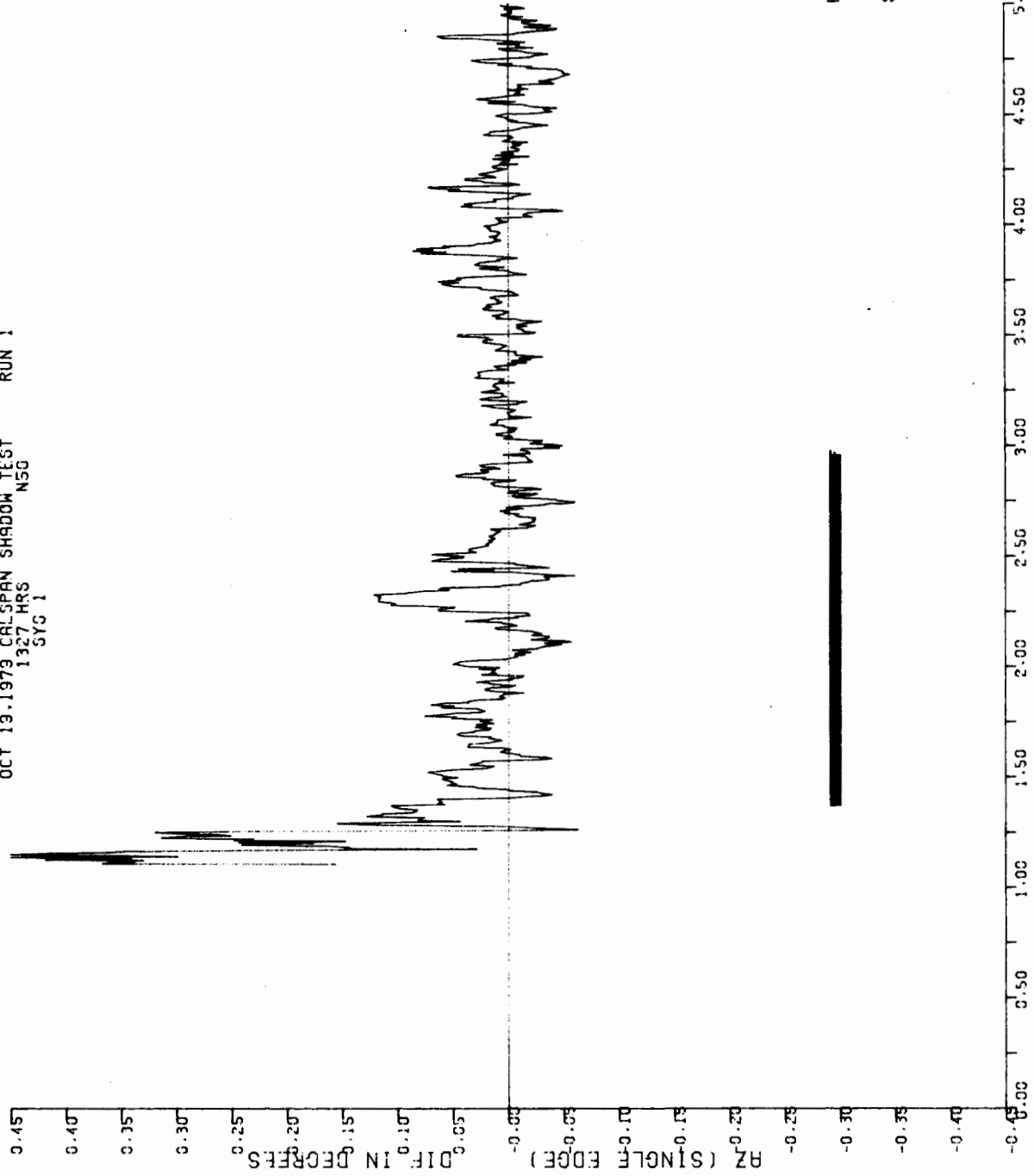


OCT 19 1979 CALSPAN SHADOW TEST RUN 1  
1327 HRS N50  
SYS 1



NM FROM AZ PHASE CENTER  
80-19-A-51

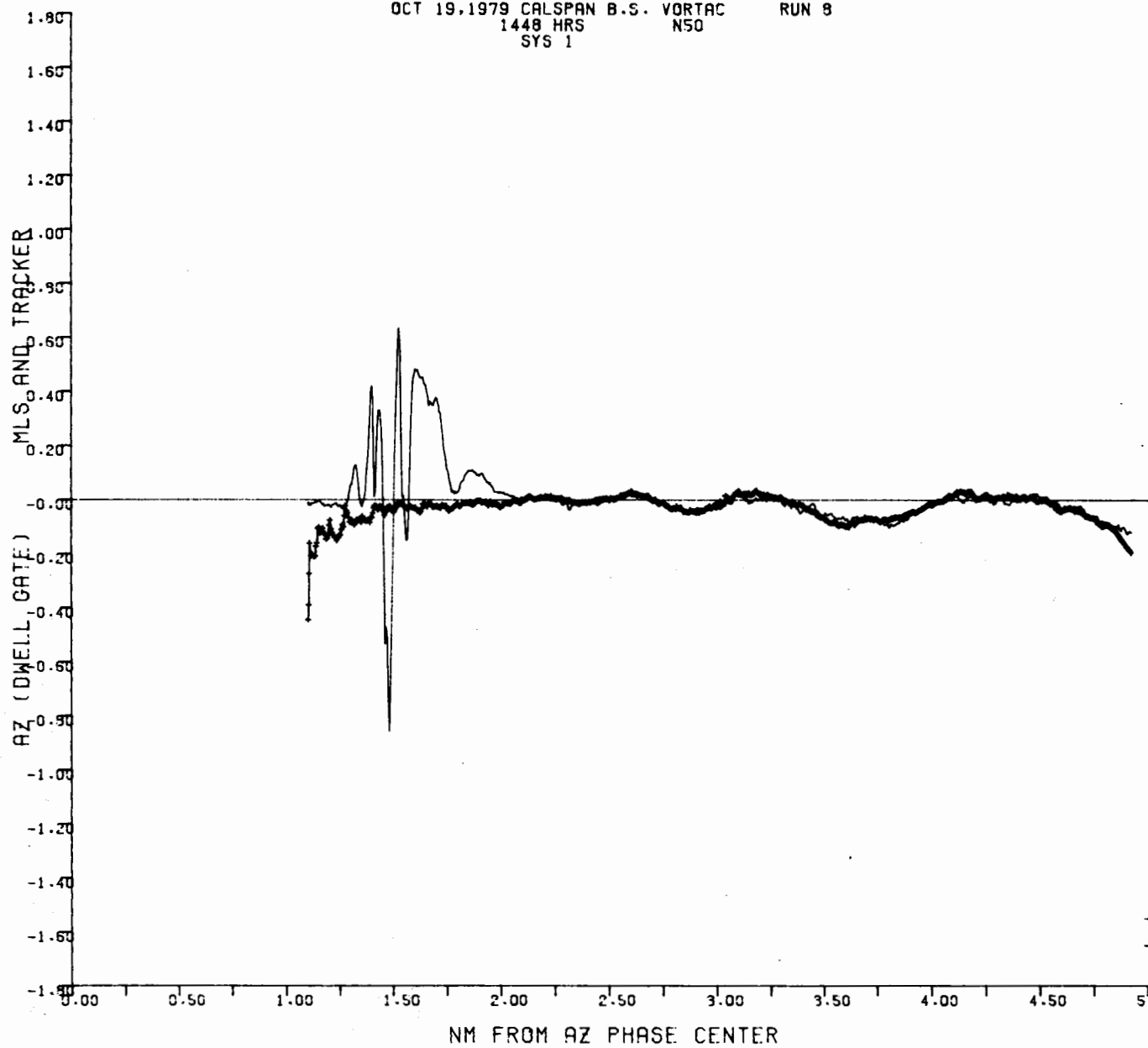
OCT 19.1979 CALSPAN SHADOW TEST RUN 1  
1327 HRS NSG  
SYG 1



80-19-A-52

OCT 19, 1979 CALSPAN B.S. VORTAC RUN 8  
1448 HRS N50  
SYS 1

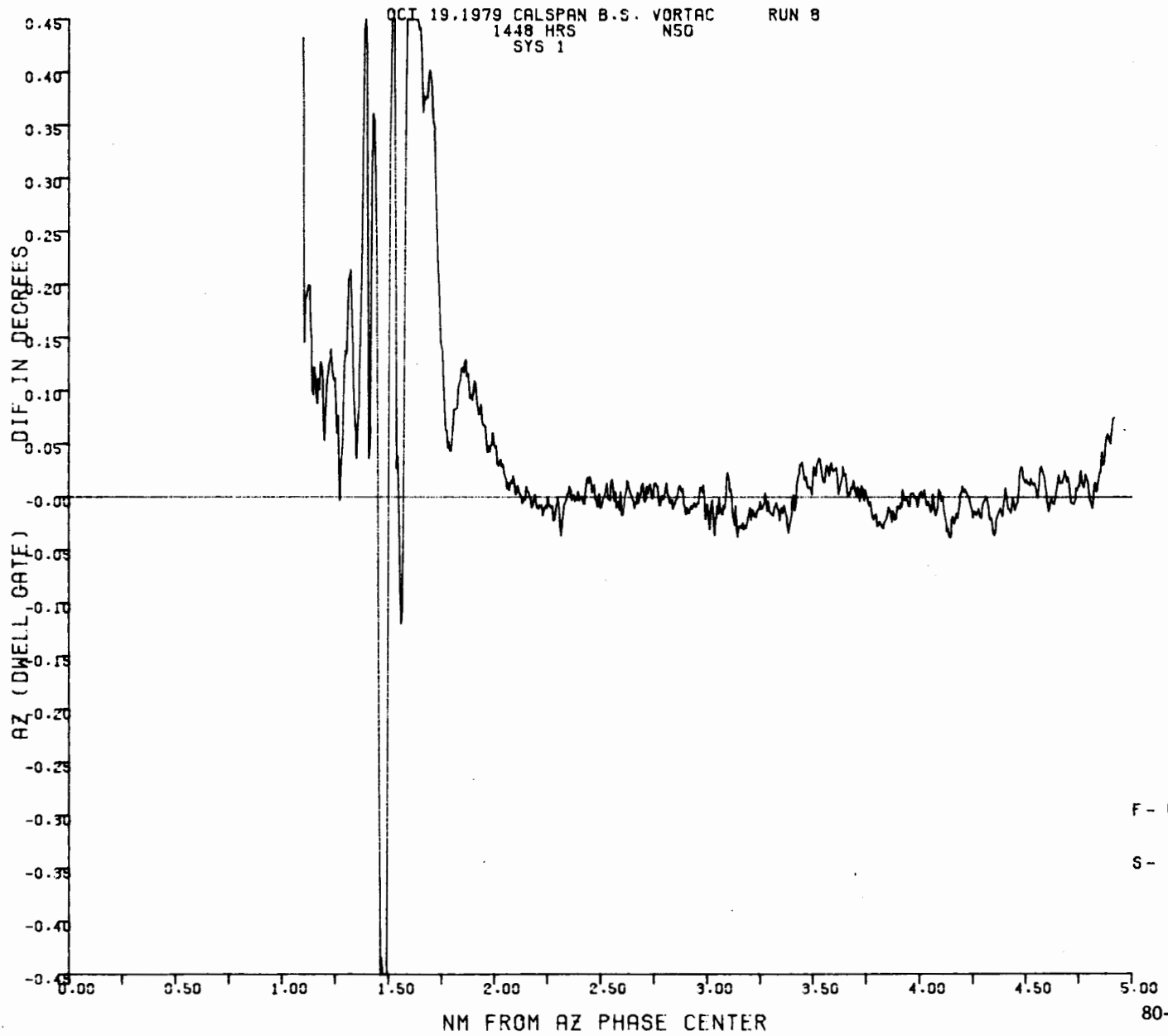
A-53



F - FRAME FLAG  
S - SYSTEM FLAG  
- - MLS  
+ - TRACKER

80-19-A-53

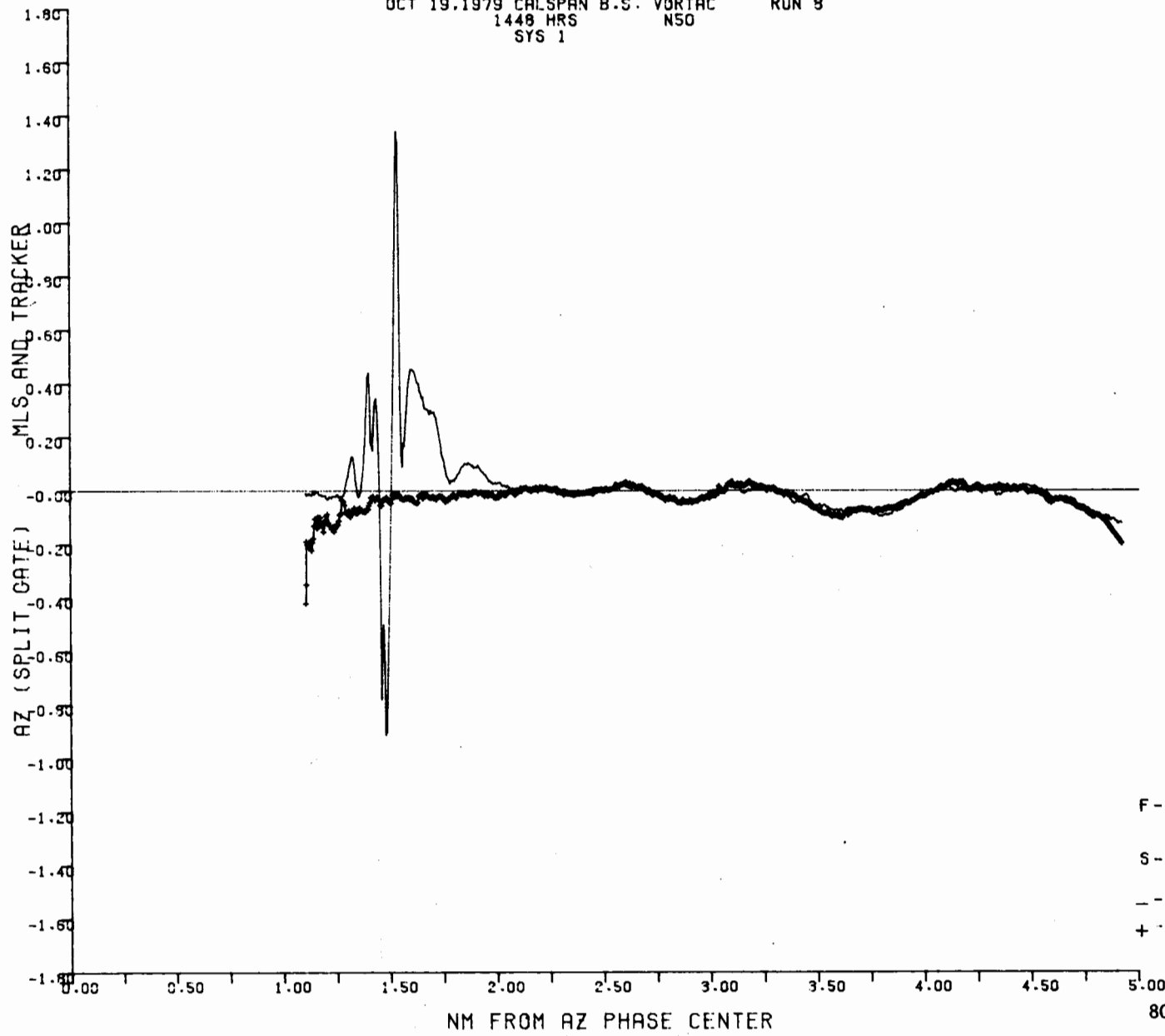
A-54



80-19-A-54

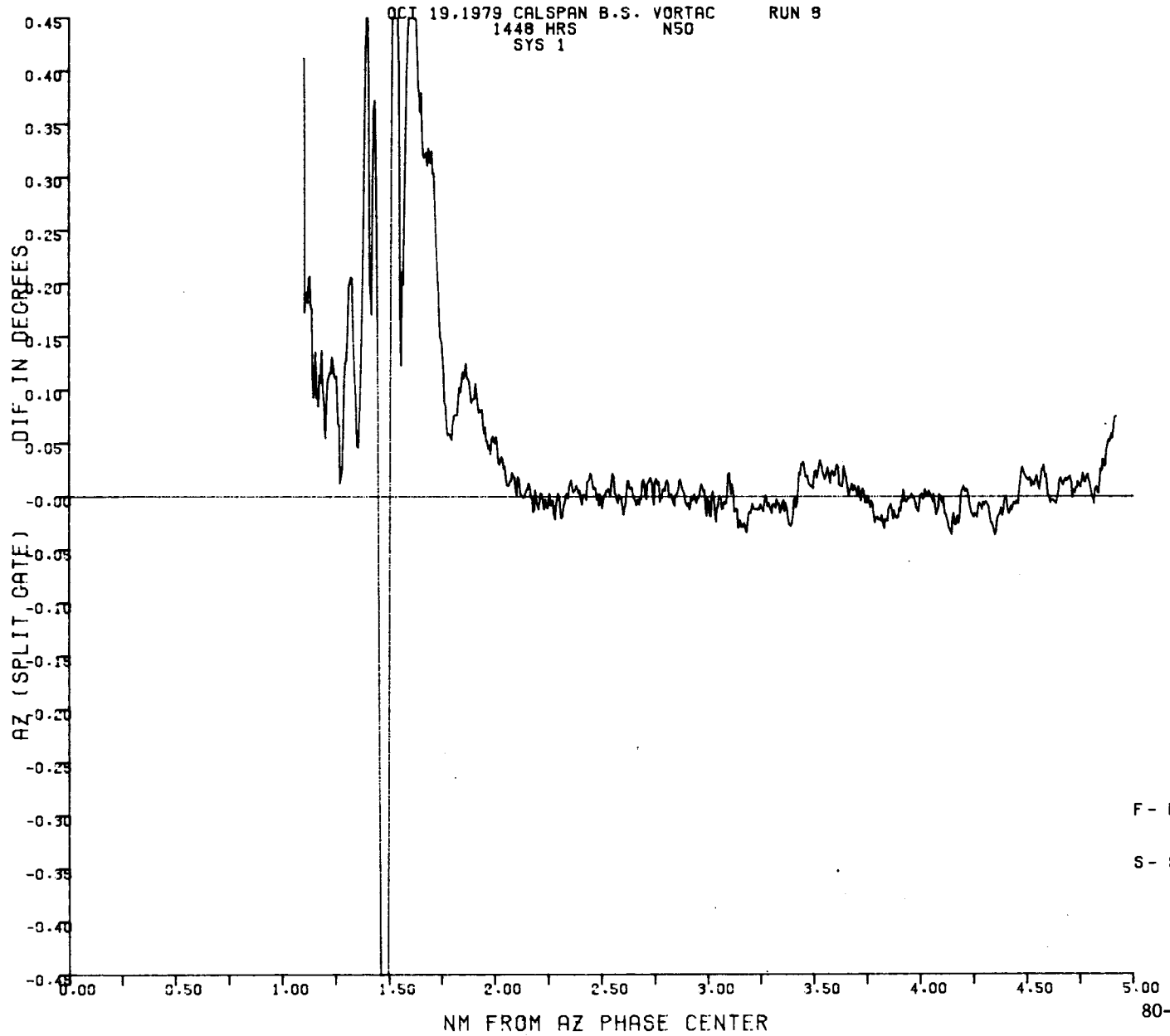
OCT 19.1979 CALSPAN B-S. VORTAC RUN 8  
1448 HRS NSO  
SYS 1

A-55



80-19-A-55

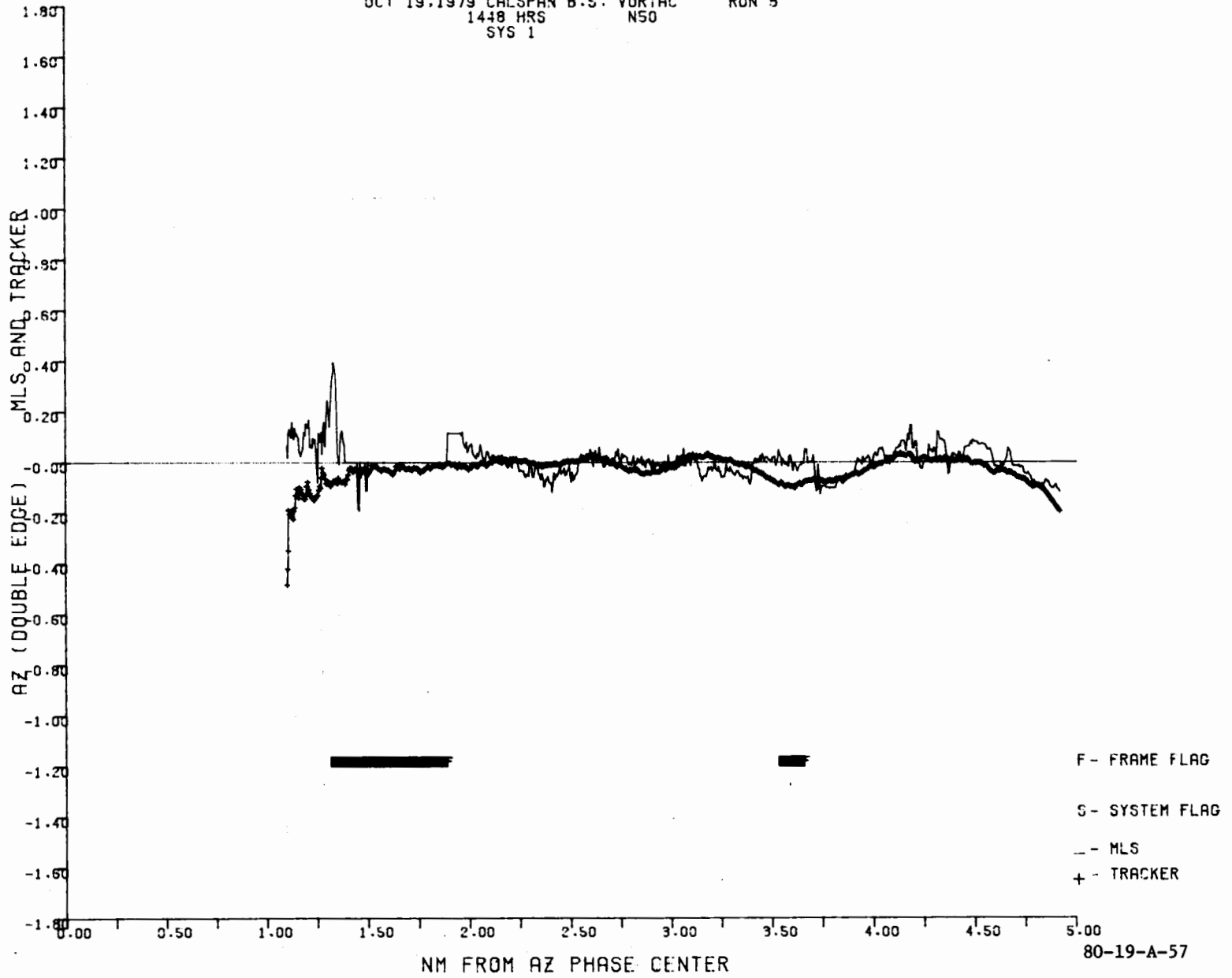
A-56



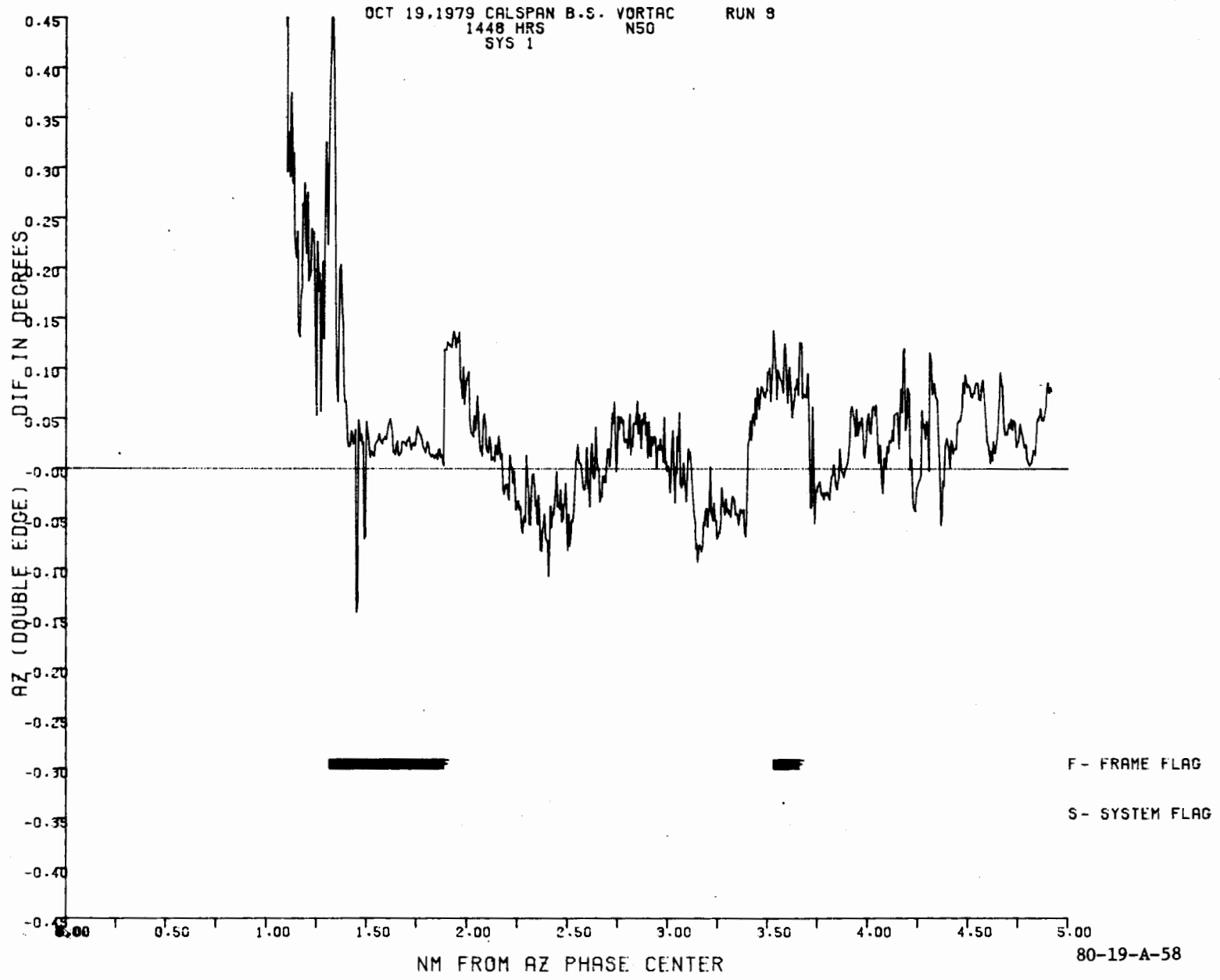
80-19-A-56

OCT 19, 1979 CALSPAN B.S. VORTAC RUN 9  
1448 HRS N50  
SYS 1

A-57

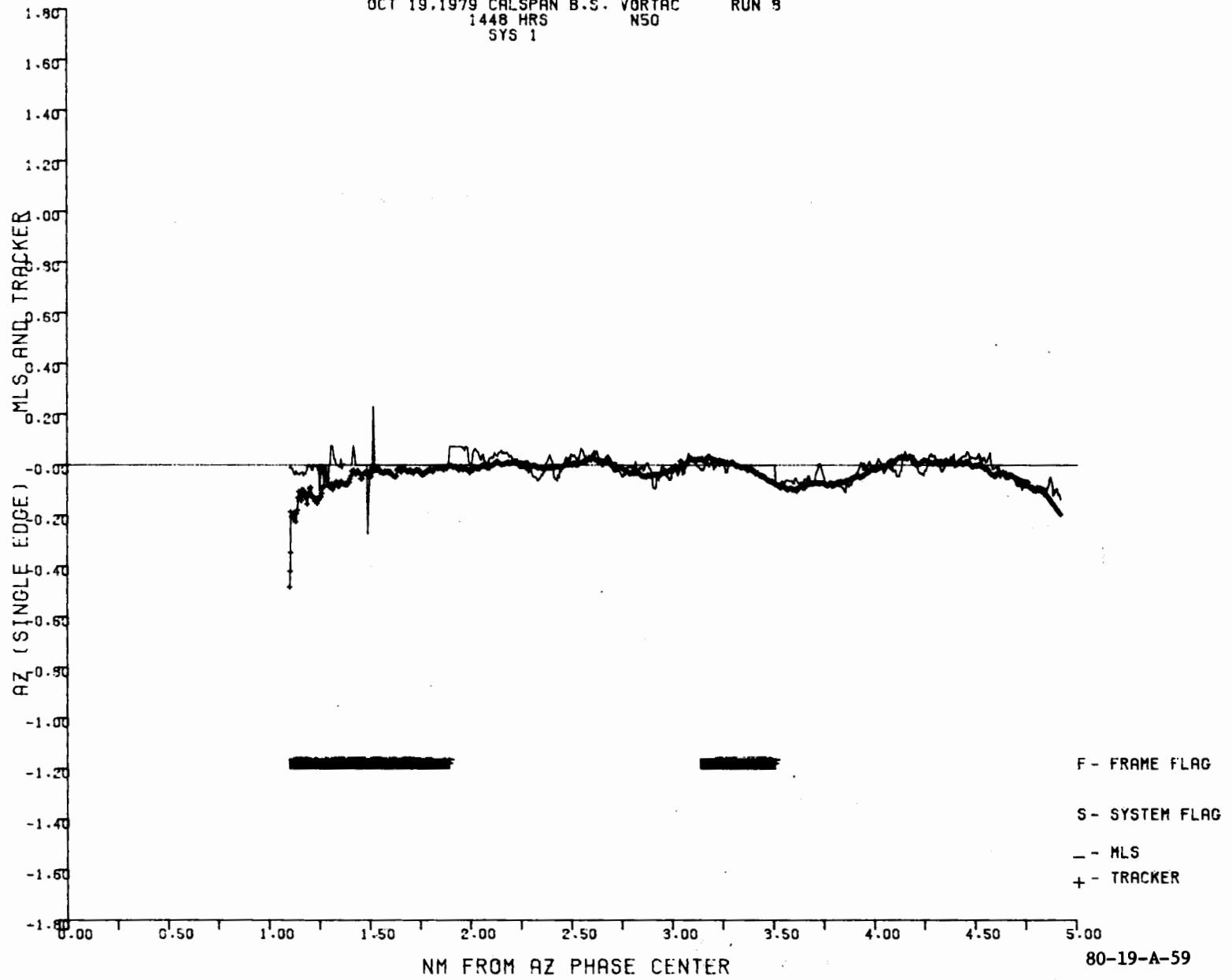


A-58



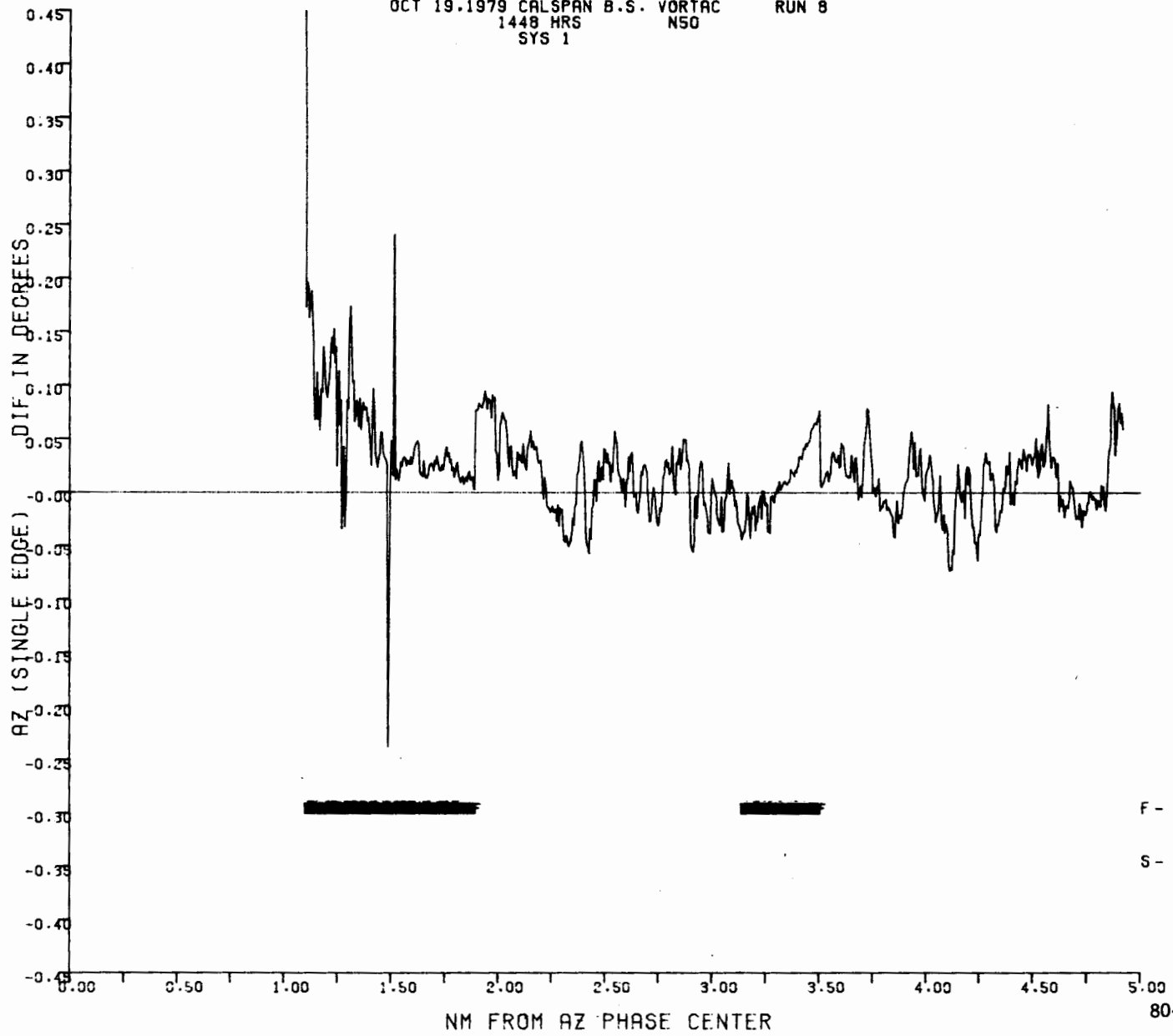
OCT 19, 1979 CALSPAN B.S. VORTAC RUN 9  
1448 HRS N50  
SYS 1

A-59



OCT 19.1979 CALSPAN B.S. VORTAC RUN 8  
1448 HRS N50  
SYS 1

A-60



80-19-A-60